INTERACTION STUDIES OF SMALL NATURAL DERIVED COMPOUNDS AND PEPTIDES WITH α-SYNUCLEIN

Direttore della Scuola: Ch.mo Prof. Maurizio Casarin

Supervisore: Ch.mo Prof. Stefano Mammi

Cosupervisore: Dr Paolo Ruzza

Dottorando: Anna Marchiani

TABLE OF CONTEST

Abstract

Proteins play a crucial role in preservation of life and their dysfunction may cause different pathological conditions. Indeed, the incorrect folding of a protein can trigger neurodegenerative diseases. A wide range of diseases, known as "Protein misfolding disorders" come from the inability of specific proteins to adopt their correct structure or native state and are characterized by the deposition of fibrillar aggregates of proteins, called amyloids, that eventually lead to cellular suffering and death. More than 20 systemic and neurodegenerative diseases are linked to this event, among which we found the well-known Alzheimer's and Parkinson's disease. Although there are no similarities between the proteins involved in these diseases, they show a common organization and morphology. Amyloid fibrils are made of protofilaments twisted around each other, with β-strands running perpendicular to the fibril axis. The mechanism by which these aggregates lead to cell death is not well understood, but it is established that prefibrillar aggregates and not the mature fibrils are the most toxic species, maybe because they interact with plasma membrane forming pore-like structures that interfere with cellular homeostasis.

α-Synuclein is a 140 amino acid presynaptic protein whose function is not well known. It has been identified in the amyloid deposits in several neurodegenerative diseases and mostly in Lewy bodies, the filament inclusions distinguished in Parkinson's disease. α-Synuclein aggregation is considered one of the causes of Parkinson's disease and a triplication or point mutations in the gene that encodes for synuclein are connected to autosomal dominant early-onset Parkinsonism. Today, there are no efficient therapies against Parkinson's and the inhibition of protein aggregation represents one of the most promising therapeutic strategies; specifically research is focused on the development of small organic molecules or peptides that may hamper this process.

Curcumin, or diferuloylmethane, is the main principle of Turmeric, a well-known Indian spice. Several properties have been proposed and then confirmed by modern medicine for curcumin, including antioxidant and antiinflammatory activities, and its ability to inhibit fibril formation *in vivo* and *in vitro* by direct binding to amyloid aggregates has been recently proposed. It has been shown that curcumin can interact with different types of fibrils, so curcumin has been proposed as a general inhibitor of aggregation. Unfortunately curcumin is insoluble in aqueous solution, it has poor bioavailability, and rapidly degrades at neutral or basic pH. All these problems limit the therapeutic use of curcumin. Dehydrozingerone, a natural compound extracted from the plant *Zingiber officinale*

corresponding to half curcumin is also one of its degradation byproduct, but it is more water soluble and stable than curcumin. Deydrozingerone has been demonstrated to possess antioxidant activity as well. Ferulic acid, another degradation product of curcumin with similar structure to dehydrozingerone, shows antioxidant and anti-inflammatory properties, as well as the ability to inhibit amyloid-β fibril deposition (or Aβ, one of the main components of neuritic plaques in Alzheimer's disease). These observations leads to the hypothesis that phenols with antioxidant properties and with a structure that resembles curcumin's, may be able to inhibit the aggregation of α-synuclein.

This research evaluate the capability of curcumin and dehydrozingerone analogues (O-methoxydehydrozingerone, zingerone and their biphenylic analogues), to interact with the monomeric form of human α-synuclein. Results obtained by CD and fluorescence spectroscopies revealed that all these compounds interact with synuclein, even though with different affinity. Moreover, their ability to inhibit the aggregation of α-synuclein was also tested.

Another important aspect to be considered in Parkinson's disease and generally in misfolding disorders is the role of metal ions. Indeed, high levels of metal ions have been detected in the brain of Parkinson's patients. These ions can generate H_2O_2 that can be further converted into the most toxic hydroxyl radical, the main responsible of the oxidative stress associated with this pathology. The ability of dehydrozingerone and analogues to chelate metal ions, specifically Cu^{2+}, Fe^{2+} and Fe^{3+}, has been evaluated by UV-Vis spectroscopy. Moreover, the ability of these compounds to scavenge free radicals was estimated by both UV-Vis and and EPR studies using the DPPH test. Except for O-methoxydehydrozingerone and its biphenylic analog, all the compounds showed good antioxidant activity, increased by dimerization. Finally, their cellular toxicity and their protective effect against oxidative stress insults have been evaluated. This study revealed the bifuctional activity of these curcumin-like molecules, i.e., their ability to chelate metal ions or to scavenge free radicals, together with their capability to interact with α-synuclein.

Additionally. "β-sheet breaker" peptides have been synthesized and tested as ligands of synuclein. The term "β-sheet breaker" refers to small peptide sequences able to interfere with the aggregation process of misfolded protein. Nine peptides, analogues to two sequences able to inhibit protein aggregation, and containing some substitutions in the sequence to overcome some of the drawbacks connected with the use of peptides in therapy (e.g., degradation by proteases), and improve their inhibitory activity have been synthesized by Solid Phase Peptide Synthesis (SPPS). The influence of the aromatic

residue phenylalanine into one sequence in peptide interaction with α-synuclein has been studied using conformational constraints of this residue. Binding studies by CD and fluorescence spectroscopies revealed that all the peptides are able to bind the α-synuclein monomer and that the phenylalanine residue is not important for the interaction with synuclein.

Riassunto

Le proteine giocano un ruolo cruciale nella conservazione della vita e una loro disfunzione può essere causa di differenti condizioni patologiche. Infatti, il non corretto ripiegamento di una proteina può essere causa di patologie neurodegenerative. Un ampio gruppo di malattie, note come "protein misfolding disorders" nascono dall'incapacità di specifiche proteine di adottare la loro struttura nativa e sono caratterizzate dalla deposizione in aree specifiche dell'organismo di proteine in forma di aggregati fibrillari che sono considerati causa della sofferenza e della morte cellulare. Oltre 20 sono le malattie sistemiche e neurodegenerative collegate a questo evento, tra le quali si ritrovano le più note patologie di Alzheimer e Parkinson. Sebbene non si riscontrino somiglianze tra le proteine correlate a tali patologie, le fibrille amiloidi presentano un'organizzazione e morfologia comune. La struttura delle fibrille amiloidi consta di protofilamenti avvolti tra loro costituiti da impilamenti a β-sheet che si propagano lungo la direzione della fibrilla. Non si conosce ancora bene il meccanismo con cui questi aggregati portano a morte cellulare, ma è ormai certo che gli aggregati pre-fibrillari, e non i depositi di fibrille mature, siano responsabili della tossicità, forse per interazione con la membrana plasmatica e formazione di pori che rompono l'omeostasi cellulare.

L'α-sinucleina è una proteina presinaptica di 140 amminoacidi la cui funzione non è ancora ben nota. Essa è stata identificata nei depositi amiloidei di differenti patologie neurodegenrative e soprattutto nei corpi di Lewy, inclusioni filamentose caratteristiche della malattia di Parkinson. L'aggregazione di tale proteina è oggi ritenuta una delle cause del Parkinson e una triplicazione dell'espressione del suo gene o mutazioni puntiformi sono associate ad una forma autosomica dominante di Parkinson giovanile. Ad oggi non esiste ancora una cura efficace per il Parkinson e l'inibizione dell'aggregazione proteica rappresenta una delle strategie terapeutiche più promettenti; in particolare la ricerca è rivolta allo sviluppo di piccole molecole organiche o piccoli peptidi che interferiscano con tale processo.

La curcumina, o diferuloilmetano, è il principale costituente del Curry, nota spezia di origine Indiana. Alla curcumina sono state associate e in seguito dimostrate dalla moderna medicina differenti proprietà, tra cui capacità antiossidanti e antiinfiammatorie, e di recente, la capacità di bloccare la formazione di fibrille in vivo ed in vitro, andandosi a legare direttamente agli aggregati amiloidei. È stato dimostrato che la curcumina, più che ad una specifica proteina, abbia la capacità generale di legare fibrille amiloidi, ipotizzando quindi

che essa agisca come generale inibitore dell'aggregazione. Sfortunatamente la curcumina è insolubile in ambiente acquoso, presenta scarsa biodisponibilità e degrada rapidamente a pH neutro o basico. Tutti questi problemi limitano l'uso terapeutico della curcumina. Il deidrozingerone è un composto naturale estratto dallo *Zingiber officinale* e strutturalmente corrisponde a metà curcumina. Esso risulta essere uno dei prodotti di degradazione della curcumina ma è stabile a pH neutro o basico e inoltre possiede maggior solubilità in solvente acquoso. Per il deidrozingerone sono state riportate proprietà antiossidanti. L'acido ferulico, un altro prodotto di degradazione della curcumina e strutturalmente simile al deidrozingerone, presenta attività antiossidanti e antiinfiammatorie, oltre alla capacità di inibire la deposizione di fibrille del peptide Aβ (uno dei principali componenti delle placche senili nell'Alzheimer). Alla luce di queste considerazioni è ipotizzabile che fenoli con proprietà antiossidanti e struttura simile alla curcumina possano anch'essi possedere proprietà inibitorie nei confronti dell'aggregazione dell' α-sinucleina.

In questo progetto L'attenzione è stata focalizzata l'attenzione sulla curcumina e su altre 6 molecole di struttura simile (deidrozingerone, zingerone, O-metossideidrozingerone e i corrispondenti analoghi bifenilici) ed è stata valutata la loro capacità di interagire con la forma monomerica della sinucleina. Dalle analisi effettuate mediante spettroscopia CD e di fluorescenza è stato evidenziato come tutti i composti in esame siano in grado di interagire con la sinucleina, e le relative costanti di *binding* sono state determinate. Inoltre è stata valutata la capacità inibitoria di questi composti nei confronti del processo di aggregazione dell' α-sinucleina.

Un altro aspetto di notevole importanza è il ruolo degli ioni metallici nel Parkinson e più in generale nella patologie da misfolding proteico. Sono stati infatti evidenziati elevati livelli di ioni metallici redox-attivi nel cervello di pazienti affetti da Parkinson. Tali ioni possono generare H_2O_2 che poi può essere convertita nel più aggressivo radicale idrossile, principale responsabile del danno ossidativo associato a tale patologia. La capacità di deidrozingerone e dei suoi analoghi di chelare ioni metallici, in particolare Cu^{2+}, Fe^{2+} e Fe^{3+} è stata quindi valutata mediante spettroscopia UV-Vis. Questo ha permesso di evidenziare come i derivati bifenilici siano dei buoni chelanti degli ioni metallici. Inoltre, è stata determinata la capacità dei composti oggetto di studio di sequestrare radicali liberi mediante DPPH test e studi EPR. Ad eccezione di O-metossideidrozingerone e del suo analogo bifenilico, gli altri composti hanno dimostrato una buona capacità antiossidante, e, in particolare, si è osservato come la dimerizzazione aumenti tale capacità. Infine, è stata valutata la loro tossicità cellulare e la loro efficacia protettiva nei confronti di insulti da

stress ossidativo: tra tutti i composti il bi-O-metossideidrozingerone si è dimostrato il più tossico a livello cellulare. Tale studio ha quindi voluto mettere in risalto la bifunzionalità delle molecole in esame, ossia la loro capacità di agire da chelanti di ioni metallici o sequestratori di radicali liberi associata alla loro capacità di interagire con la sinucleina.

Un'altra parte del progetto riguarda la sintesi di peptidi aventi proprietà "β-sheet breakers". Tale termine viene utilizzato per indicare piccole sequenze peptidiche in grado di interferire con il meccanismo di misfolding e aggregazione proteica. Mediante la tecnica SPPS (solid phase peptide synthesis) sono stati sintetizzati 9 peptidi analoghi a due sequenze capaci di inibire l'aggregazione proteica e contenenti delle sostituzioni nella sequenza peptidica al fine di superare alcuni svantaggi associati all'uso di peptidi in terapia (es.: degradazione da parte di proteasi), migliorare le loro capacità inibitorie e analizzare l'importanza del residuo aromatico fenilalanina nell'interazione con la sinucleina. Studi di binding mediante spettroscopia CD e di fluorescenza hanno evidenziato come tutti i peptidi siano in grado di interagire con la sinucleina monomero e come la presenza del residuo di fenilalanina non sia importante nell'interazione con la proteina.

Abbreviations

6-OHDA	6-hydroxydopamine
Aib	α-aminoisobutyric acid
AS	α-synuclein
ASI	α-synuclein inhibitors
BAD	
BBB	blood-brain-barrier
BCSG1	breast cancer-specific-gene-1
BDMC	bisdemethoxycurcumin
Bi-DHZ	Bi-dehydrozingerone
Bi-OMe-DHZ	Bi-methoxydehydrozingerone
Bi-Zing	Bi-zingerone
Boc	tert-butyloxycarbonyl
BS	β-synuclein
BSBs	β-sheet breakers
CAP	capsaicin
CD	Circular dichroism
CNS	central nervous system
COMT	cathecol-O-methyltransferase
CR	Congo Red
Ct	C-terminal domain
DA	Dopamine
DAs	dopamine agonists
DAT	plasma-membrane dopamine transporter
DC	dopaminochrome
DCC	Dicyclohexylcarbodiimide
DCM	Dichloromethane
DFS	dynamic force spectroscopy
DHI	5,6-dihydroxyindole
DHZ	dehydrozingerone
DIEA	N,N-diisopropylethylamine
DLB	dementia with Lewy bodies
DMC	demethoxycurcumin
DMF	N,N-Dimethylformamide
DMN	dorsal motor nucleus of the vagus
DNA	Desoxyribose nucleic acid
DOPA	dihydrophenylalanine
DOPAC	didydroxyphenylacetate
DOPAL	3,4-dihydroxyphenylacetaldehyde
DOPET	3,4-dihydroxyphenylethanol
DPPH	2,2-Diphenyl-1-picrylhydrazyl
DQ	dopamine-o-quinone
E1	ubiquitin-activating enzyme

E2	ubiquitin-activating enzyme
E3	ubiquitin ligase
EDTA	Ethylene Diamine Tetraacetic Acid
EPR	Electron paramagnetic resonance
ER	endoplasmic reticulum
ERK	extracellular regulated kinase
ESI-MS	electrospray ionization mass spectrometry
FE	4'(diethylamino)-3-hydroxyflavone
Fmoc	Fluorenylmethyloxycarbonyl
GABA	γ-aminobutyric acid
GSH	Glutathione
HBTU	O-Benzotriazole-N,N,N',N'-tetramethyl-uronium-hexafluoro-phosphate
HOAt	1-Hydroxy-7-azabenzotriazole
HOBt	1-Hydroxybenzotriazole
HPLC	High Performed Liquid Cromatography
HSA	human serum albumin
HVA	homovanillic acid
IAEDANS	**5-((((2-iodoacetyl)amino)ethyl)amino)naphthalene-1-sulfonic acid**
IQ	indole-5,6-quione
LBs	Lewy bodies
LNs	Lewy neurites
LRRK2	leucine-rich repeat kinase 2
MALDI	Matrix-assisted laser desorption/ionization
MAO	monoamine oxidase
MeCN	Acetonitrile
MPP	1-methyl-4-phenyl pyridine
MPP$^+$	1-methyl-4-phenylpyridinium
MPTP	1-methyl-4-phenyl-1,2,3,6-tetrahydropyridine
MSA	multiple system atrophy
MTT	3-(4,5-dimethylthiazol-2-yl)-2,5-diphenyltetrazolium bromide
Myr	myricetin
NAC	non Aβ component
NACP	non-amyloid-β-component precursor
NBIA1	neurodegeneration with brain iron accumulation type 1
NM	neuromelanin
NMR	Nuclear magnetic resonance
OG	Oregon Green 488
OMe-DHZ	methoxydehydrozingerone
OtBu	tert-butyl ester
PA	phosphatidic acid
Pbf	2,3-dihydro-2,2,4,6,7-pentamethyl-5-benzofuranyl)sulfonyl
PD	Parkinson's disease
PD2	phospholipase D2
PKA	protein kinase A

PKC	protein kinase C
PLD2	phospholipase D2
PMDs	Protein Misfolding Disorders
Rg	Radius of gyration
ROS	reactive oxygen species
RP-HPLC	Reverse phase high performance liquid chtomatography
SAC	S-allylcysteine
SDS	sodium dodecyl sulfate
SNC	substantia nigra pars compacta
SOD	superoxide dismutase
SPPS	Solid phase peptide synthesis
SRCD	Synchrotron radiation circular dichroism
SVD	singular value decomposition
TBTU	O-(Benzotriazol-1-yl)-N,N,N',N'-tetramethyluronium tetrafluoroborate
TC	tetracycline
TCSPC	Time-Correlated Single Photon Counting
TFA	Trifluoroacetic acid
ThT	Thioflavin T
TIPS	Triisopropylsilane
TOF	Time Of Flight
TOH	tyrosine hydroxilase
Tris-HCl	tris(hydroxymethyl)aminomethane
TSEs	transmissible spongiform encephalopathies
UCH-L1	ubiquitin C-terminal L1
UPS	ubiquitin-proteasome system
UV	ultraviolet
WT	wild-type
Zing	zingerone

Amino acids abbreviations.

Name	Three letter code	One letter code
Aspartic acid	Asp	D
Glutamic acid	Glu	E
Alanine	Ala	A
Arginine	Arg	R
Asparagine	Asn	N
Cysteine	Cys	C
Phenilalanine	Phe	F
Glycine	Gly	G
Glutamine	Gln	Q
Isoleucine	Ile	I
Histidine	His	H
Leucine	Leu	L
Lysine	Lys	K
Methionine	Met	M
Proline	Pro	P
Serine	Ser	S
Tyrosine	Tyr	Y
Threonine	Thr	T
Triptophan	Trp	W
Valine	Val	V

IUPAC-IUB Commission, *Eur. J. Biochem.*, **1994**, *138*, 9-3

Introduction

Protein Misfolding Disorders (PMDs)

Protein folding and quality control system

Protein folding is the fundamental process that allows a protein to assume the correct structure or the native state [1]. The correct folding is essential for a protein to carry out its biological function and is encoded in the amino acid sequence of the protein itself because it has been shown that proteins can reach their correct folded structure *in vitro* in the absence of any auxiliary factors [2,3]. The dependence of the folding on the aminoacid sequence of a protein is not completely understood but it is believed that hydrophobic and polar residues favor specific and preferential interaction that lead to the final compact structure. The folding process is extremely rapid (milliseconds-to-seconds) much more rapid than expected if the folding were to proceed through a random search of all possible conformations. To explain this contradiction, Levinthal proposed that folding is not a random search for the correct conformation, but that proteins fold along specific "folding pathways" through which the protein experiences well-defined partially-structured intermediate states.
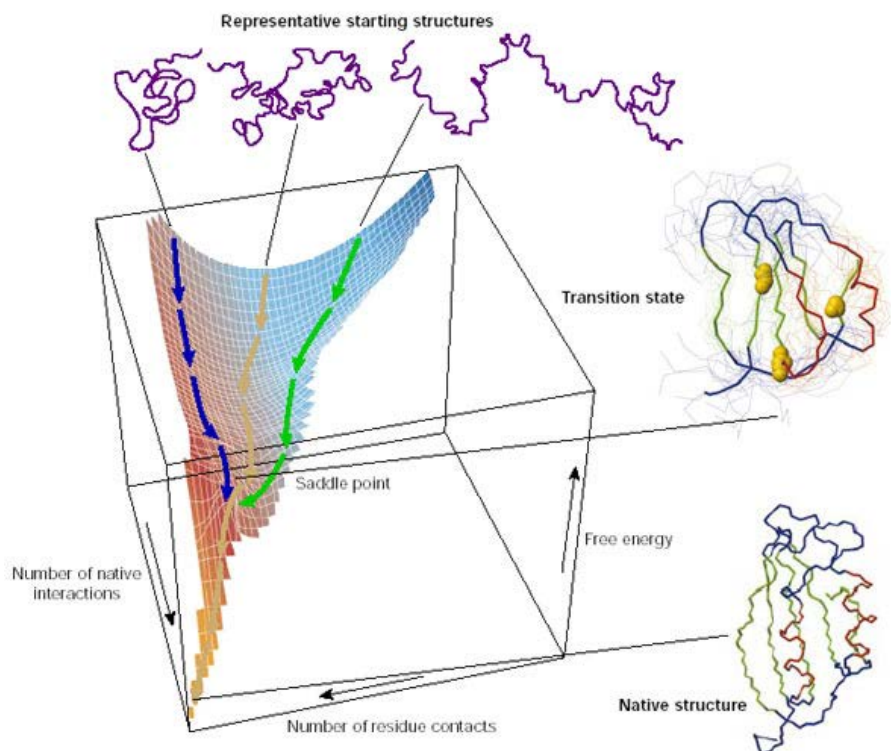

Figure 1: A schematic energy landscape for protein folding [4].

Researchers now describe the entire process via the landscape view of protein folding, in which there is a rugged energy surface or "landscape" through which the unfolded polypeptide chain searches for the native conformation until the unique native structure is formed. Native interactions between residues are more stable than non-native contacts; therefore, while these contacts form and the polypeptide heads towards the native structure, the number of available conformations is reduced. Hence, natural selection has enabled proteins to evolve so that they are able to fold rapidly and efficiently [1,4,5].

The genetic information that encodes for proteins is contained in cellular DNA and ribosomes are the designated structures for protein synthesis. From the ribosome, the unfolded polypeptides are either released into the cytosol or translocated into the endoplasmic reticulum (ER) where they begin to assume their native conformation. Here, they find a complex and crowded environment, with high concentration of proteins and other cell components, and relatively high temperatures. In these cellular conditions, hydrophobic interactions between emerging polypeptides and other protein and cell components are promoted [6]. After release from the ribosome, a competition between successful folding and rapid hydrolysis decides life or death of the newly synthesized polypeptide. It seems that a large fraction of these species is rapidly degraded because of the inherent inefficiency in protein folding [7]. To avoid these unfavorable conditions, the intracellular folding process is monitored and supported by a set of molecular system that all organism possess. The role of these molecular systems is to reduce non-productive interactions rather than catalyze the folding during the process, hiding hydrophobic domains and allowing them to bury inside the native structure [6]. Two main protein groups assist the protein folding process: molecular chaperones and folding catalysts. The molecular chaperones are present in all types of cells and cellular compartments [4]. Some of them are involved in the first step of the folding process, since they interact with the nascent chain that emerges from the ribosome, whereas others are involved at later stages. They often act in concert to ensure that each step of the process is completely efficient, by reducing the probability of competing reactions, especially aggregation. Besides protecting proteins during their folding, some chaperones also rescue misfolded and aggregated proteins to give them a second opportunity to fold correctly. In addition, several classes of folding catalysts accelerate potentially slow steps in the folding process.

Molecular chaperones and folding catalysts are contained in the ER, but there is also a so-called "quality control system" that checks the final conformation before a protein is exported. The quality-control mechanism permits to distinguish between the correctly

folded proteins from the misfolded ones through glycosylation and deglycosylation reactions. This is of crucial importance because abnormal proteins have the propensity to misfold and aggregate, hence they must be removed so that the cell maintains its integrity [8]. This function is carried out by a wide range proteases, among which the most important are the autophagy/lysosomal and ubiquitin-proteasome system (UPS). The autophagy/lysosomal system is responsible for clearing insoluble bulk material such as protein aggregates, whereas the ubiquitin-proteasome system is responsible for the degradation of soluble proteins in eucaryoctic cells. The UPS removes abnormal protein through sequential steps. The first one is an ATP-dependent process, where a chain of the 76-aminoacid polypeptide ubiquitin is conjugated to the unwanted protein. To this end, a ubiquitin-activating enzyme (E1) binds to and activates ubiquitin, followed by the action of a ubiquitin-conjugating enzyme (E2) and a ubiquitin ligase (E3). Ubiquitination is the signal that allows the transfer of the unwanted protein to the protease system where is thus degraded and eliminated from cell [5,7,8].

Misfolding, aggregation and therapy

Despite cell controls, a range of debilitating human diseases is associated with protein misfolding events that result in the malfunctioning of the cellular machinery and eventually lead to pathologies [9]. Many diseases, known as Protein Misfolding Disorders (PMDs) or conformational diseases, result from the presence in a living system of protein molecules with structures that are "incorrect" [10].
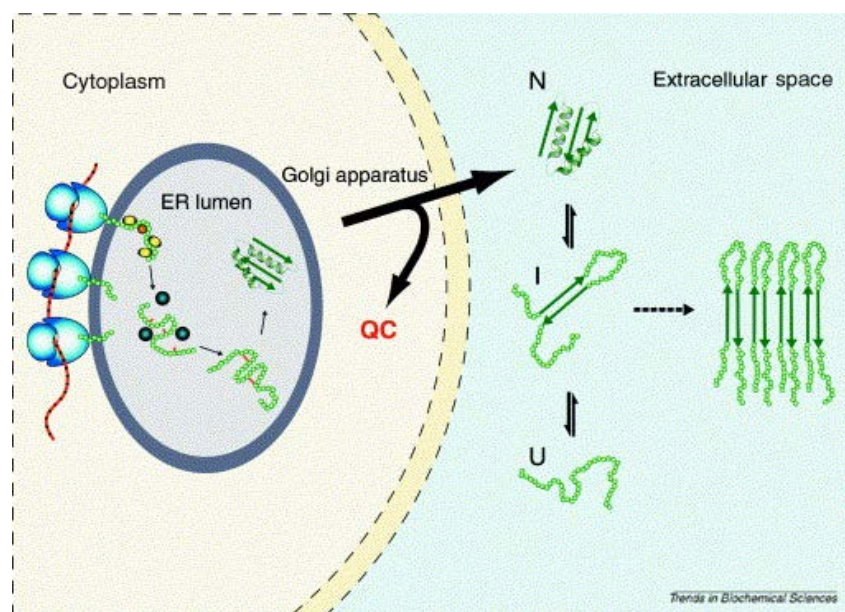

Figure 2: Schematic representation of the possible mechanism of amyloid fibril formation by a globular protein. ER, endoplasmic reticulum; QC, quality control mechanism; N, native; I, intermediate; U, unfolded [9].

Above all, a group of protein folding diseases is gaining the attention of the scientific world: these diseases are generally named "amyloidoses" and are characterized by the failure of specific proteins or peptide to fold correctly or to hold the correct conformation, followed by aggregation that consequently leads to the formation of "amyloid" deposits in tissue.

The term amyloidoses was initially chosen to describe diseases that show accumulation of normally soluble proteins as insoluble deposits in the extracellular environment: an exhaustive analyses of their morphology reveals a thread-like fibrillar structure, sometimes assembled further into larger aggregates or plaques [10]. Some of these disorders are neurodegenerative diseases that affect the brain and the central nervous system such as Alzheimer's disease, while others are systemic diseases that involve peripheral tissue and organs such as the liver, heart and spleen (e.g., type II diabetes). Today, however, the term amyloidoses is also used to describe intracellular depositions, localized in the cytoplasm or in the nucleus, since they resemble those found in the extracellular environment.
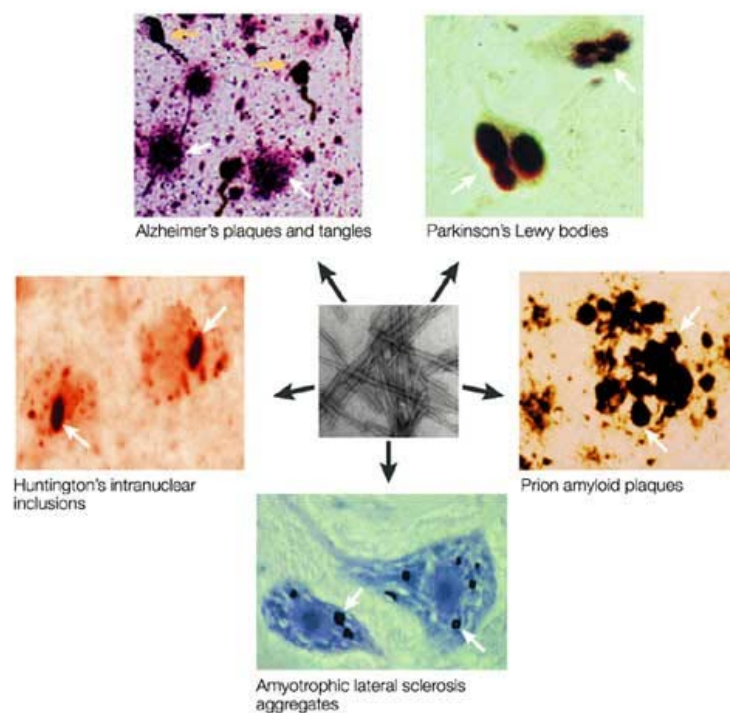

Figure 3: Cerebral aggregates in neurodegenerative diseases [11].

About 20 amyloid diseases are recognized as "amyloidoses" for the presence of extracellular or intracellular aggregates of a specific protein; among them we find: Alzheimer's and Parkinson's disease, spongiform encephalopaties such as Creutzfeldt-Jakob disease, type II diabetes and other less well-known pathologies but with equally severe conditions, such as fatal familial insomnia [9].

These diseases can be sporadic, inherited or infectious, and they often arise late in life. Every disease is associated with a particular protein, and aggregation of these proteins are considered the triggering event directly or indirectly associated with the pathological condition related to the disease in question. Examples of proteins involved in amyloid-related human disorders are lysozyme (in Ostertag type amyloidosis, a non-neuropathic amyloidosis), transthyretin (in familial polyneuropathy), and the prions (in transmissible spongiform encephalopathies or TSEs) [12]. These proteins show no sequence similarity among them and in general they exhibit exclusive and specific native folds, usually an α-helical motif or unfolded structure, while in the form of amyloid fibril they present a conformation rich in β-sheets [11]. The fibrils that they form in their respective pathologies are extremely similar in their overall appearance, but vary in the distribution and composition leading to different deposition profiles and pathologies [12]. Two different driving forces can lead to the formation of similar fibrillar structures: hydrophobic interaction or polar hydrogen bonding among side-chain groups [11].
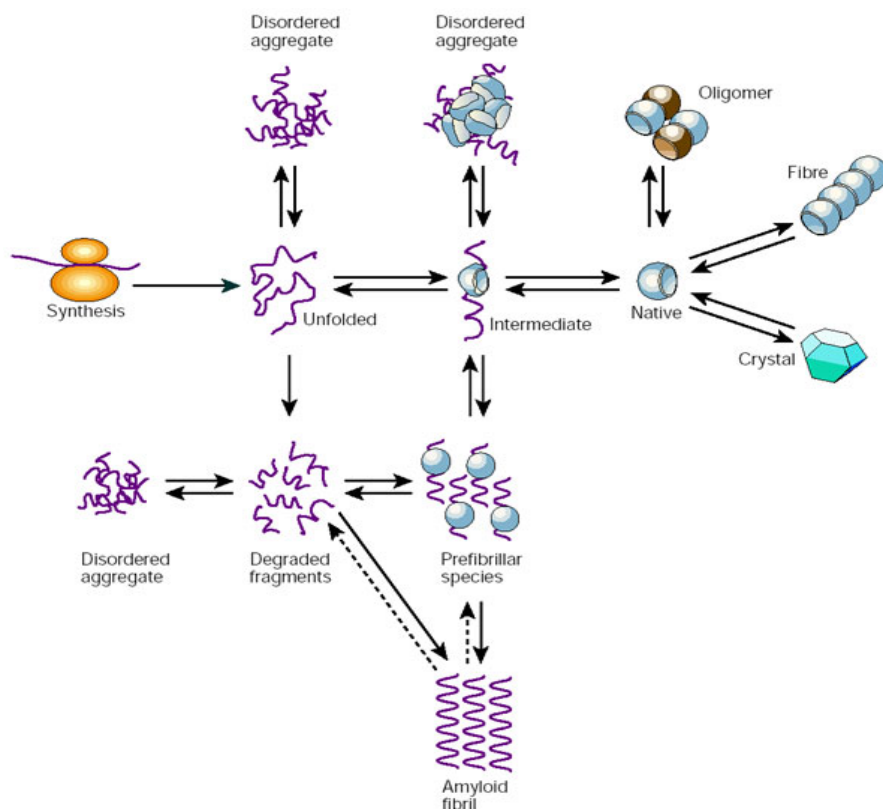

Figure 4: A unified view of some of the types of structure that can be formed by polypeptide chains [4].

Protein aggregation is a slow process that can be described by an ordered mechanism, the nucleation-dependent polymerization model, that features a slow and thermodynamically unfavorable nucleation phase followed by a rapid elongation phase [12]. The rate determining step of the nucleation phase is the formation of a stable seed or nucleus of

polymerized protein. Through the binding of the seed to multiple molecules of the normal protein, the initial nucleus can be converted into a thread of aggregated small oligomers which subsequently leads to the formation of amyloid fibril and in some cases, plaques.

There are conspicuous similarities in the aggregation process of different peptides and proteins [4]. In the first phase of amyloid fibril formation, soluble species appear. They resemble small bead-like structures, sometimes linked together, and are often described as amorphous aggregates or as micelles. These first aggregates are quite disorganized structures and expose to the external environment a variety of segments of the protein that are usually buried in the native state. In some cases, however, they adopt distinctive structures, like well-defined annular species. The early 'prefibrillar aggregates' are then converted into the so-called 'protofilaments' or 'protofibrils' species that show a more distinctive morphology. Usually these structures are short, thin, sometimes curly, and fibrillar species that eventually assemble into mature fibrils, perhaps by lateral association accompanied by some degree of structural reorganization.

The name "amyloidoses" comes from the observation that, like starch (amylose), the aggregated polypeptides stain with dyes such as Congo Red (CR) so the name "amyloid" was first used to describe the insoluble fibrous deposits [3]. Today, amyloid is a generic term that refers to aggregates organized in a cross β structure in which hydrogen bonds are formed between polypeptide chains in a direction parallel to the fiber axis, and possess specific tinctorial properties, higher resistance to proteolitic degradation and a fibrillar appearance under electron microscopy. X-ray diffraction of insoluble amyloid fibrils shows that in general they are straight, unbranched structures about 70-120 Å in diameter and of indeterminate length [13]. X-ray analysis of *ex-vivo* transthyretin amyloid fibrils lead to a model in which several β-sheets turn around a central axis and this is proposed as a generic model for amyloid protofilament structure since collection of fibre diffraction patterns from many other amyloid fibrils demonstrate similar profile.
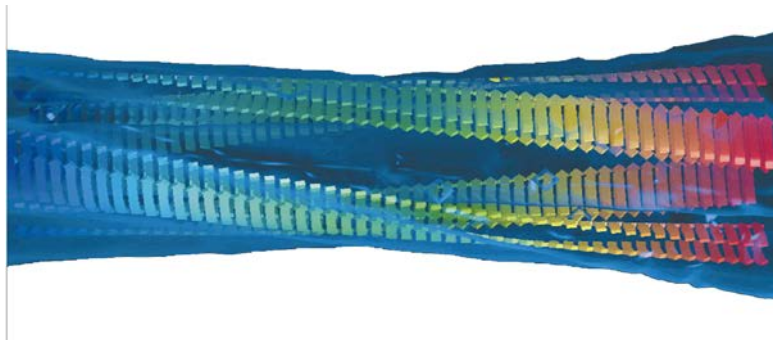

Figure 5: Model of an SH$_3$ domain amyloid fibril [12].

Several genetic and environmental factors have been associated with protein misfoldig and aggregation [11]. Genetic mutations of proteins involved in PMDs can cause conformational changes that then give rise to destabilization of normal protein conformation with subsequent misfolding and aggregation. Some of the environmental factors that might trigger protein misfolding are: changes in metal ions, pathological chaperone proteins, pH or oxidative stress, macromolecular crowding and increases in the concentration of the misfolding protein. Up until recently, it was believed that the most toxic species responsible for cell death were the mature amyloid fibrils, the type of aggregates that are usually found in pathological deposits [10]. However, an increasing quantity of recent experimental data suggests that in many cases the prefibrillar aggregates and not the final mature fibrils are responsible for cell toxicity and death. These findings highlight the importance of these intermediate species, but unfortunately, little is known about their structure and this is due to the nature of the soluble oligomers: they are intermediates in the aggregation process, hence they are supposed to be extremely labile and transient [14].

Kayed et al. [15] evaluated the membrane perturbation caused by amyloid oligomers and protofibril from different proteins involved in PMDs. They demonstrated that soluble oligomers share a common structure that is associated with cellular toxicity, suggesting that soluble oligomers share a common primary mechanism of pathogenesis. This suggests that they should share a common target, and since some types of amyloid oligomers are cytosolic, while others are extracellular, the common target must be accessible to both compartments, and for example it might be the plasma membrane. Kayed et al. have demonstrated that different spherical oligomers increase the membrane conductivity suggesting that this may represent the common primary mechanism of pathogenesis. Several other studies confirmed that prefibrillar assemblies are able to interact with phospholipid bilayers and with the cell membrane that is subsequently destabilized. This interaction is accompanied by a reduced or loss of function of specific membrane-bound proteins. It is thought that this is due to the ability of soluble oligomers to form pore-like structures within cell membranes impairing the ion balance across these structures [10]. Further observations show that low molecular weight species and mature fibrils have no effect on membrane conductivity. From these observations, some investigators have proposed that the formation of the mature amyloid like fibrils might be a protection mechanism of the cell eliminate toxic misfolded intermediates [11].

Toxic aggregates are also able to induce a quick increase of intracellular reactive oxygen species (ROS) and, in addition, changes have been observed in reactive nitrogen species, lipid peroxidation, deregulation of NO metabolism, protein nitrosylation and up-regulation of heme-oxigenase-1, a specific marker of oxidative stress [10]. These data suggest that exposure to early species implicated in amyloid formation can trigger and/or worsen oxidative stress which is another factor responsible for cell damage and eventually cell death.

Currently, therapies for PMDs are just palliative. Protein misfolding plays a leading role in the development of PMDs: therefore preventing and/or inhibiting the misfolding process, as well as reversing already misfolded proteins, might be the best strategy for delaying the disease progression and/or avoiding this unwanted event. Today, this represents the major challenge and a potentially efficient disease-modifying therapy [12]. A large number of strategies have been studied and are under investigation in clinical trials, among which:

- Decreased expression of the aberrant protein: this can be achieved by repairing the gene defect or suppressing the expression of the variant protein;
- Increased elimination of the aggregation-prone proteins, by alleviating the aggregation tendency or stimulating the elimination of the accumulated aberrant protein. Another way is to introduce specific antibodies designed for the particular disease against the aggregation-prone proteins or to target the general β-sheet structure;
- Inihibition of aggregate formation, by the use of small molecules or peptides, or by overexpression of chaperone components of the folding and degradation pathways;
- Enhancement of protein function that means the introduction of chemical and pharmacological chaperones.

Parkinson's disease

Parkinson's disease was first described by James Parkinson in 1817 and is a debilitating pathology that affects approximately 0.3% of the general population and 1-2% of individuals who are 65 years or older [16]. It is a progressive, neurodegenerative disorder that is characterized by severe motor impairments involving resting tremors, bradykinesia, postural instability and rigidity accompanied by non-motoric symptoms like autonomic, cognitive and psychiatric problems [17]. Dementia is 6.6 fold more frequent in elderly patients with the disease compared to those without it. Life expectancy of affected individuals is greatly influenced, with a two to five-fold higher mortality among patients with PD than in age-matched controls [16]. The main pathological hallmark of this

disorder is a pronounced loss of dopaminergic neurons in the substantia nigra pars compacta (SNC), which results in a drastic depletion of dopamine in the striatum, to which these neurons project [18].

Parkinson's disease affects the part of the brain known as the basal ganglia, which consists of five interconnected, subcortical nuclei that cover the telencephalon (forebrain), diencephalon, and esencephalon (midbrain). These nuclei include the striatum (caudate and putamen), globus pallidus, subthalamic nucleus, substantia nigra pars compacta, and substantia nigra pars reticulata [16]. In normal striatum, the neurotransmitter dopamine, which is released from nerve terminals of dopaminergic cells originating in the substantia nigra, modulates the activity of inhibitory γ-aminobutyric acid (GABA) neurons. In turn, striatal GABAergic neurons, through a series of complex "direct" and "indirect" neuronal pathways, modulate neuronal outflow to the talamus, which provides excitatory (glutamatergic) input to the motor cortex. In normal conditions, the direct pathway is dominant, but in PD, the situation is reversed, and the indirect pathways becomes more apparent, with a net effect of decreased excitatory input to the motor cortex. The striatal dopamine deficiency is responsible for the major motor symptoms of the disease but other cathecolaminergic nuclei are also affected, although less severely, contributing to brain disfunction in PD. Direct degeneration of non-dopaminergic cholinergic, adrenergic and serotoninergic nuclei may accounts for several of the non-motor features seen in PD, including fatigue and abnormalities of blood pressure regulation [16,19]. It has been shown that degeneration in PD likely begins in the olfactory region and/or the dorsal motor nucleus of the vagus (DMN), later on spreads into the substantia nigra pars compacta neurons and upper brain stem, and eventually affects the cerebral hemispheres [8].

PD causes

Determining the causes of Parkinson's disease has been a focus of neuroscience research for many decades. Both environmental and genetic factors contribute to the onset of the illness, however, the one factor that most strongly relates to the onset of PD is age or the ageing process [18]. To explain the reasons why PD takes decades to manifest, age-dependent deficits in protective mechanisms have been proposed, whose direct consequence is that abnormal protein aggregation escapes the quality control system [20]. In sporadic PD, the pathogenic mechanisms have been more difficult to understand because a wide range of factors are implicated [18]. Among environmental factors we find: industrialization, rural environment, well water, plant-derived toxins, bacterial and viral

infections, exposure to organic solvents, carbon monoxide and carbon disulfide, pesticide exposure [8]. As an example, evidence shows that carbon monoxide poisoning can trigger parkinsonism within a few days or weeks of exposure with necrosis of the globus pallidus [21]. A similar condition is due to manganese dioxide exposure, termed manganism, with symptoms resembling Parkinson's disease. Manganese primarily damages the globus pallidus with substantia nigra affected to a lesser extent.

Oxidative stress is caused by excessive production of reactive oxygen species (ROS), such as hydrogen peroxide, nitric oxide, superoxide and the highly reactive hydroxyl radicals. Oxidative stress occurs when the cell endogenous defense mechanism is impaired. [22]. Cells possess different markers of oxidative stress: lipid peroxidation is one of these, as unsaturated lipids represent one of the preferential targets of ROS. Several mechanisms exist that lead to the production of ROS: one is redox-active metals and oxygen species that catalyze reactions such as the Fenton and the Haber-Weiss reaction, but there are also other indirect pathways like calcium activation of metallo-enzymes such as phospholipase, nitric oxide synthase and xanthine dehydrogenase.
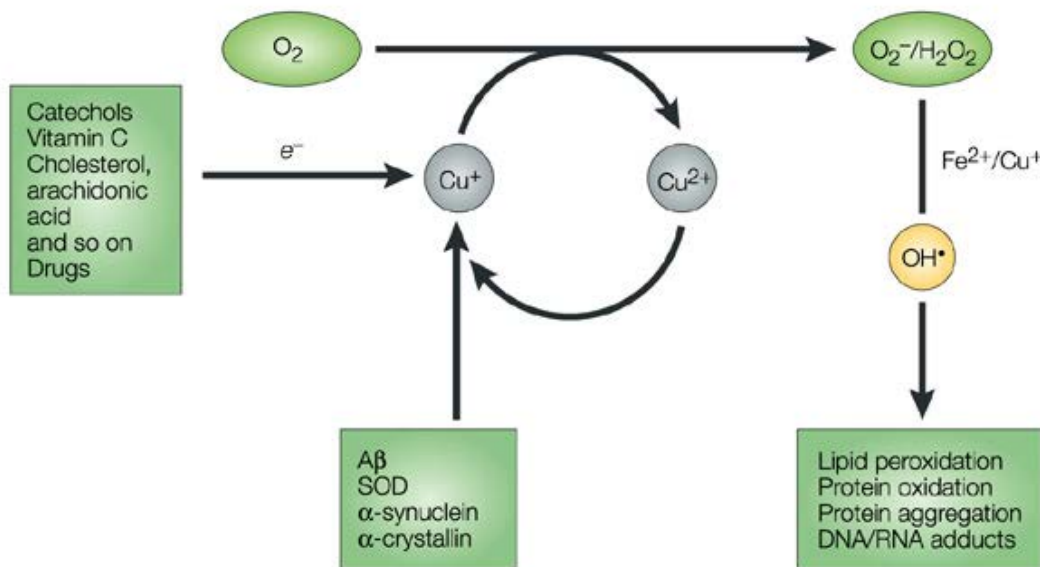

Figure 6: ROS generation by abnormal reaction of O_2 with protein-bound Fe or Cu [22]. One of the consequences of normal aging is that the levels of the redox-active metals copper and iron in the brain increase. This increase could lead to hypermetallation of proteins that normally bind redox-active metals at shielded sites. Adventitial binding — for example: at a loading site — will increase the likelihood that ROS are generated inappropriately as illustrated, leading to the oxidative stress that is observed in neurodegenerative diseases. Aβ, amyloid-β; ROS, reactive oxygen species; SOD, superoxide dismutase.

Deficiency in the major antioxidant enzyme system (i.e. catalase and glutathione peroxidase), but increase in the activity of superoxide dismutase, low mitochondrial complex I activity, and reduction of reduced glutathione levels, suggested that oxidative stress in PD was real and contributes to pathogenesis [23]. Further data that oxidative

stress is involved in PD comes from studies of parkinsonism induced by the toxin 1-methyl-4-phenyl-1,2,3,6-tetrahydropyridine (MPTP), a secondary product that is produced during the synthesis of the drug meperidine. [18]. The active metabolite of MPTP, 1-methyl-4-phenylpyridinium (MPP$^+$) is responsible for PD, because after entering into dopaminergic neurons, it provokes nigral cell death leading to clinical symptoms that resemble those of sporadic PD. People that usually assume this drug can develop the symptoms that are akinetic rigid syndrome with or without resting tremors, within 7-14 days. Once inside the cell MPP$^+$ is concentrated inside the mitochondria, where it inhibits complex I; there are also confirmations for a role in generating free radicals [21].

Finally, deficiency in the ubiquitin-proteasome system as well as proteolytic stress should be considered among the factors implicated in sporadic PD [24]. Chaperones may also play a role, as they have been found in Lewy bodies after immunostaining human postmortem tissues.

Genetic PD

Several gene mutations have been found in inherited forms of PD [17] and they are listed below.

First, PARK1 encodes for a protein named α-synuclein: this is considered a natively unfolded protein with presynaptic localization and it is believed to play a role in synaptic vesicle recycling, storage and compartmentalization of neurotransmitter and associates with vesicular and membrane structures. Genomic triplication of a region of the α-synuclein gene and three missense point mutations in the α-synuclein gene (A53T, A30P and E46K) are associated with autosomal dominant PD. These substitutions were found in different family through the world: the Ala to Thr substitution at position 53 in certain Greek and Italian families; the Ala30 to Pro mutation in a family of German origin, the E46K mutation was discovered in a Spanish kindred, and a triplication of the wild-type gene in a large family from Iowa [25].

This familial form of PD is characterized by an early stage of onset and a high occurrence of dementia, with features that resemble those of sporadic PD.

PARK2 encodes a protein named parkin that functions as an E3 ubiquitin protein ligase by targeting misfolded proteins to the ubiquitin-proteasome system for degradation and is considered a neuroprotective agent in a variety of toxic insults crucial for dopamine neurons survival. Mutations in the parkin gene leads to an autosomal recessive early onset PD (about 50% of the cases) and causes the loss of its E3 ligase activity.

Mutations in PARK7 locus are associated with rare forms of autosomal recessive early-onset parkinsonism. Approximately 1-2% of all early-onset PD are due to mutation in the PARK7 gene. PARK7 is responsible for the expression of DJ-1 protein that loses its function in the mutated form. DJ-1 is a homodimeric protein that acts as an antioxidant protein: it has been demonstrated that cells lacking DJ-1 are more susceptible to damage due to free radicals. DJ-1 is present in various mammalian tissue including brain and can be localized to mitochondria.

Another missense mutation affects the gene encoding ubiquitin C-terminal L1 (UCH-L1) (PARK5 locus). The I93M mutated form of UCH-L1 caused PD in two siblings. This form of PD is characterized by impairment in the ubiquitin-proteasome system since the role of UCH-L1 is to de-ubiquitinate proteins so that they can enter into the proteasome for subsequent degradation. It also makes free ubiquitin available, necessary for the clearance of other unwanted proteins.

Early-onset familial PD is also caused by mutations in the PINK1 (PARK6) gene. PINK1 mutations account for 1 to 9% of PD cases, but there are substantial differences among different ethnic groups. PINK1 is localized to mitochondria, but its function is mostly unknown: perhaps it has a role in mitochondrial dysfunction, protein stability and kinase pathways in pathogenesis of PD.

Finally mutations in the leucine-rich repeat kinase 2 (LRRK2) or dardarin (PARK8 locus) cause autosomal dominant PD and are the most common genetic cause of PD. LRRK2 encodes a 2527 amino acid multidomain protein, that includes a central catalytic region with GTPase and kinase activities. Its precise physiological role and how LRRK2 mutations lead to neurodegeneration are unknown, but the observation that toxicity related to LRRK2 mutations can be attenuated with kinase inhibitors suggests that altered kinase activity contributes to the pathogenic process [17, 8, 21].

Parkinson's disease therapies

Administration of levodopa was introduced in the late 1960s as a treatment to control the motor symptoms of Parkinson's disease [19]. Catechol-O-methyltransferase (COMT) inhibitors were lately introduced as adjunct therapies, leading to an increase in both half-life and bioavailability of single levodopa doses. Soon after, ergot-derived dopamine agonists (DAs) were established in addition to levodopa in advanced PD because of their ability to reduce side-effect of levodopa, such as dyskinesia. Another strategy in PD treatment is the use of MAO inhibitors as neuroprotective agents. Rasagiline was the first

putative disease-modifying agent of this class to be tested although the beneficial effects of this drug remain controversial. Non-dopaminergic antiparkinsonian medications targeting systems outside the striatal dopamine synapse were also developed. Among all these treatments, today levodopa remains the preferred and most effective medicine for symptomatic treatment.

New therapeutic strategies are under investigation: cell-based therapy may be one of the future approaches with the aim to replace nigrostriatal dopamine neurons in PD; another one is gene therapy, that utilizes viral vectors carrying therapeutic genes to be injected intracerebrally, but the discovery of novel molecular target and drug candidates is the major challenge in PD therapy.

α-synuclein

The synucleins

α-Synuclein (AS) is a 140-aminoacid protein that belongs to the class of intrinsically unstructured proteins [26]. At least four different labs discovered synuclein proteins independently: Maroteaux et al. first discovered AS localized to a restricted area of the nucleus and to the presynaptic nerve terminals, in the central nervous system (CNS) of *Torpedo californica* and in rat. It was named synuclein, on the initial evidence for both synaptic and nuclear localization, even though nuclear localization has not been consistently observed in subsequent studies [27, 28]. Najako et al. described the purification of a brain specific bovine protein that they named phosphoneuroprotein-14-kDa. Later, Ueda et al. discovered a new intrinsic peptide component in the human AD amyloid and called it "non-amyloid-β-component precursor" (NACP). Finally, Clayton et al., studied, cloned and sequenced a new protein and named it sylnefin [27]. For hystorical reasons, the name synuclein has survived. In 1994, another sequence was identified, the human homologue of rat phosphoneuroprotein-14, named β-synuclein (BS) because of its similarity with α-synuclein. BS is a phosphoprotein that contains 134 amino acid [29]. More recently, Clayton et al. suggested the name γ-synuclein to refer to a third form related to the original *Torpedo* synuclein sequence [27].

The human α-synuclein gene maps to chromosome 4q21, whereas β-synuclein gene maps to chromosome 5q35 [29]. There is a considerable degree of homology with α-synuclein and the main difference between AS and BS is that an 11-aminoacid segment, from residue 73 to 83, is absent in β-synuclein [30]. They are shown to be concentrated in nerve

terminals in close proximity to synaptic vescicles [31], with little staining of somata and dendrites. β-Synuclein was also found in Sertoli of the testis cells and recently it has been detected at low levels in other tissues than brain, while α-synuclein was also found in platelets [32]. γ-Synuclein is a 127 amino acid protein found in large amounts in human breast cancer tissue and corresponds to the "breast cancer-specific-gene-1 (BCSG1). The γ-synuclein homology to AS accounts for only 55% of the AS sequence: it contains about twice the number of amino acid substitutions than β, and lacks the tyrosine-rich C-terminal. [27,29]. γ-Synuclein is present in neurons of the peripheral nervous system, although it has also been found at low levels in brain but diffusely distributed throughout the cytoplasm [33].
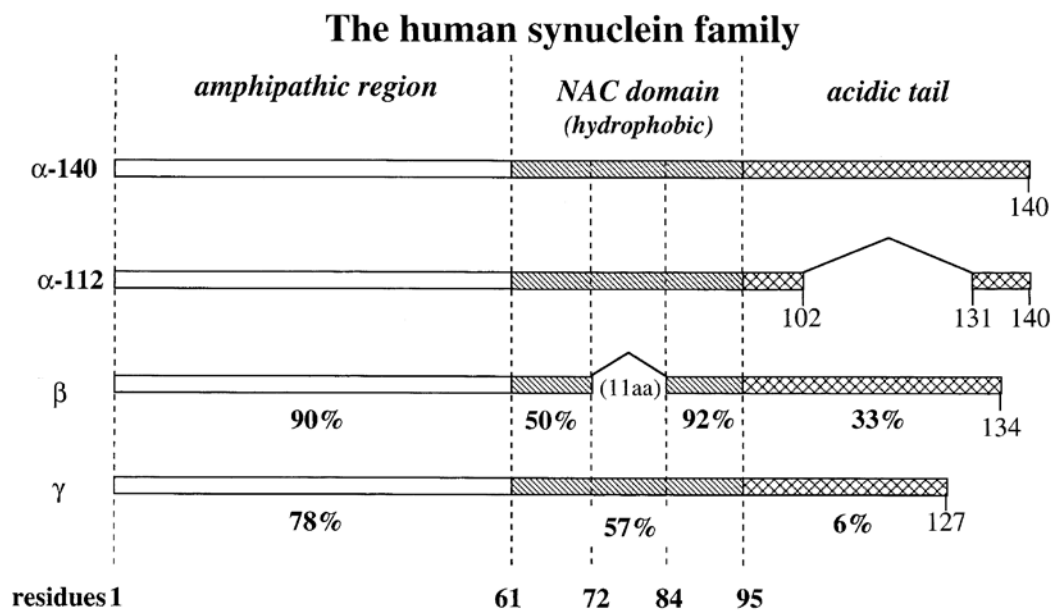
Figure 7: The human synuclein family [7].

Analysis of the structure

α-Synuclein, in aqueous solution, is natively unfolded, without a hydrophobic core and with an extended random coil structure [7]. Usually, natively unfolded proteins lack the amino acids which normally form the core of a folded globular protein, that is the hydrophobic (Ile, Leu and Val) and the aromatic (Tyr, Trp, Phe) residues. They also possess low contents of Cys and Asn residues [32]. On the other hand, the disorder-promoting polar amino acids (Ala, Arg, Gly, Ser, Pro, Glu and Lys) are present in large amounts.

The primary sequence of α-synuclein can be divided into three region: (i) residues 1-60 constitute the N-terminal region, containing four 11-aa imperfect repeats with the motif

KTKEGV; (ii) the central region, containing two additional KTKEGV, that includes the highly amyloidogenic NAC sequence (residues 61-95); and (iii) the C-terminal region (aminoacids 96-140), disordered under most conditions, rich in acidic residues and prolines, with three highly conserved tyrosines [34].
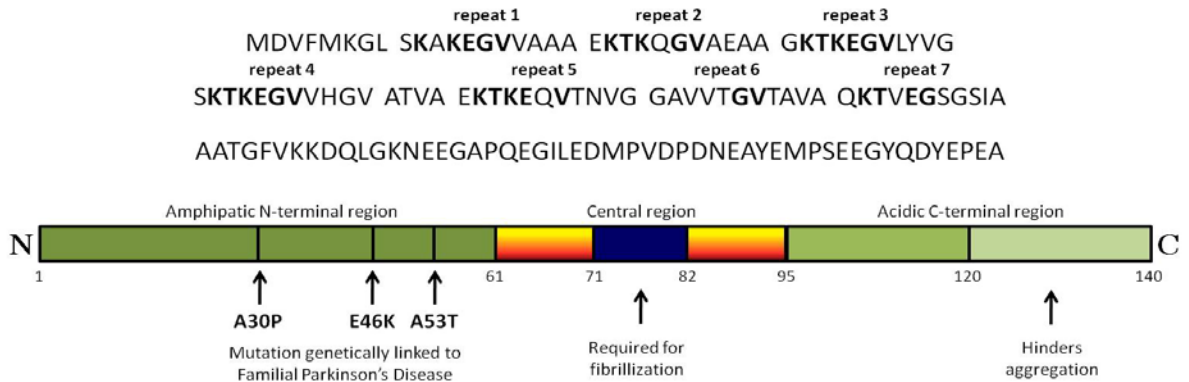

                    repeat 1   repeat 2   repeat 3
        MDVFMKGL SKAKEGVVAAA EKTKQGVAEAA GKTKEGVLYVG
        repeat 4   repeat 5   repeat 6   repeat 7
        SKTKEGVVHGV ATVA EKTKEQVTNVG GAVVTGVTAVA QKTVEGSGSIA

        AATGFVKKDQLGKNEEGAPQEGILEDMPVDPDNEAYEMPSEEGYQDYEPEA

Figure 8: Primary structure of α-synuclein.

AS binds lipid and its conformation upon binding has been extensively studied. The first 100 residues of the N-terminal region are responsible for the binding to SDS-micelles or phosphatidic acid/phosphatidylcholine vesicles, with acquisition of an α-helical conformation, while the C-terminus remains substantially unstructured [35]. The KTKEGV motif assumes a distinct disposition when bound to lipids, with separation of hydrophobic and polar domain, resembling the behavior of apolipoproteins and other lipid-binding proteins [36].
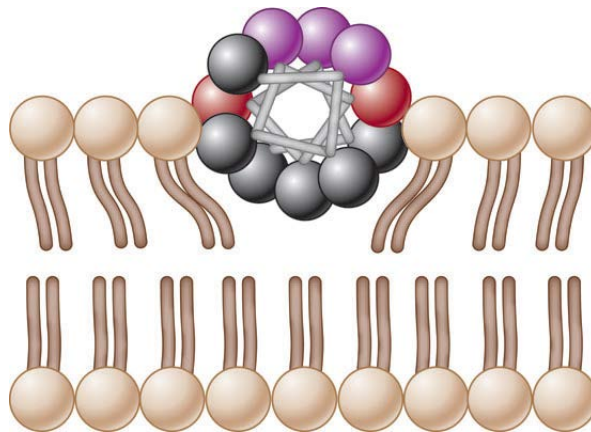
Figura 9: Model of AS bound to lipids. Grey sphere: hydrophobic residues; red: charged lysine residues; purple, hydrophilic residues [36].

The A53T mutant form of α-synuclein is also able to bind lipid vesicles, while the A30P mutation shows lower affinity perhaps because the proline residue disrupts the α-helical structure and interferes with the conformation required for lipid binding [31]. The E46K α-synuclein shows similar affinity for lipids as the A53T, as the charged amino acid lysine 46 favors the formation of hydrogen bonding between AS and the phospholipid surface [36].

15

The hydrophobic peptide NAC (non Aβ component) was first discovered in AD amyloid and later recongnize to belong to the synuclein sequence. It is a 35-amino acid peptide and corresponds to residues 61-95 of AS [30]. NAC can aggregate in vitro acquiring a distinct fibrillar morphology: electron microscopy has revealed the presence of short irregular fibrils of variable length, mainly 4-11 nm in diameter. Interestingly, the N-terminal sequence of NAC shows similarity to sequence fractions crucial for the aggregation and toxicity of other three amyloidogenic proteins: Aβ (AD), prion protein (TSEs) and islet amyloid polypeptide (type II diabetes). The four residue group, Gly-Ala-X-X, where X is an aminoacid with an aliphatic side chain, is common to all four peptides. The N-terminal fragment of NAC gives rise to characteristic amyloid fibrils enriched in β-sheet structure, whereas the C-terminal fragment of NAC has no tendency to aggregate under similar conditions. These data confirmed the importance of the NAC region in AS aggregation, especially that the N-terminal section of NAC is the principal determinant that drives β-sheet formation and hence aggregation and deposition of NAC in neuritic plaques. It has been proposed that the toxicity of NAC and AS is sequence specific and increased by ageing in solution [37]. Further studies confirm the role of the NAC region in AS aggregation, such as evidence that the fibrillation kinetics of β-synuclein, which lacks 11 residues within the middle region of the sequence (residue 73-83), is much slower than that of AS [38].

Among the three synuclein, β-synuclein is the only one that cannot form "amyloid pores", the neurotoxic oligomeric species. In addition, it has been shown that a small amount of β-synuclein is able to completely suppress the oligomerization of AS [39], although the mechanisms is not completely understood. One of the hypotheses to explain this behavior is that β-synuclein might indirectly bind to AS and prevent further aggregation, or that β-synuclein might also facilitate interaction of AS with fatty acids in the membrane, favoring the α-helix conformation. Furthermore, it has been proposed that β-synuclein might have antioxidant or neuroprotective properties thus decreasing AS oxidation and preventing its aggregation [40].

The influence of the C-terminal domain of AS on aggregation, specifically residues 109-140, was evaluated [41]. Truncation of the 16 or 32 C-terminal amino acid residues of wild-type α-synuclein ([syn(1-124)] and [syn(1-108)]), resulted in a marked acceleration of aggregation. This truncated region is rich in acidic residues, with four aspartate and eight glutamate residues in aa 109-140, whereas basic amino acids are absent. Since charge changes affect the overall property of the protein, the net charge of the sequence must be

considered. The presence of cations such as monovalent Na^+, divalent Mg^{2+}, or polycationic polyamines is cause of accelerated aggregation, due to the shielding of the negative charges. We can conclude that the C-terminal domain of AS sequence plays a crucial role in the aggregation process, by regulating AS properties both in its monomeric and aggregated forms, because its presence can avoid the encounter and association of aggregation-prone regions by charge-charge repulsion and by formation of intramolecular contacts. Another piece of evidence for the regulatory role of the C-terminal domain in fibril formation was supported by Mazzulli et al. [42] who demonstrated that dopamine and other catechols have the ability to modulate the progression of PD through C-terminal interactions with AS.

The importance of the C-terminal domain has been confirmed by recent NMR structural analysis, that have revealed the existence of a number of long-range interactions in the AS structure, the most important ones being long-range interactions between the C-terminus and the NAC region (residues 120-140 of the C-terminus and residues 30-100 in the central region) [43].

The conclusion of the study was that AS is composed of an ensemble of structures that are, on average, significantly more compact than a random coil, as demonstrated by the smaller hydrodynamic radius of AS in its native state compared to a completely unfolded polypeptide chain in 8M urea. It has been proposed that the highly charged C-terminus may be in close proximity to the central region, thus shielding and protecting hydrophobic residues from aggregation. Destabilization of long-range interactions could favor the exposure of the polypeptide chain, making it available for aggregation [44].
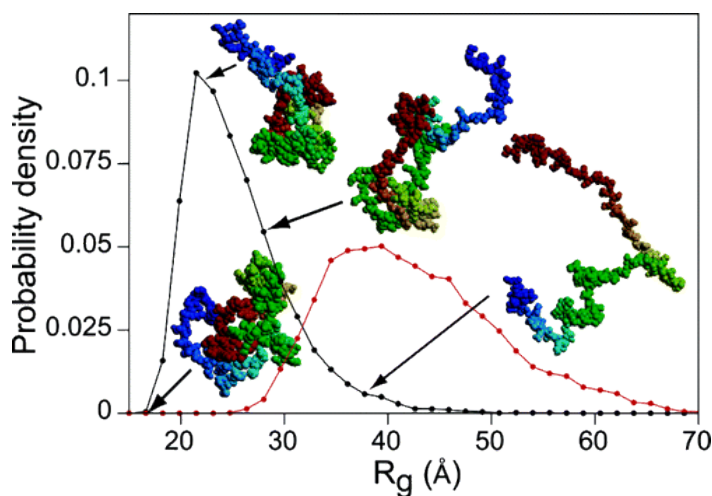

Figure 10: Radius of gyration (Rg) probability distributions for native (black) and random coil (red) models of AS. Representative structures are shown with arrows pointing to their corresponding Rg values. The structures are color-coded according to sequence, ranging from dark blue to red at the N- and C-termini, respectively [43].

More recently Bartels et al. [45] revealed an absolute new and different model of AS folding. They studied the conformational features of AS extracted from red blood cell (that have been demonstrated in recent times to contain the protein) and neuroblastoma cells expressing AS: several different analyses revealed that AS adopts a tetrameric fold rich in α-helical content, opposite to the unfolded AS obtained from bacteria. They proposed that AS is natively unfolded when expressed in bacteria because of the denaturing conditions used for its purification. From the observation that unfolded AS is highly prone to adopt an α-helical structure, they assert that the monomer represents an incomplete, nonfunctional, and less abundant species in the cells. Furthermore, tetrameric AS shows a completely different behavior towards aggregation compared to the monomer, with a much lower propensity to aggregate and to form fibrils. Thus, they conclude that AS tetramers in the cells could undergo conformational destabilization before AS aggregation, like the transthyretin amyloid formation mechanism.

AS functions

The normal functions of α-synuclein have been hypothesized based on its structure, physical properties and interacting partners [7]. The seven imperfect repeats of the 11-amino acid motif in the N-terminal domain of AS are similar to the lipid binding α-helical domain of many apolipoprotein [30,46]. Through the N-terminal repeats AS binds to acidic phospholipids, indicating that it might be a lipid-binding protein [30, 31].
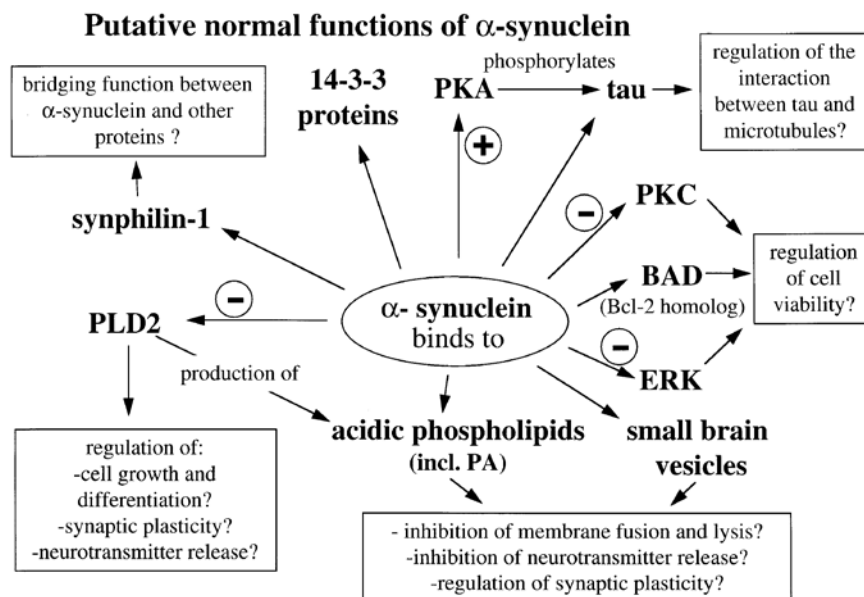
Figure 11: Putative normal function of AS [7]. The binding partners of AS are indicated by arrows. "-" and "+" indicate enzyme inhibition or activation by AS respectively. The boxes describe potential functions of AS interacting with the respective partner. PA, phosphatidic acid; PLD2, phospholipase D2; PKC, protein kinase C; PKA, protein kinase A; ERK, extracellular-regulated kinase.

All synucleins may be members of the chaperone proteins superfamily due to their homology to a region of the chaperone 14-3-3. The fact that 50% of AS is found in the cytosol is another indication of its proposed chaperone activity. The chaperon-like activity of AS is lost when the entire C-terminal domain is deleted [46]. α-Synuclein inhibits protein kinase C (PKC) and it binds to dephospho-BAD and extracellular signal regulated kinase (ERK), as well as 14-3-3 [7]. It is thus possible that α-synuclein plays a role in the regulation of cell viability like these three proteins do. Synphilin-1 is another protein that binds to α-synuclein, specifically to its first 39 residues, and it has been proposed that it may anchor α-synuclein to other proteins that are involved in vesicles transport and cytoskeletal function. So it is also possible that α-synuclein regulates vesicular transport processes. Regulation of synaptic plasticity and neuronal differentiation is another role proposed for AS. This may be mediated by the selective inhibition of phospholipase D2 (PLD2), an enzyme localized to the plasma membrane, since isoforms of PLD2 were shown to be implicated in cell growth and differentiation. [31]. AS can also interact and modulate the activity of tyrosine hydroxylase, the enzyme involved in the rate-limiting step of dopamine synthesis [35]. Moreover, AS may have a regulatory role in DA neurotransmission by negatively regulating dopamine release through its interaction with vesicles membranes (modulating the releasable dopamine pool). In addition, AS knockout mice show increased dopamine release at synaptic terminals when stimulated with electrical pulses [46]. Finally, AS can regulate cell viability (pro-apoptotic role) [31].

Lewy bodies and neurites

The main feature of Parkinson's disease is the presence of Lewy bodies (LBs) and Lewy neurites (LNs) in neurons of the substantia nigra pars compacta and other region of the central and peripheral nervous system [8]. Lewy bodies were named after their discovery in the neurons of substantia nigra innominata by Heinrich Lewy in 1929. They are intracytoplasmic inclusions that show a proteinaceous core with a pale halo after staining with hematoxylin/eosin [26]. The major component of Lewy bodies is the protein α-synuclein, as revealed by strong staining of LBs from idiopathic PD with antibodies for α-synuclein [47], but also neurofilament, ubiquitin, and a wide range of other proteins were found. Lewy neurites represent protein accumulations as well, but they are detected in the axons of affected neurons. Lewy body is a form of aggresome. An aggresome is an intracellular inclusion that rises as a consequence of excess levels of unwanted proteins to facilitate their segregation and degradation. This happens when proteins/aggregates cannot

be eliminated locally so they are transported through the microtubular system to the centrosome, which expands and becomes an aggresome. Lewy bodies are considered an aggresome because they contain centrosome/aggresome specific proteins and, above all, they have heat shock proteins and components of the UPS typically found in aggresomes. Moreover, LBs also contain high levels of oxidized, 4-hydroxynonenal conjugated, nitrated, phosphorylated, and ubiquitinated proteins that usually are not present in the cell. These observations suggested that Lewy bodies might act as sequestrators of unwanted and potentially toxic proteins, thereby representing a protective mechanism to proteolytic stress [8]. LBs are also found in other pathologies, such as dementia with Lewy bodies, Alzheimer's disease, where LBs constitute the second most common nerve cell pathology after the neurofibrillary lesions of AD, Down's syndrome, multiple system atrophy (MSA) and neurodegeneration with brain iron accumulation type 1 (NBIA1) [32, 33, 47].

AS aggregation: morphology and kinetics

Several observations implicate α-synuclein in the pathogenesis of PD [32]. Braak et al. [48] proposed that AS pathology begins at caudal levels of brainstem perhaps years before affecting the substantia nigra; pathology then progresses rostrally to affect limbic and cortical regions.

In high concentrations or in mutant form, AS has a propensity to misfold into β-pleated sheets and form toxic oligomers and aggregates [8]. For a globular protein fibrillation requires the destabilization of its native structure leading to a partially unfolded conformation [32]. This conformation permits specific intermolecular interactions which are necessary for oligomerization and then fibrillation, e.g. hydrogen bonding and hydrophobic contacts. Fibrillogenesis of intrinsically unstructured proteins requires the stabilization of a partially folded conformation. These observations leads to a general hypothesis of fibrillogenesis: a partially folded conformation intermediate state is an important prerequisite for protein fibrillation.

AS aggregation resembles the model proposed for PMDs: the aggregation is slow and displays a distinct lag phase [49], indicating that it follows a nucleation-dependent polymerization mechanism.

Several factors can trigger AS aggregation such as: increased temperature and concentration, lowered pH, interaction with metal ions and interaction with Aβ and apolipoprotein E, mutations and truncation of AS sequence [7]. As mentioned above, genetic mutations are responsible for familial form of PD: three different missense

20

mutation in the AS gene, corresponding to A53T, A30P and E46K substitution in AS and triplicated gene expression of AS have been recognized. In these cases, the propensity of AS to aggregate is increased [32]. El-Agnaf et al. [50] reported that mutant AS proteins developed more β-sheet structure and formed more mature filaments than wild-type AS.

In agreement with several experimental data (X-ray fiber diffraction, cryoelectron microscopy, NMR and EPR studies) a possible fold of the core of AS fibrils was proposed, where a motif of five-layered β1-loop-β2-loop-β3-loop-β4-loop-β5 fold like a sandwich and then, when it finally converts into a protofilament, it builds up five layers of parallel, in-register β-sheets [51]. Fibrils with diameters from 6 to 8 nm wide are referred to as protofibrils, while those with diameters 10 nm and above are referred to as mature fibrils [30].
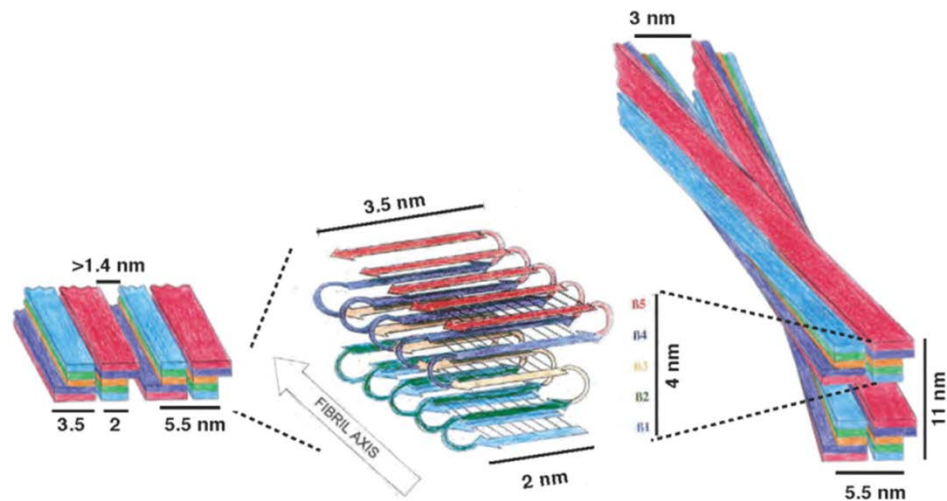
Figure 12: Proposed fold of AS fibril. The proposed fold of a monomeric AS within a protofilament is shown in the center. The incorporation of a protofilament into the straight (left) and twisted (right) fibril type is indicated by a schematic drawing [51].

The final fibril can be either straight, with two protofibril aligned with each other to give the fibril that subsequently can align again itself, or twisted, in which the two protofibrils twist around each other forming a twisted filament that can further twist around another one. It has been shown that β3- and β4- strands (74-84 residues) are in the center of the fibril fold and their elimination is deleterious for the formation of fibrils. In contrast, deletion in either β1, β2 and β5 (61-67 and 72-86 residues) might not be sufficient to stop fibril formation. The two termini are excluded from the β-sheet-rich core region [52]. Through adjacent side chains, layers of the parallel β-sheet may associate to form channels: these channels have been proposed as binding sites for Thioflavin T (ThT), the probe most commonly used for detection of amyloid fibrils, with its short axis perpendicular to the fibril axis [53].

It is worth noting that the fibrils from a given polypeptide can exhibit polymorphism. Under altered conditions, variations in the fibril appearance, such as in the diameter, twist, pitch, and number of protofilaments, may arise [52].

Celej et al. highlighted the presence of subtle variations in the structure of AS fibrils using an extrinsic multiple-emission probe 4'-diethylamino-3-hydroxyflavone (FE) that showed distinct spectroscopic characteristics upon binding to fibrils formed either by wild-type AS or its variants (A53T and A30P). Moreover, Serpelli et al. demonstrated that the A53T substitution of gives rise to different filament morphologies. The wild-type AS and the A30P mutant have been shown to form predominantly straight filaments similar to those found in dementia with Lewy bodies (DLB): in detail, aggregates of the A30P mutant present various morphologies, including single-5-nm-wide straight protofibrils, similar to those seen in the wild-type, but the majority of long mature fibrils had 10-nm-wide straight bundles. On the contrary, the A53T mutation produced mainly twisted filaments that resemble those found in multiple system atrophy (MSA), with branched twistedsingle fibrils with a width varying between 6 and 12 nm. Mature fibrils with slim 6- to 10-nm-wide extensions at the end of 25-nm-wide fibrils have been also seen.
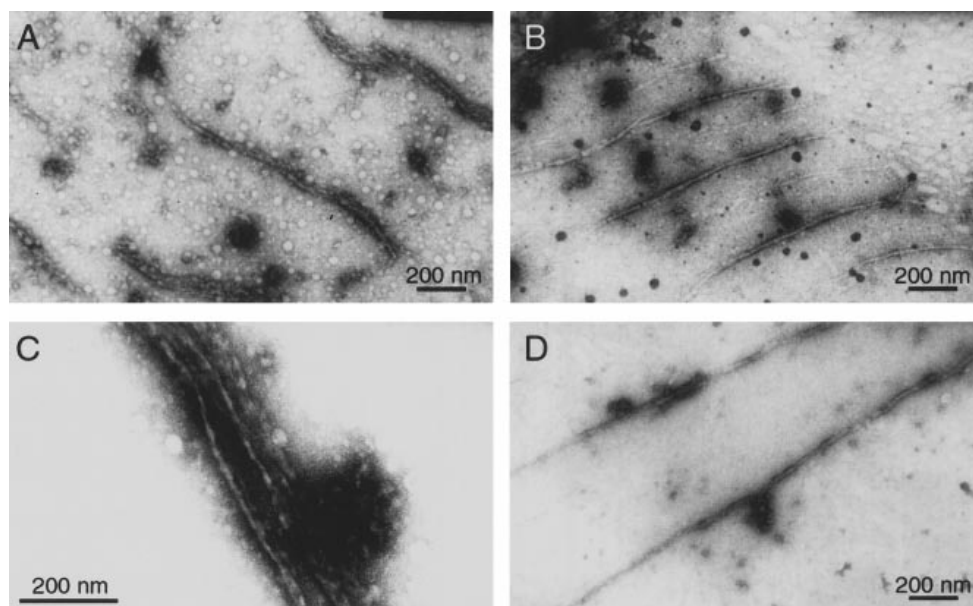
Figure 13: Negatively stained electron micrographs of fibrils obtained from AS proteins aged for 7 days at 37 °C in PBS [30]. (A) AS; (B,C) A30P mutant; (D) A53T mutant.

Conway et al. [54] characterized three different species of AS oligomers that may be sequential species in aggregation pathway. These are: "spheres" of several heights, some of which resemble early Aβ protofibrils, "chains" that appear to comprise linearly-associated 4-5 nm spheres, analogous to elongated Aβ protofibrils, and "rings", apparently comprising

circularized chains. These findings underscore the polymorphic nature of the α-synuclein assemblies [30, 55].

As previously mentioned, accumulating evidence suggests that it is not the insoluble aggregates but rather soluble oligomers that are the most neurotoxic species to neuronal cells. This theory was supported also for AS. Lashuel et al. studied the morphology of AS and its mutants oligomers [56]. In addition to previously reported spherical and chain-like oligomeric structures, electron microscopy images revealed novel annular, pore-like structures, whose morphology resembles membrane pores formed by protein toxins. The protofibrils were shown to permeabilize synthetic vesicles [56,57], while monomers and fibrils showed only minor or no channel-forming activity [14]. These observations led to the conclusion that there exists a relationship between formation of pore-like protofibrils, membrane permeabilization and the mechanism of neurotoxicity in PD and that increased levels of protofibrils or the selective population of particular protofibrillar morphologies may initiate early PD.
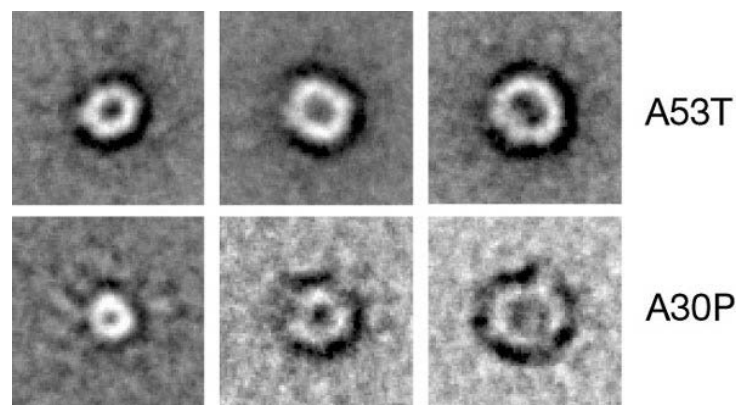
Figure 14: Annular protofibrils formed by the PD α-synuclein mutants A53T and A30P [57].

Beside the influence on fibrils morphology, AS mutants also influence the rate of aggregation. Conway et al. [58] reported that the cause of early onset PD might be an acceleration of fibril formation for the A53T and A30P mutations while idiopathic PD can be explained by the presence of other mechanisms (for example, increased expression or decreased degradation) that accelerate AS fibrillation. In the conditions tested, the A53T sample contained fibrils after two weeks, whereas no fibrillar material was detected in the wild-type (WT) or A30P samples after 3 weeks. In particular, A30P sample contained many spherical assemblies, that looked like prefibrillar intermediates of the the Aβ protofibrils. After 9 more weeks, fibrillar material was detected in both the WT and A30P incubation. Atomic force microscopy and electron microscopy analyses of each sample

(A53T, A30P and WT) showed that all the fibrils were similar to those found in Lewy bodies.
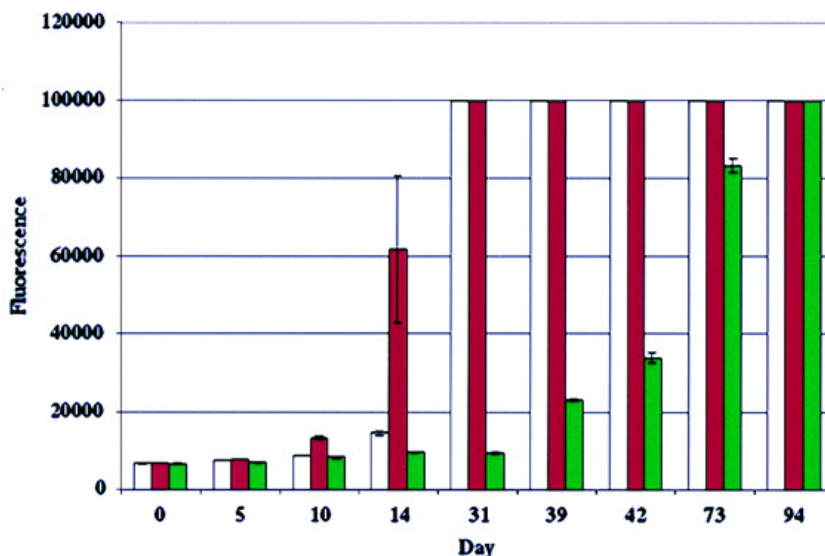

Figure 15: ThT fluorescence assay of A53T (red), wild-type AS (white) and A30P (green) [54].

The same research group [54] demonstrated that the common property of the two mutants protein is acceleration of oligomerization, rather than acceleration of fibrillation and that it is the critical step in the pathogenesis of PD. While the A53T mutant accelerates AS fibrillization, the A30P mutant shows a lag time longer than both wild-type and A53T synuclein, but the A30P monomer disappears with the same or slightly faster rate than the WT. For the E46K mutant it has been shown that it seems even more prone to aggregation than either A53T or A30P [20].

Covalent modifications of AS

Early stages of the AS aggregation process were analysed by dynamic force spectroscopy (DFS) and especially the very first step of this reaction was characterized: the formation of AS dimers [59]. The dimers formed by misfolded AS are enormously stable (about 10^6-10^9 times more than the original monomers) and the accumulation of dimers defines the lag phase for the AS aggregation process. This is in accordance with previous studies, demonstrating that the final aggregates of wild-type AS are resistant to denaturation, suggesting that AS deposits may contain covalently modified AS [60].

The presence of modified AS is further supported by several other studies. For example, it has been found that Lewy bodies also contain nitrated AS. In aqueous solution, AS is unfolded and exposure of the tyrosine residues may be favored. Tyrosine can be the target

for nitrating agents to form 3-nitrotyrosine and/or o,o'-dityrosine cross-links that stabilize short oligomers and/or elongated AS polymers. Later on, the same group demonstrated that dityrosine is not essential for fibrillogenesis even though it can begin the polymerization process [61].
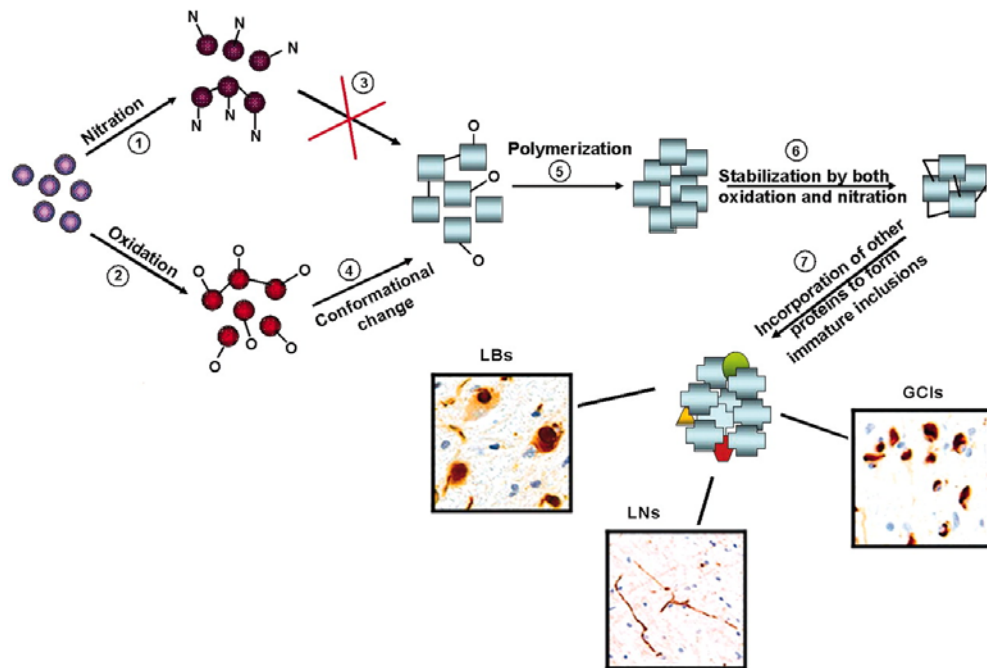

Figure 16: Proposed model for the role of nitration and oxidation in the formation of stable AS fibrils [61].

Another modification of wild-type α-synuclein found in *in vitro* studies is the extensive phosphorylation at Ser129 by a subset of protein kinases, that promotes formation of AS filaments as well as oligomers [62]. All these findings strongly suggest that every abnormality of α-synuclein would cause aggregation, eventually leading to neuronal cell death. On the contrary, Uversky et al. [63] reported that oxidation of the methionine residue in AS by H_2O_2 prevents fibril formation.

AS and oxidative stress

Oxigen-derived free radical damage have been considered to play a critical role during the process of neurodegeneration. The vulnerability could be due to the facts that: (i) neurons exibit a relatively low glutathione level, which limits their defense against oxidative stress; (ii) neurons also contain high levels of polyunsaturated fatty acids that may be susceptible to peroxidative damage; (iii) neurons in general exhibit higher oxygen consumption which would produce a large amount of ROS [64]. Protein modifications induced by ROS comprise carbonyl formation on amino acid residues such as arginine, lysine and proline;

reactions such as aldol or Schiff base condensation can then lead to the formation of cross-linked proteins. Specifically, divalent metal ions are considered as risk factors for PD [65]. Iron levels in the substantia nigra in PD and imbalance of the iron-ferritin ratio are responsible for the mechanism that leads to free-radical production. Fe^{3+} is a potent initiator of aggregation: it is a catalyst of the Fenton reaction that converts hydrogen peroxide into the toxic hydroxyl free radical [66]. Iron is the most abundant transistion metal in the body and is considered a possible major catalyst of oxidative reactions in PD. Iron can promote NAC self-aggregation, as observed by Hashimoto et al. [67], hence aberrant accumulation of ferric iron may be a risk factor in PD. Indeed, substantia nigra pars compacta of PD patients shows increased amount of ferric iron compared to controls. Fe^{3+} catalizes the oxidation of cathecols and then they can stabilize AS oligomers by covalent ligation leading to soluble oligomers [46]. Fe^{3+} can induce fibrillation of AS to form ThT-positive, SDS-sensitive, insoluble species. The influence of Cu^{2+} and compared to Fe^{3+} on AS self-oligomerization has been analysed. Both metals, Cu^{2+} and Fe^{3+}, induced SDS-resistant protein aggregates and for Cu^{2+} the formation of dityrosine cross-link has been observed in oligomers. Results obtained by Paik et al. [64] show that the metal effects on AS are dependent upon the C-terminus of the protein. This was confirmed by Binoldi et al. [65]: they demonstrated that the divalent metal ions Mn^{2+}, Cu^{2+} and Fe^{2+} bind preferentially to the C-terminal domain of AS in the native state, especially to the region between amino acids 110 and 140, that is also the binding site for polycationic polyamines. Their data proved conclusively that AS binds metal ions into the C-terminus with very low selectivity. On the other hand, they also showed that AS binds Cu^{2+} with high affinity ($K_d \approx 0.1$ μM) in the N-terminal domain, affecting the ^{1}MDVFMKGLS^9 and ^{48}VAHGV^{52} regions.

AS and dopamine

Dopamine (DA) is a neurotransmitter biosynthesized from tyrosine that is hydroxylated by tyrosine hydroxylase (TOH) to form dihydrophenylalanine (DOPA) [16]. DOPA is then decarboxylated by L-aromatic amino acid decarboxylase to give dopamine. Newly synthesized dopamine is stored in vesicles, from which it is released into the synaptic cleft by depolarization of the presynaptic neuron in the presence of Ca^{2+}. The dopamine released may stimulate postsynaptic D1- and D2-type autoreceptors that negatively modulate DA synthesis (through inhibition of TOH) and release. The action of DA is suppressed through reuptake into the presynaptic neuron by high-affinity DA neurotransport proteins located

on the nerve terminal membrane. Free cytoplasmic dopamine negatively modulates DA synthesis via feedback inhibition of tyrosine hydroxylase and it may undergo metabolic deamination by monoamine oxidase (MAO), an enzyme bound to the outer membrane of mitochondria, to form dihydroxyphenylacetaldehyde, that later oxidizes to give didydroxyphenylacetate (DOPAC). Eventually, DA or DOPAC may undergo methylation by catechol-O-methyltransferase (COMT) to give homovanillic acid (HVA), a metabolite excreted in urine.
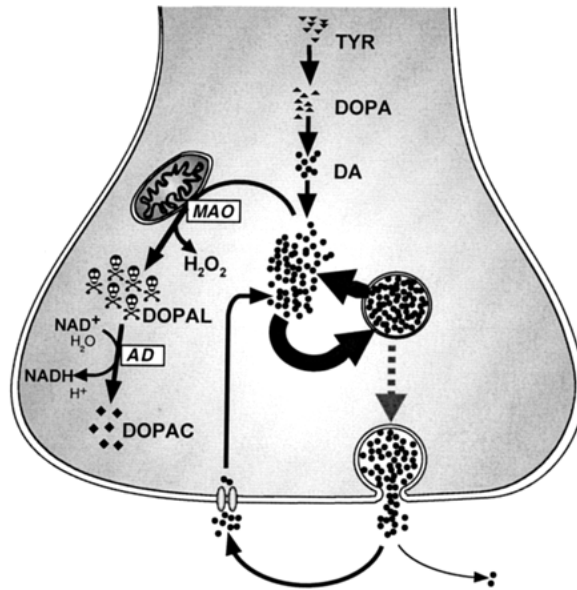

Figure 17: Biosynthesis and metabolism of dopamine [68].

A link between dopamine biology and AS has been hypothesized. It has been proposed that DA can induce, either through a direct covalent interaction or indirectly, changes in AS conformation that may influence the oligomerization state. Specifically, Outeiro et al. [57] demonstrated that DA or its oxidized derivatives can induce changes in AS structure, which adopts a conformation where its N- and C-termini become close together. These observations may explain why the increased vulnerability of dopamine neurons may be due to deficits in DA sequestration into synaptic vesicles with consequent undesired DA-AS interactions. The susceptibility of dopaminergic neurons to oxidative stress was further on highlighted with the discovery of the ability of 6-hydroxydopamine (6-OHDA) to destroy cells [70]. The toxicity of 6-OHDA may be related to its ability to produce free radicals and oxidative stress.

In both generic and sporadic forms of PD, a dopamine-dependent pathway for dopaminergic neuronal loss has been recognized, in which a defective sequestration of DA into synaptic vesicles leads to the generation of reactive oxidative species (ROS) in the cytoplasm and consequent cell death. Indeed cytoplasmic DA can quickly form ROS, but

DA sequestration protects neuronal cells from DA oxidation in normal conditions. Aggregated AS can indirectly trigger overproduction of DA and, in oxidative conditions, dopamine can autoxidize at normal pH into toxic dopamine-quinone (DQ) species, superoxide radicals and hydrogen peroxide [18,46]. DA-quinone can form covalent adducts with AS, probably through formation of dityrosine cross-links and/or through a nucleophilic attack via lysine side chain. The adducts stabilize AS oligomers and inhibit their conversion into fibrils, resulting in increased cellular damage. DA-quinone can also interact and alter the normal functional activity of a number of other proteins including tyrosine hydroxylase, DA transporter and parkin [66].

DA is able to dissociate preformed AS fibrils into soluble non ordered aggregates [46] while the incubation of DA with fresh AS over time resulted in a dose-dependent formation of SDS-resistant and soluble oligomers. Formation of soluble oligomers mediated by the interaction between AS and DA could lead to the accumulation of the putative toxic protofibrillar form of AS [20], even though AS, in presence of DA, displayed no significant increase in ThT fluorescence indicating that DA-mediated AS oligomers are not amyloidogenic. What is unknown is whether the DA-mediated AS oligomers constitute a toxic species. Prolonged incubation of AS in the presence of an equimolar concentration of DA resulted in AS fibril formation as observed by electron microscopy [66].
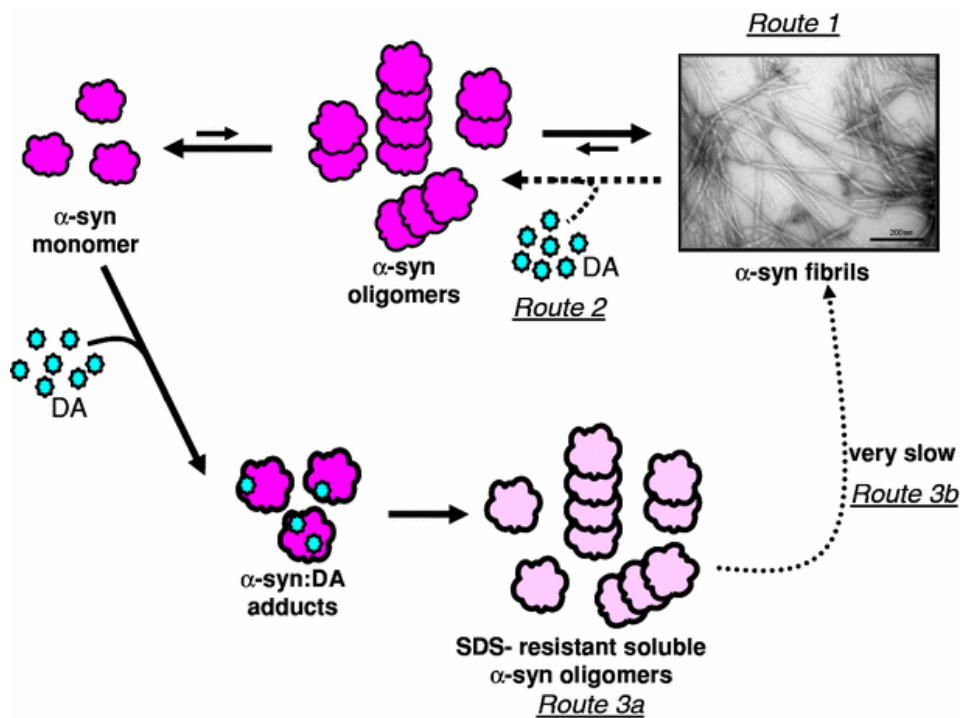
Figure 18: Model of AS aggregation pathways [66].

Galvin [20] focused on the effect of DOPAL, the immediate monoamine oxidase metabolite in DA catabolism.
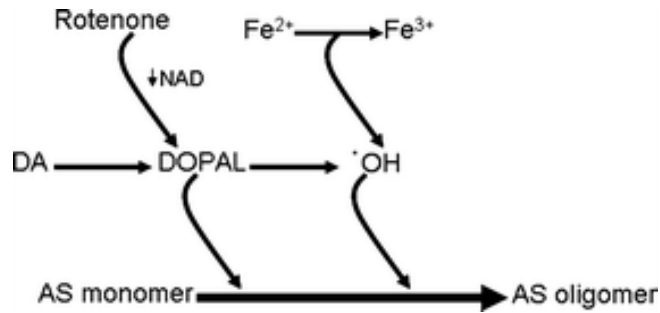

Figure 19:Pathways linking AS mutations, DA metabolism and environmental toxins in the selective vulnerability of nigral neurons in PD [20].

MAO metabolism of catecholamines is a two-step process, where 3,4-dihydroxyphenylacetaldehyde (DOPAL) is initially formed from DA. DOPAL is then converted to DOPAC by aldehyde dehydrogenase or to 3,4-dihydroxyphenylethanol (DOPET) by aldheyde reductase. A unique effect of DOPAL is the production, in the presence of H_2O_2, of toxic hydroxyl radicals that can trigger AS aggregation. Furthermore, dopaminochrome has been shown to inhibit fibril formation and to promote the oligomerization of AS [66].
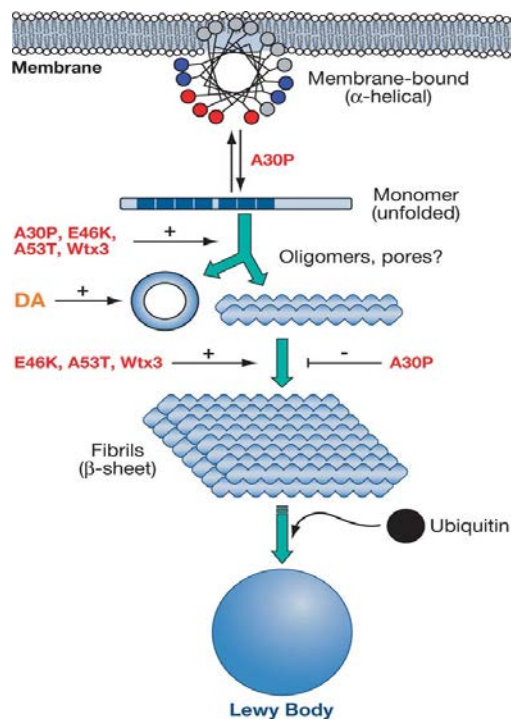
Figure 20: The pathogenic cascade of α-synuclein aggregation. Inside the cell, the monomer is in equilibrium with membrane-associated forms with higher helical content. In the helix, blue and red circles indicate charged residues, gray circles are nonpolar and hydrophobic amino acids. The A30P mutation disfavors membrane binding. All mutations indicated in the picture increase the rate of formation of oligomers or protofibrils, which may also produce pores. Oligomers and other intermediates are kinetically stabilized by dopamine (DA) but they are transient species that eventually aggregate to form mature fibrils. The formation of Lewy bodies is presumed to be a consequence of fibrillation. Events such as the attachment of ubiquitin (black dot) are thought to be secondary to the initial aggregation and deposition processes [25].

Therapy

It is now ascertained that AS deposition plays a central role in the pathogenesis of PD and other synucleinopathies. This suggests that therapeutic agents designed to inhibit or reverse AS aggregation and fibrillation may have potential disease-modifying effect and may be a feasible strategy for therapeutic intervention in PD and other related disorders [71,72]. One approach is based on the observation that some small molecules such as Congo Red (CR) and derivatives, curcumin and quinacrine, have the ability to prevent the misfolding and aggregation of proteins involved in PMDs. Another approach is based on β-sheet breakers, short peptides containing a self-recognition motif (usually the region of the protein responsible for protein-protein interactions and early stage of misfolding) and a β-sheet disrupting element in their amino acid sequence. Several attempts for immunization against PMDs have been tried based on the belief that immunization using sequence specific peptides can decrease the clinical features of PMDs. Another strategy is the use of antibodies that target specific misfolded aggregates of amyloidogenic proteins: the enormous advantage of this approach is that only the structure responsible for the toxicity is hit [12]. An alternative approach is the intervention on those systems that oppose the abnormal accumulation of misfolded protein, i.e. the normal proteolytic pathways, the ubiquitin proteasome system, and the autophagic system [72].

Curcumin and derivatives

Natural plants have been used throughout human history for various purposes and medicines derived from plants have played a crucial role in the health care of many cultures [73].

Curcumin, is an active principles contained in the root of the plant *Curcuma longa* (or Turmeric). Turmeric is a member of the Curcuma botanical group, which is part of the ginger family of herbs, the Zingiberacee, and is cultivated extensively in south and south-east tropical Asia [74]. It was first isolated in 1815 and its structure was delineated in 1920 as diferuloylmethane or 1,6-heptadiene-3,5-dione-1,7-bis(4-hydroxy-3-methoxyphenyl)-(1E,6E) with a molecular weight of 368.37. It is estimated that 1-2% of turmeric is curcumin [75]. Curcumin is a yellow-orange powder, insoluble in water and ether but soluble in ethanol, dimethylsulfoxide, acetone and oils [73]. Commercially available curcumin also contains ≈17% and 3% demethoxycurcumin (DMC) and bisdemethoxycurcumin (BDMC), respectively [76].

A β-dichetone moiety connects symmetrically the two aryl rings having ortho-methoxy phenolic OH groups. The β-dichetone functionality is also responsible for the intramolecular hydrogen atom transfer leading to the keto and enol tautomeric configurations [77].

There are two kinds of acidic hydrogens in curcumin. One is a phenolic hydrogen, the other is the methylene hydrogen of the β-diketone. Widely varying pKa values have been reported for curcumin depending on the solvent used and the method of estimation. Taking all the studies together, an average pKa value of 8.38 is estimated for the loss of enolic proton from curcumin and a pKa of approximately 10-10.5 for the two phenolic protons [78]. At the physiological pH of 7.4, nearly 10-25% of curcumin is in the monoanionic form and the remaining in the neutral form [77].
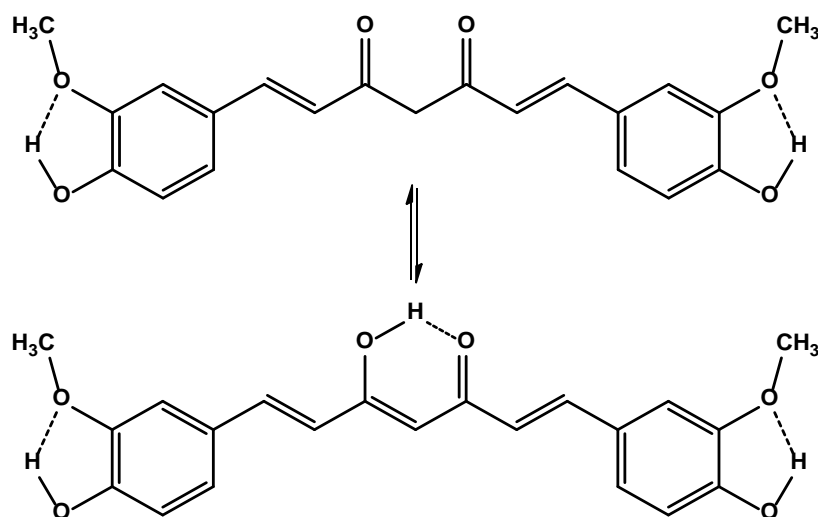
Figure 21: Chemical structure of curcumin in keto-enol tautomeric equilibrium.

The excited state photophysical properties of curcumin are greatly influence by the solvent.
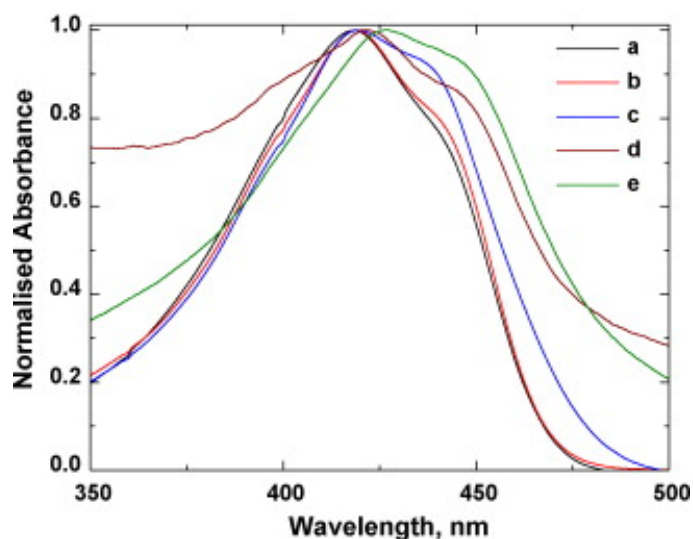
Figure 22: Normalized absorption spectra of curcumin in: (a) chloroform, (b) acetone, (c) methanol, (d) PC liposomes and (e) HSA [77].

31

Curcumin exhibits a strong absorption in the UV-vis region with an absorption maximum in the range from 408 to 434 nm, depending on the solvent.

The extinction coefficient of curcumin varies from 20000 to about 50000 $M^{-1}cm^{-1}$ [77,79]. The nature of the solvent affects the absorption spectrum of curcumin, producing a red shift on going from *n*-hexane to methanol, which indicates that the excited singlet state must be very polar [80]. The strong absorption band at about 410-430 nm has been assigned to the π-π* transition of the conjugated system of the curcumin structure. The fluorescence spectrum, fluorescence maximum and the fluorescence quantum yield of curcumin have been found to be very sensitive to the nature of the solvent, with a strong red-shift in protic solvents such as ethanol. The Stokes' shift depends on the nature of the solvent and varies significantly from 2000 to 6000 cm^{-1} (≈ 30-140 nm) [77, 81]. The fluorescence spectra exhibit no wavelength dependence, i.e. the spectra recorded at different excitation wavelengths were identical with the fluorescence spectrum obtained by excitation at the absorption maximum of curcumin. This is indicative of the existence of only one fluorescent species, that is the conjugated system existing in the enolic configuration [80,81].
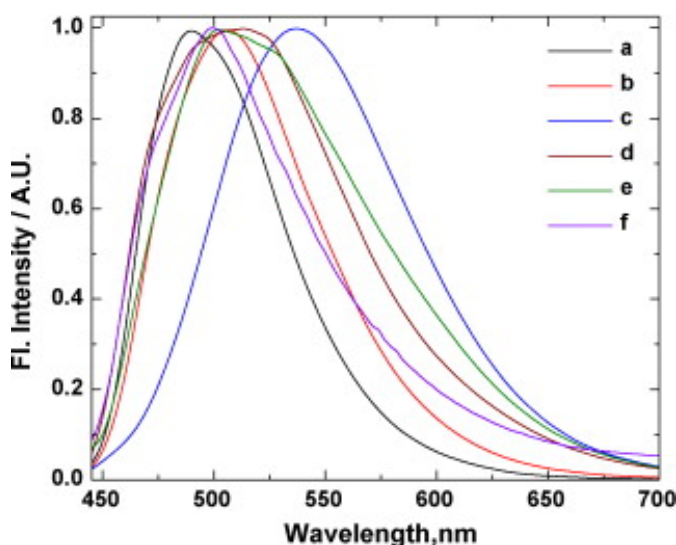

Figure 23: Normalized fluorescence spectra of curcumin in (a) chloroform, (b) acetone, (c) methanol, (d) PC liposomes and (e)EL4 cell line, (f) EL4 cell line [77].

The phosphorescence spectrum of curcumin is weak and its intensity is dependent on the excitation wavelength, probably due to multiple phosphorescence emission from different keto-enol tautomeric triplet excited states. Polarity, π-bonding nature, hydrogen bond donating properties of the solvent influence the excited state photophysics of curcumin [77].

Traditionally, turmeric is widely used in the India subcontinent in different areas, from health care to the preservation of food and coloring of textiles [75]. In Ayurvedic medicine, it is used for various respiratory conditions as well as for liver disorders, anorexia, rheumatism, diabetic wounds, cough and sinusitis. In traditional Chinese, medicine the primary application is for diseases associated with abdominal pain while in ancient Hindu medicine it is a treatment for sprains and swelling. In general, throughout the Orient, it has traditionally been used as an anti-inflammatory remedy. Many effects of curcumin have been confirmed by modern scientific research, including antioxidant, anti-inflammatory, anticarcinogenic and antimicrobial, hepatoprotective, thrombosuppressive, cardiovascular, hypoglycemic and antiarthritic. Furthermore, curcumin possesses antirheumatic activity and has a potential palliative therapy for cancerous skin lesions. It can lower serum cholesterol and lipid peroxide levels in healthy individuals, it beneficially affects psoriasis, it may improve cognitive function in the elderly [73-76,78]. It has been used in digestive disorders and against bacterial infections [74]. Preclinical studies on curcumin demonstrated that it is a potent chemopreventive agent, exhibits antitumor activity in animals and inhibits proliferation of tumor cells in vitro [73]. Curcumin has been shown to be a more potent antioxidant than even vitamin E [76].

To date, studies in either animals or human have discovered no toxicity associated with the use of curcumin, even at high doses [73]. Three different Phase I clinical trials performed to determine the safety of curcumin have indicated that doses as high as 15 g/day orally for 3 months is safe. No dose limiting toxicity was reported [76].

Curcumin's molecular target were discovered within the last three decades and the effect of curcumin on most of these targets has been analyzed. The results have shown that curcumin can modulate several transcription factors, cytokines, growth factors, kinases, and other enzymes [73,75].

Among all the therapeutic effects proposed, curcumin is also effective in Alzheimer's disease [76] as demonstrated by its ability to bind β-amyloids and thereby reducing plaque burdens [73]. Interest on curcumin comes from the observation that there is a decreased prevalence of AD and PD in India, where approximately 200 mg of dietary curcumin is ingested daily [82]. It has also been proposed that the anti-Alzheimer's effect of curcumin could be due to its antioxidant properties, since oxidative stress is considered a significant factor associated with the decline of function in the aging brain. Polyphenols such as curcumin, resveratrol and epigallocatechin are becoming recognized for their protective effect against inflammatory diseases, cancer, cardiovascular and neurodegenerative

diseases thanks to increasing studies that support their antioxidative, anti-inflammatory, antiapoptotic and metal chelating properties [83]. Curcumin has been shown to bind certain divalent metal ions such as Fe, Cu, Mn and Zn, with high affinity for Fe and Cu.

Chronic dietary curcumin has been shown to lower Aβ deposition in 16-month-old transgenic mice. Curcumin is highly hydrophobic and should readily cross the blood-brain barrier (BBB) and bind to plaques *in vivo*. Yang et al. [84] showed that curcumin inhibits Aβ aggregate formation in a dose-dependent manner and prevents formation of oligomers at low micromolar or even submicromolar concentrations. Shoval et al. [85] studied the effect of several polyphenols such as curcumin and epigallocatechin. From TEM images, they observed that polyphenols induced dissociation of amyloid fibrils and that this effect depends on the dose of the compound. As mentioned earlier, oligomerization kinetics and mechanism of amyloid formation are similar in Parkinson's and Alzheimer's disease, hence Pandey et al. [82] investigated the effect of curcumin on AS aggregation. Their results demonstrated that curcumin increases AS solubility and prevents the formation of high molecular weight AS aggregates in a dose-dependent manner. Beside reducing Aβ and AS aggregate, curcumin also inhibits the accumulation of protease-resistant prion-protein, suggesting that curcumin acts as a general amyloid breaker rather than being specific to one PMDs.
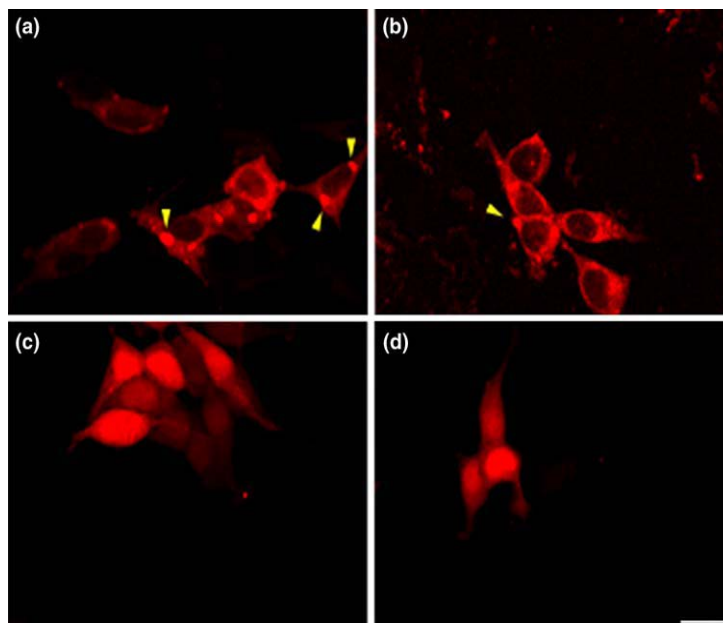

Figure 24: Panel (a) demonstrates aggregation of A53T_AS_DsRed2 fusion protein. Panel (b) demonstrates reduction in aggregation of A53T_AS_DsRed2 fusion protein upon treatment of 5Y cells with 5 M curcumin. Panels (c) and (d) demonstrate hardly any aggregation in DsRed2-expressing 5Y cells (c), which is unchanged upon treatment with 5 M curcumin (d) [82].

Masuda et al. [86] have investigated the effect of 79 compounds belonging to 12 different chemical classes, including curcumin, on AS filament formation compared to Aβ and tau

assembly. The analysis revealed the presence of dimeric and oligomeric AS in the presence of the inhibitory compound. These are SDS-resistant soluble oligomers, instead of oligomers formed in absence of the inhibitor that are SDS-sensitive.
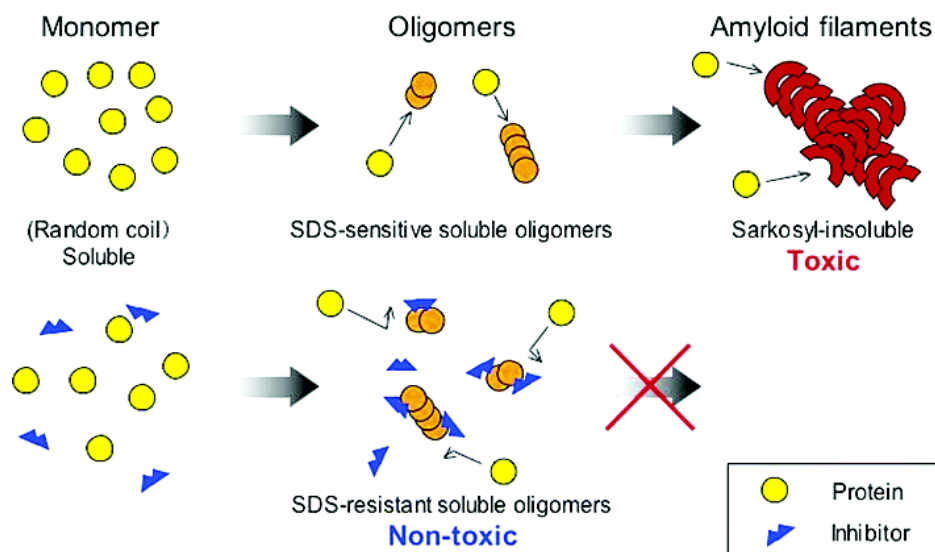

Figure 25: Model for the inhibition of amyloid filament formation by small compounds [86].

The compounds investigated in this study may inhibit filament formation of AS by stabilizing soluble, prefibrillar intermediates. The toxicity of soluble oligomers was investigated in SH-SY5Y cells and compared with that of monomeric AS, protofibrils and filaments. Monomer and soluble oligomers did not reduce cell viability. By contrast, protofibrils and filaments were markedly cytotoxic. These results indicate that the compound investigated inhibit not only filament formation but also the toxicity of α-synuclein and may have therapeutic potential.

Similar results were obtained by Ono et al. [87]: curcumin could destabilize AS fibrils and inhibit the formation of aggregates.
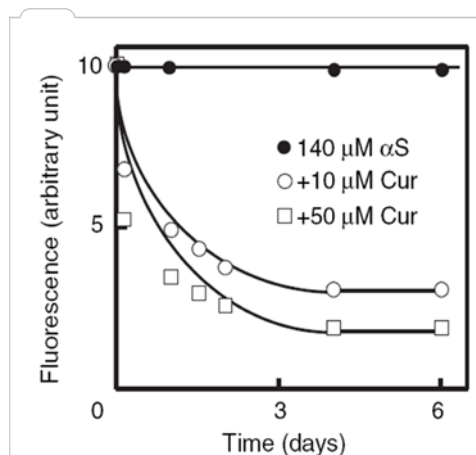

Figure 26: Effect of curcumin on the kinetics of destabilization of α-synuclein fibrils (fαS). The reaction mixtures containing 140 μM fαS, 20 mM Tris buffer, pH 7.5, 100 mM NaCl and 0, 10 or 50 μM curcumin were incubated at 37°C for the indicated times [87].
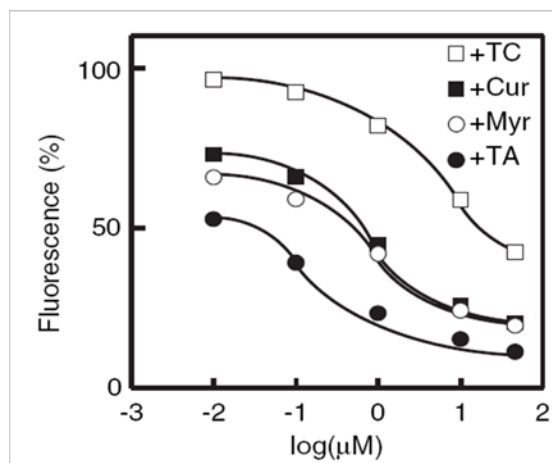
Figure 27: Dose-dependent destabilization of α-synuclein fibrils (fαS). The reaction mixtures containing 70 µM αS, 20 mM Tris buffer, pH 7.5, 100 mM NaCl, and 0.01, 0.1, 1, 10 or 50 µM TA (tannic acid), Myr, (myricetin) Cur (curcumin) or TC (tetracycline) were incubated at 37 °C for 6 hours [87].

A structure-activity relationship has been proposed for amyloid disaggregators based on curcumin's structure [88]. The influence of the linker region, the two aromatic groups and the substitutions on the aromatics has been evaluated. The features important for the activity are: (i) aromatic substitutions capable of taking part in hydrogen bonding; (ii) a linker length between 6/8Å and 16/19 Å, and (iii) inclusion of 2-3 freely rotatable carbons centers is not well tolerated; (iv) compounds lacking a second terminal aromatic group are less active at inhibiting amyloid formation, thus, the second phenyl group is important for activity.
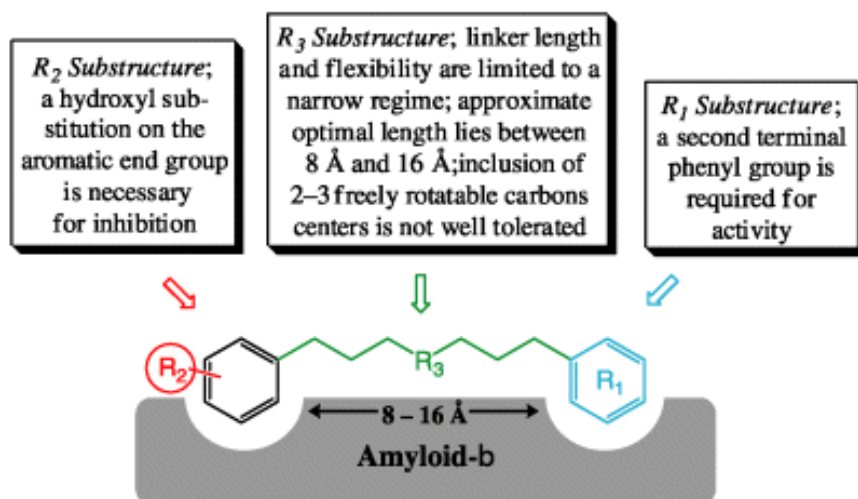

Figure 28: Schematic depiction of the three regions (R1, R2, and R3) that were identified and the approximate features that describe potent ligands [88].

Research has demonstrated that antioxidants and metal chelators may be of beneficial use in the treatment of neurodegenerative disorders. As curcumin has antioxidant activity, its effect on PMDs may also be due to this property. Dairam et al. [89] showed that curcumin potently scavenges the DPPH free radicals and superoxide anion, and possesses Fe^{2+} ion

chelating activity. The metal binding is mediated through the β-diketone group of curcumin [76] and the phenolic OH groups [81].
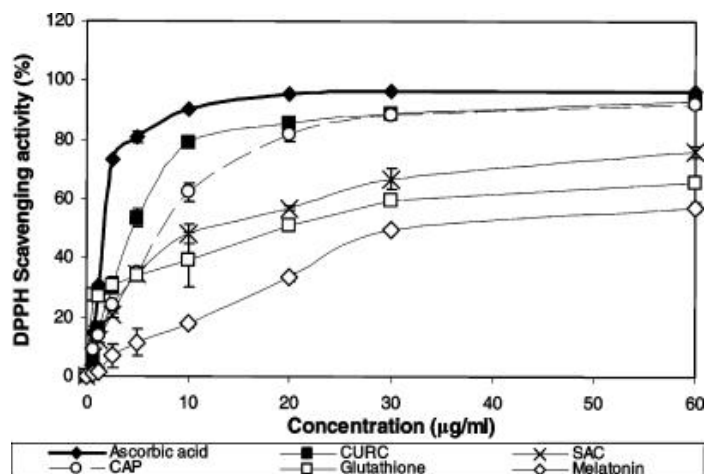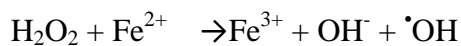

Figure 29: DPPH scavenging activity of curcumin (CURC), capsaicin (CAP), S-allylcysteine (SAC), ascorbic acid, glutathione and melatonin. Each point represents the mean ± standard deviation of five separate determinations [89].

Transition metals such as iron and copper can react with hydrogen peroxide, which is a product formed by the dismutation of the superoxide anion by superoxide dismutase to produce the highly reactive hydroxyl radical. This reaction is known as the Fenton reaction:

$$H_2O_2 + Fe^{2+} \rightarrow Fe^{3+} + OH^- + {}^{\bullet}OH$$

The Fe^{2+} ion chelating activity diminishes the available Fe^{2+} that reduces H_2O_2 to the potent hydroxyl radical.

It has been suggested that the methoxy group on the phenol ring as well as the β-diketone moiety are the important functional groups responsible for the potent antioxidant and free radical scavenging properties.
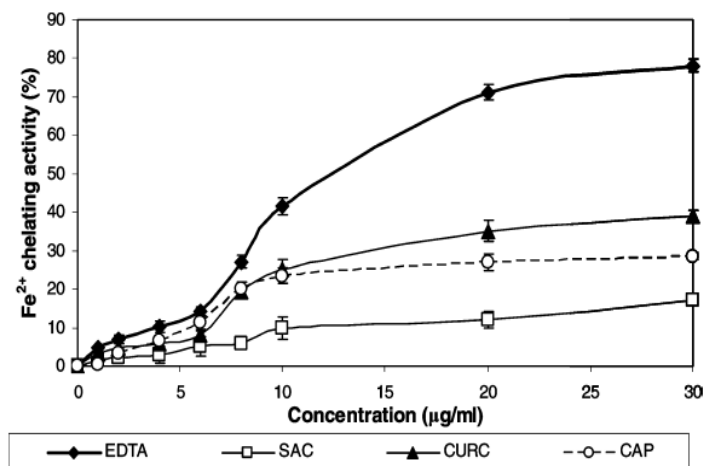

Figure 30: Fe2+ ion chelating activity of curcumin (CURC), capsaicin (CAP), S-allylcysteine (SAC) and EDTA. Each point represents the mean ± standard deviation of five separate determinations [89].

Antioxidant activity has been proved also for demethoxycurcumin and bisdemethoxycurcumin, the other two active compounds found in turmeric root [90]. An event that significantly contributes to the oxidative load in dopaminergic neurons is glutathione depletion. Curcumin and bioconjugates of curcumin restore the cellular GSH pool, thus protecting against oxidative stress. Curcumin treatment also leads to significant protection against protein oxidation and preservation of mitochondrial complex I activity lost because of GSH depletion [91,92]. On the other hand, it is worth noting that curcumin may also produce pro-oxidative effects, depending on conditions; therefore, more studies are needed to understand the different modes of action of curcumin [78,83].

One of the most important limitations with curcumin is its bioavailability. Studies have shown that when administered orally, curcumin is poorly bioavailable. Either no curcumin at all was found or only low levels of curcumin metabolites were detected in the serum or in the tissue. Curcumin seems to be metabolized through conjugation and reduction [76]. When administered orally, curcumin is metabolized into curcumin glucuronide and curcumin sulfonate. However, when administered systematically or intraperitoneally, it is metabolized to tetrahydrocurcumin, hexahydrocurcumin and hexahydrocurcuminol [75]. The low bioavailability of curcumin is due to the hydrophobic nature of the molecule. Numerous approaches have been undertaken to enhance the bioavailability, which involve: (i) the use of adjuvants such as piperine that interfere with glucuronidation, (ii) the use of liposomal curcumin, (iii) the use of curcumin nanoparticles, (iv) the use of curcumin phospholipid complexes and (v) the use of structural analogs of curcumin [76].

The potential use of curcumin as coloring agent, a pharmaceutical prescription, or a drug is closely related to the stability of the compound. Its color is not constant in aqueous media or in an organic solvent because of its degradation or conversion to its dissociated form. pH also influences the color of curcumin/turmeric, that turns from yellow to deep red when exposed to acidic conditions [75,80]. Curcumin alone undergoes loss of absorbance at 420 nm in phosphate buffer, indicating that it is unstable at physiological conditions in vitro. The degradation follows an apparent first-order kinetics at 37 °C and constant ionic strength.

Vanillin, vanillic acid, ferulic aldehyde and ferulic acid have been identified as the degradation products. At short-time reaction, trans-6-(4'-hydroxy-3'-methoxyphenyl)-2,4-dioxo-5-hexenal has been identified as the major degradation product, while vanillin becomes the major degradation product as the incubation time increases. The stability of

curcumin can be improved by lowering the pH. Furthermore, curcumin is sensitive to light, and the combined effect of air and light is the most deleterious [93,94].
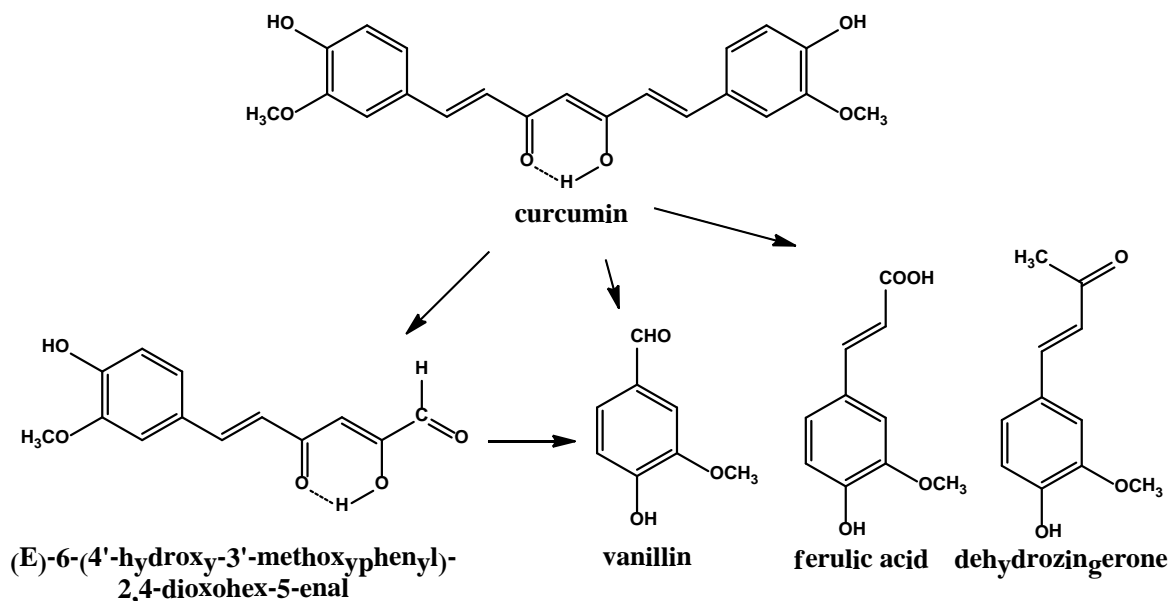

Figure 31: Curcumin and its degradation products [93].

Leung and Kee [95] showed that plasma proteins such as human serum albumin (HSA), fibrinogen and transthyretin suppress the degradation of curcumin as shown by the high fluorescence yields of curcumin in presence of HSA, fibrinogen and transthyretin. This implies that curcumin is segregated from the aqueous solvent due to strong binding to these proteins.

Ferulic acid, one of the degradation productS of curcumin, haS been reported to have antioxidant activity that may be of interest in the therapy of AD, PD and other neurodegenerative diseases. Ferulic acid dose-dependently inhibits formation of Aβ fibrils from fresh Aβ, and it destabilizes preformed Aβ fibrils *in vitro* [96]. Thus, it may be reasonable to speculate that ferulic acid could prevent the development of AD not only through scavenging reactive oxygen species, but also through direct inhibition of Aβ fibrils deposition in the brain. A natural extract from ginger (*Zingiber officinale*) that matches another degradation product of curcumin, is dehydrozingerone (DHZ) or feruloylmethane and, like ferulic acid, it exhibits antioxidant activity. Studies on DHZ and its derivatives demonstrated that the antioxidant activity is enhanced by the presence of the hydroxyl substituent on the phenyl nucleus. The dihydroxyl substitution at 2' and 3' of the phenyl group is particularly important for the radical scavenging activity and the double bond at the C-3 and C-4 position would be essential for antioxidant activity [97,98]. Zingerone, another active extract from ginger roots, has shown antioxidant activity through scavenging superoxide anion and inhibiting neurotoxicity induced by 6-OHDA [99], an

endogenous neurotoxin found in urine of PD patients. Vanillin is also a powerful scavenger of superoxide and hydroxyl radicals and it inhibits iron-dependent lipid peroxidation in rat brain homogenates, microsomes and mitochondria [93].

β-sheet breakers

The understanding of fibril sequence and structure has allowed the design and synthesis of peptide-based inhibitors of fibrillogenesis through a rational approach. The development of these types of inhibitors may represent a potential therapeutic goal in PMDs treatment [100]. The term "β-sheet breakers" (BSBs) refers to compounds (mostly peptides and peptide mimetics) rationally designed to break β-sheet structure. Since fibrillogenesis is a process of self-association, it is noticeable to affirm that inhibitors should be homologous to the presumed site of self-association [100]. Protein misfolding and aggregation requires two properties for the self recognition polypeptide fragments: a high hydrophobicity and a large propensity to adopt a β-sheet conformation. The hydrophobicity appears to be important for triggering monomer interactions leading to aggregation, while the β-sheet conformation might determine ordering of the aggregates into amyloid fibrils. Soto and Estrada [101] suggested to separate these two properties in short synthetic peptides homologous to the targeted peptide/protein, bearing a similar degree of hydrophobicity but a very low propensity to adopt a β-sheet conformation. β-sheet breaker peptides probably inhibit amyloid formation by binding to monomeric/dimeric peptides, thereby blocking the formation of oligomeric β-sheet precursors of the fibrils [102].

Their mechanism for inhibition of aggregation may be the formation of β-strands that would compete for association with the homologous sequence in the targeted peptide. The β-strand must be at least four amino acid residue in length and better if it is at least as long as the segment of the targeted sequence [103]. β-Breakers peptides that combine a sequence similarity to the region of the protein responsible for fibril formation with the ability to block the pathologic conformational changes may be the therapeutic compounds directed specifically to each of these diseases [102].

The β-sheet breakers group comprise: unmodified peptides and peptides with modifications to their side chains and termini, peptidic polymers with changes of the main chain backbone, and peptidomimetics. There are several pros and cons. Among the advantages, we find the possibility of a rational design of the peptide inhibitor and specificity toward a specific target [100]. A major drawback with the *in vivo* use of peptides is that they are degraded by natural enzymes and have poor blood-brain-barrier (BBB) permeability [102].

An efficient inhibitor should have affinity for the fibril-forming protein or peptide and should also be water-soluble, resistant to proteases and not form fibrils itself.
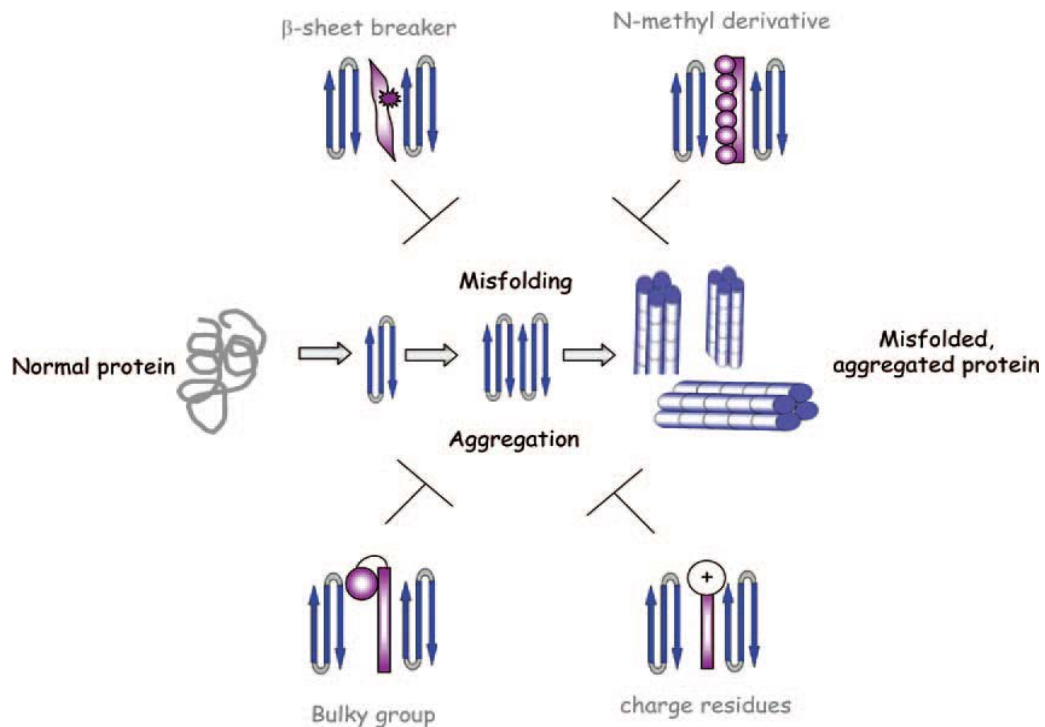

Figure 32: Strategies to inhibit protein misfolding and aggregation by small rationally-designed peptides. As disrupting elements, different groups have used distinct strategies, including: the use of a bulky group that sterically inhibits protein aggregation; N-methylations (or N-alkylations) to generate peptides having a blocking face; β-sheet breaker amino acids to disrupt β-sheet conformation; and addition of charged residues to reduce the hydrophobic interactions which trigger protein aggregation [101].

Strategies for the design of fibrillogenesis inhibitors are:

❖ Side chain modification. Modification of the side chain can decrease the susceptibility of inhibitor peptides to proteases.

❖ Proline substitution and addition. Their rigid structure restrains the φ and ψ angles outside of the β-sheet range and they also lack the amide proton needed for the hydrogen bonding found in β-sheet.

❖ Modification of the peptide termini. The addition of a short sequence of a group (peptide and non peptide) to the termini, that is intended to disrupt propagation of the fibril. The disrupting element can disrupt aggregation in several ways: first, by steric effects; second, by increasing the solubility of prefibrillar aggregates thanks to the addition of highly polar or charged groups; finally, by increasing their stability against proteases.

❖ Modification of peptide backbone atoms. This includes:
  ➢ N-methylation: the methyl group replace the amide proton that stabilize β-sheets through hydrogen bonding interactions between individual β-strands. In addition, the methyl group is larger than the amide proton and could thus prevent interactions

between peptide chains by steric hindrance. Thus, peptides containing N-methyl amino acids are torsionally constrained to adopt the β-strand conformation. Furthermore, N-methylated peptides tend to have increased solubility (by preventing self-aggregation), increased resistance to proteolytic degradation and increased blood-brain barrier penetration.

➢ Peptoids: these are polymers of N-substituted glycines. They lack backbone hydrogen bond donors but adopt a polyproline type I helical structure.

➢ Ester bonds: in this case, amides are replaced by ester bonds, because esters lack the potential hydrogen bond donor present in amides, but share many structural similarities with amides.

➢ Modification at the α-carbon: this modification cannot interfere with hydrogen bonding, but peptides containing such modifications could, through steric effects or restrictions of conformational freedom, disrupt fibril propagation.

❖ Peptide cyclization. In general, cyclization of peptides increases their stability, but in the case of amyloidogenic peptides, the stabilized form may be fibrillogenic. The introduction of a lactam between the ith and i+4th residues strongly favors the α-helical conformation, rendering the cycle more effective at disrupting β-sheets.

❖ Use of D-amino acids. D-amino acids are used to inhibit proteolysis [100,104].

Some of the first fibrillogenesis inhibitory peptides targeting β-amyloid aggregation were based on the amyloidogenic sequence within the Aβ.

Soto et al. [102] used the central hydrophobic region in the N-terminal domain of Aβ, aminoacids 17-20 (LVFF), as a template to design the β-sheet breaker peptide iAβ5 (**LPFFD**). The iAβ5 peptide was shown to inhibit amyloid formation by Aβ1-40 and Aβ1-42 *in vitro* in a dose-dependent manner; it prevents amyloid neurotoxicity in cell culture, it reduces *in vivo* cerebral Aβ deposition and completely blocks amyloid fibril formation in rat brain. The iAβ5 peptide contains a proline residue to decrease its propensity to adopt a β-sheet structure, and a charged residue was added at the end of the peptide to increase solubility. The iAβ5 peptide was then protected against degradation by proteases with the N-terminal acetylation and C-terminal amidation, yielding iAβ5p (Ac-LPFFD-NH$_2$) [101]. Moreover, iAβ5p is able to cross the BBB at a rate higher than most proteins and peptides known to be selectively taken up by the brain [105].

Laczkó et al. [106] synthesized an analog of Soto's pentapeptide, in which Phe3 is replaced by the more hydrophilic Tyr. Their aim was to establish whether LPYFD-NH$_2$ was a more efficient inhibitor of fibrillogenesis or a better disrupting element for preformed Aβ(1-42)

compared to LPFFD-OH. From analyses of conformational changes during the aggregation and fibril formation of Aβ(1-42) alone or in the presence of BSBs it was demonstrated that the time-dependent cross β-sheet structure of Aβ(1-42) was not prevented by LPFFD-OH, whereas LPYFD-NH2 exerted some inhibitory effect.

Starting from the KLVFF sequence, several N-methylated peptides have been synthesized, and analyzed, their inhibitory activity towards fibrillation compared, and their effect on the Aβ cell toxicity evaluated. Much effort has been devoted to suppress the oligomer formation of Aβ. In contrast to this inhibition strategy, acceleration of the fibrillogenesis of Aβ has also been shown to reduce toxicity. If the formation of mature fibrils is really a protective mechanism, the toxicity of Aβ might be reduced by conversion of toxic oligomers into the final mature aggregated forms [107]. Oligolysine and oligoglutamic acid units were incorporated within the KLVFF peptide with the aim to obtain binders to Aβ that would lead to the formation of large aggregates with less cell toxicity. The oligolysines as disrupting elements for Aβ toxicity were effective when the length was three or more residues [107]. This behavior suggests that the new fibrils are not toxic or that they are no longer in equilibrium with the toxic oligomeric intermediates; the ability of these peptides to accelerate fibril formation while decreasing toxicity may represent a new interesting approach. However, a different result was reported with a variant of the Aβ core domain (KLVFF) containing a polycationic disrupting region appended to the C-terminus, KVLFFKKKKKK. An enhancement in the rate of fibril formation was found, and the rate increased with the number of lysine residues, but the association did not reduce cell toxicity of Aβ as determined using the monitoring reagent for the cell viability MTT (3-(4,5-dimethylthiazol-2-yl)-2,5-diphenyltetrazolium bromide) [104,107].

Aib, (α-aminoisobutyric acid), a Cα-tetrasubstituted α-amino acid, was proposed as a β-sheet disrupting element because of its propensity to adopt a $3_{10}/α$-helical conformation [108]. It was demonstrated that a single substitution with Aib, (but the same could be affirmed for any Cα-tetrasubstituted α-amino acids) completely disrupts the β-sheet structure of a pentapeptide related to the sequence 17-21 of Aβ.

The protein αA-crystallin possesses about 70% homology to αB-crystallin, a member of the small heat shock family of proteins that was found in brains of AD patients, and it has been demonstrated that it is able to inhibit amyloid fibrillation and toxicity. Using mini-αA-crystallin, Santhoshkumar and Sharma [109] demonstrated the importance of the chaperone region (sequence 70–88) of αA-crystallin in the prevention of Aβ aggregation. Interestingly, the N-terminal sequence of mini-αA, K(D)FVIF, is very similar to the highly

amyloidogenic domain (KLVFF) of Aβ(1–40). The best anti-fibrillogenic activity against Aβ fibrillation seems to be achieved with compounds containing residues Lys, Leu, Val and Phe and, incidentally, the chaperone sequence of αA-crystallin has all of these critical residues required to bind Aβ. Thus, the authors proposed that this sequence in mini-αA as well as αA-crystallin may compete with the binding domain in Aβ(1–40) and prevent its polymerization.

In AS, the 61-95 hydrophobic NAC region is considered responsible for aggregation, with the N-terminal part of NAC mostly responsible for amyloid formation. An N-methylated derivative of the AS fragment 67-78, where Gly73 was replaced with sarcosine, was shown to prevent fibril formation and reduced toxicity markedly [101].

El-Agnaf et al [110] chose the hydrophobic residues 68–72 of AS (GAVVT). They designed several peptides, referred to as α-synuclein inhibitors (ASI), where they maintained the original sequence GAVVT and varied the length or the amino acid substitution through the introduction of hydrophilic arginine residues or glycines at the N- and/or the C-terminus.

Table 1: Primary structure of the native sequence AS (68-75) and ASI peptides synthesized by El-Agnaf et al. [110].

Name	Structure	M.W.
NAC(8-18)	**GAVVTGVT** α-syn(68-75)	702
ASI1	**RGGAVVTGR**-*NH₂*	871
ASI2	**GGAVVTGR**-*NH₂*	715
ASI3	**RGAVVTGR**-*NH₂*	814
ASI4	**RGAVVGR**-*NH₂*	713
ASI5	**RGVVTGR**-*NH₂*	743
ASI1D	**RGGAVVTGRRRRRR**-*NH₂*	1652
NTC1	**RGKGLSKGR**-*NH₂* α-syn(6-10)	957
NTC2	**RGGVVAAGR**-*NH₂* α-syn(14-18)	841
NTC3	**RGKTKEGGR**-*NH₂* α-syn(21-25; 32-36; 43-47; 58-62; 80-84)	987

Experimental data showed that some of these ASI peptides could inhibit formation of early and late AS aggregates, and the peptide RGAVVTGR-amide was the shortest that retained the ability to inhibit synuclein aggregation. Concerning the problems associated with the transport through the blood-brain barrier, they have shown that ASI peptide fused to an arginine rich carrier (ASI1D) can enter neuronal cells transfected with synuclein A53T and inhibit DNA damage induced by Fe(II). Related peptides without this delivery system did not reverse levels of Fe(II)-induced DNA damage [111].
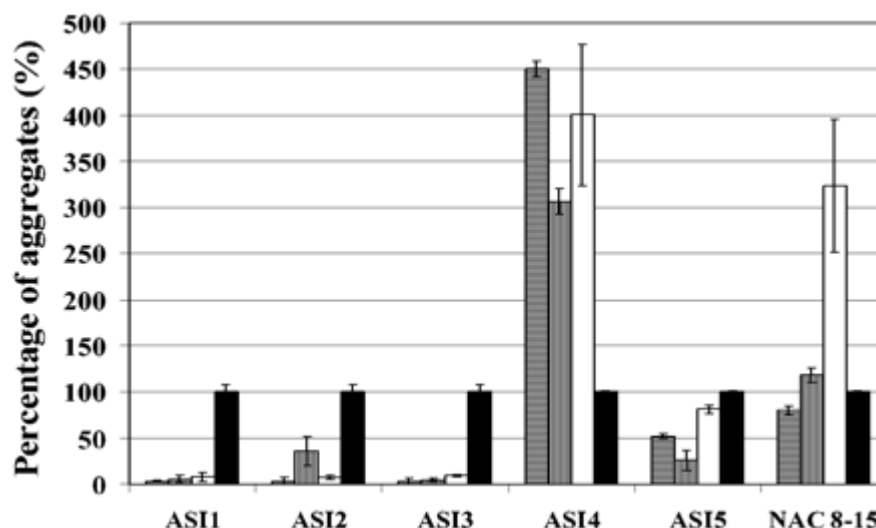
Figure 33: Effect of ASI peptides on AS fibrillogenesis. Data are representative of at least three independent experiments. Assays were performed in triplicate, and mean ± standard deviation are shown [110].

Madine et al. [112] considered the region corresponding to residues 71-82 of full length AS and developed different N-methylated peptide inhibitors. Using solid state NMR, they identified the peptide VAQKTmV as effective in preventing the aggregation of AS to form large insoluble fibrillar species.

Another strategy for β-sheet breaker therapy comes from the observation that β-synuclein is able to counteract abnormal AD aggregation in a dose-dependent manner. Small molecules based on β-synuclein sequence were developed and in particular the sequence 1-15 seems most important for antiaggregatory potential. Indeed, β-synuclein derivatives that lack this region are not able to prevent AS aggregation. Furthermore, the biological activity of β-synuclein is not restricted to interaction with AS, since β-synuclein protects against oxidative stress (i.e. it exerts protective effects after chronic $FeCl_2$ exposure) [113].

Much more effort is required in the design of β-sheet breakers to improve their ability to inhibit amyloid deposition and their pharmacokinetic characteristics. On the other hand, this strategy might help in understanding the biochemical mechanism involved in PMDs and, since current medicine is still based on palliative drugs, it might represent a new disease-modifying therapy.

Aim of the project

The present project focuses the attention on the interaction between small bifunctional molecules and α-synuclein. Specifically, curcumin and dehydrozingerone like molecules (dehydrozingerone, O-methoxydehydrozingerone, zingerone and their biphenylic analogues) have been considered.
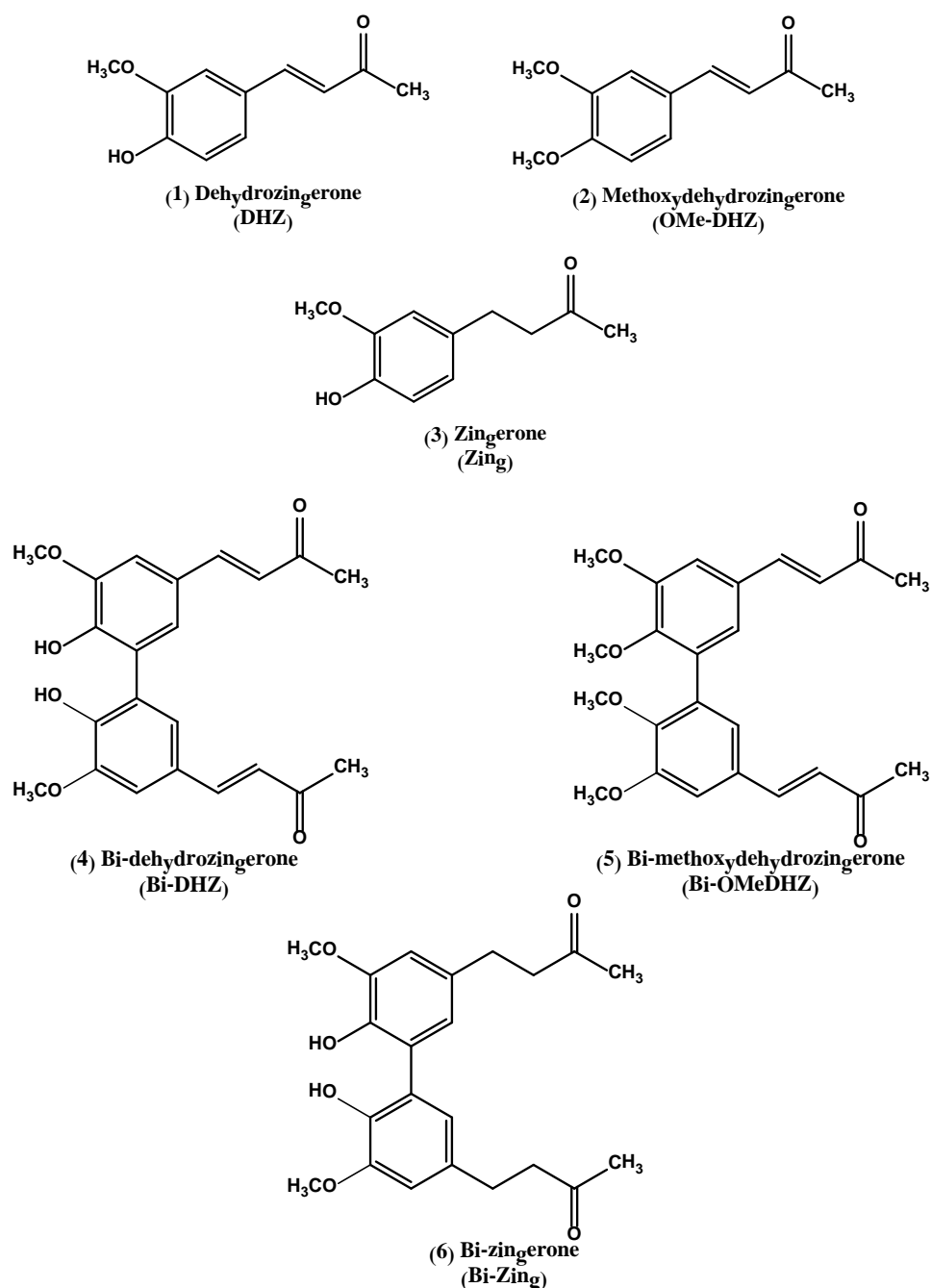

Figure 34: Chemical structure of deihydrozingerone (DHZ) and DHZ-like compounds.

Circular dichroism (CD) and fluorescence spectroscopic techniques have been used to study the binding between AS and curcumin, dehydrozingerone and its derivatives, whose

structure is shown below. Circular dichroism measurements, performed at Diamond Light Source Ltd (UK), was also used to detect any conformational change in the secondary structure of AS upon binding to the molecules and to evaluate the stability of each complex. Changes in emission fluorescence of tyrosine residues of AS was used to confirm CD results. A preliminary study of the effect of the molecules tested and their potential inhibitory properties on AS aggregation was also performed, following the kinetic of AS aggregation with UV-Vis and circular dichroism measurements. Their ability to chelate divalent metal ions was also evaluated.

Researchers of the CNR Sassari Unit analyzed the free-radical scavenger ability through EPR measurements and DPPH test. The safety of these compounds was also estimated by testing the viability of PC12 cells.

We also extracted two sequences already known from the literature and we synthesized two peptides, named BB1 and BB2, and their all-D amino acid analogues as potential amyloid aggregation modulating ligands. We also introduced some conformational constraints at the Phe residue to evaluate the influence of this residue on the binding process. The binding between the peptides and AS was monitored by fluorescence and CD spectroscopy. Changes in tryptophan fluorescence emission were evaluated to confirm results obtained from CD studies and the FRET technique was used to highlight the binding domain in AS sequence of the compounds tested.

The peptides are listed in table 2.

Table 2: List of the peptide synthesized.

Peptide	Sequenza
BB1	H-Arg-Lys-Val-Phe-Tyr-Thr-Trp-NH$_2$
BB1-D	H-arg-lys-val-phe-tyr-thr-trp-NH$_2$
BB1-MePhe	H-Arg-Lys-Val-**MePhe**-Tyr-Trp-NH$_2$
BB1-D-MePhe	H-Arg-Lys-Val-**mephe**-Tyr-Thr-Trp-NH$_2$
BB1-Tic	H-Arg-Lys-Val-**Tic**-Tyr-Thr-Trp-NH$_2$
BB1-D-Tic	H-Arg-Lys-Val-**tic**-Tyr-Thr-Trp-NH$_2$
BB1-Ala	H-Arg-Lys-Val-**Ala**-Tyr-Thr-Trp-NH$_2$
BB2	H-Arg-Gly-Ala-Val-Val-Thr-Gly-Arg-NH$_2$
BB2-D	H-arg-gly-ala-val-val-thr-gly-arg-NH$_2$

Lower case = amino acid of the D-series

Materials and Methods

Materials

Applied Biosystem (Foster City, CA):

TBTU.

Biosolve LTD (Valkenswaard, The Netherlands):

DIEA, piperidin.

Carlo Erba (Milano, Italia):

DCM,.

Fluka (Buchs, Svizzera):

DMF, TFA, anisole, triisopropylsilane, DCC, HOAt, acetonitrile and ethanol HPLC grade, orthophosphoric acid 85%

Sigma Aldrich (Munich, Germany):

Trizma base, Bovine serum albumin (BSA), sodium phosphate monobasic, sodium phosphate dibasic, 1,5-dimethoxynaphthalene 97%, anthracene, saccharose, triptone, yeast extract, sodium chloride, EDTA, kanamicin, magnesium chloride, ammonium sulphate

Novabiochem-Calbiochem AG (Laüfelfingen, Svizzera):

HOBt, Rink Amide MBHA resin, Fmoc-Trp(Boc)-OH, Fmoc-DTrp(Boc)-OH, Fmoc-Thr(But)-OH, Fmoc-DThr(But)-OH, Fmoc-Tyr(But)-OH, Fmoc-DTyr(But)-OH, Fmoc-Phe-OH, Fmoc-Dphe-OH, Fmoc-mePhe-OH, Fmoc-DmePhe-OH, Fmoc-Tic-OH, Fmoc-Dtic-OH, Fmoc-Ala-OH, Fmoc-Val-OH, Fmoc-DVal-OH, Fmoc-Lys(Boc)-OH, Fmoc-DLys(Boc)-OH, Fmoc-Arg(Pbf)-OH, Fmoc-DArg(Pbf)-OH, Fmoc-Gly-OH, Fmoc-DGly-OH.

H_2O is purified thorugh a MilliQ *Millipore* (Billerica, MA, USA) system and RP grade solvents have been used without further purification. Anidrous and peptide synthesis solvents were purchased from Fluka and stored on molecular sieves.

Dehydrozingerone analogues have been synthesized at "Istituto di Chimica Biomolecolare", Sassari Unit.

Methods

Expression and purification of AS

Human wyld-type α-synuclein was expressed in Eschrichia coli BL21(DE3) cells transformed with the pET-28b(+)synuclein plasmid, and an overnight culture was diluted to a final OD600nm of 0.1/0.15 in 1 liter of LB medium (Per litre: 10 g triptone, 5 g yeast extract, 5 g sodium chloride) supplemented with 25 μg/ml kanamicin. The culture was maintained under agitation at 37°C and was induced after cell growth equal to an OD600 value of 0.3/0.4 with 0.1 mM IPTG. After 5 hours cell suspension was centrifuged at 6000 rpm for 10 minutes using a TA-10-250 Beckman-Coulter rotor at 20°C and resuspended in 100 ml Osmotic Shock Buffer (30 mM Tris, 2 mM EDTA, 40% v/v sucrose, pH 7.2), according to Huang et al. [114]. The suspension was incubated at room temperature for 10 min, then it was centrifugated at 12000 rpm for 10 min using a TA-14-50 Beckman-Coulter rotor. Resuspension of the pellet in 90 ml cold deionized water added with of 37.5 μl of MgCl2 saturated solution permitted the protein release from periplasmatic space. Then the suspension was kept on ice for 3 min, and subsequently centrifugated at 12000 rpm for 20 min. The supernatant was boiled for 10 min, and centrifugated at 12000 rpm for 30 min. The solution was adjusted to 20mM Tris-HCl pH 8 ml with 1M Tris-HCl and diluted to a final volume of 100 ml. Then, the protein was precipitated with addition of ammonium sulphate in two steps: in the first step a 35% saturation of ammonium sulphate protein solution was reached and then centrifuged for 40 minutes at 12000 rpm, in the second step ammonium sulphate was added to the supernatant until 55% solution saturation and the solution was again centrifuged for 40 minutes at 12000 rpm. Ammonium sulphate precipitate was resuspended in 20 mM Tris buffer, pH 8 and purified by anionic exchange chromatography with a ResourceQ column (Amersham Parmacia) using a linear gradient from 0 to 0.5M NaCl in 60 minutes. Fractions were collected, dialyzed overnight against water and lyophilized, yielding 25 mg of AS. Purity was checked by SDS-PAGE and MALDI-TOF mass spectrometer analysis.

Stability studies

Stability studies were performed at room temperature in phosphate buffer 20 mM, pH 6.8 and in presence of α-sinuclein or BSA (10 μM), with a protein to curcumin ratio of 1:2. Spectra were recorded every 3 minutes over a period of 36 minutes with a Shimadzu UV-2501 spectrophotometer and analized with UV-probe software.

The molar absorbivity of DHZ-like molecules was determined by measuring the absorbance of each compound at four known concentration (2.5 µM, 5 µM, 10 µM and 25 µM) and the relative calibration curve was determined. The slope of the calibration curve corresponds to the molar absorptivity.

Fluorescence quenching studies

For fluorescence quenching measurements, a 3 µM solution of AS in 10 mM Tris-HCl buffer pH 6.8 was titrated with aliquots of each molecule (3 mM in ethanol). Fluorescence measurements were recorded on a Perkin Elmer LS50B spectrofluorimeter from 285 nm to 385 nm with an excitation wavelength of 275 nm, excitation and emission slit, 7.5nm; scans, 4; scan speed, 50 nm/min, pathlength 1 cm. Each spectrum was subtracted of the solvent contribute and corrected for the dilution and inner filter effect when needed.

Lifetimes studies

The lifetimes of α-sinuclein measures was performed by a TCSPC (Time-Correlated Single Photon Counting) instrument using solutions of AS 15 µM in phosphate buffer 20 mM pH 6.8 with or without curcumin at different concentrations (30 µM and 75 µM).

CD studies

Far-UV CD measurements

Synuclein (4 µM in 20 mM phosphate buffer, pH 6.8) was titrated with aliquots of curcumin (2 mM in ethanol; λ_{max} = 430 nm; ε = 55000 M^{-1} cm^{-1}). CD spectra were recorder with a Jasco J715 spectropolarimeter from 190 to 260 nm at 25 °C with a speed of 100 nm/min, bandwidth, 1 nm, response 0.5 sec, data pitch, 0.5 nm, sensitivity, 100 mdeg, with a 1 mm pathlenght quartz cell (Hellma, Ltd) and are the average of 4 scans: Each spectrum was subtracted of the solvent contribute and corrected for the dilution.

For DHZ-like molecules, far-UV CD. Spectra were collected at Diamond Light Source Ltd (UK) with a ChirascanTM-plus spectrometer from 180 to 260 nm at 25 °C, bandwidth 1.5 nm, step 1 nm, time per point 2 sec, 4 scans and with a 1 mm pathlenght quartz cell (Hellma, Ltd), titrating a solution of AS 5µM in 20 mM phosphate buffer pH 6.8 with increasing aliquots of each compound (two stock solution, 100 and 200 µM in 20mM phosphate buffer pH 6.8/20% v/v EtOH) to a final ratio protein/peptide 1:3.5. Each spectrum is subtracted of the solvent and corrected for the dilution.

Visible CD measurements

Titration of synuclein with increasing amount of curcumin were performed using the same concentrations for far-UV measurements. Each spectrum was collected from 350 to 550 nm at 25 °C, with a scan speed of 100 nm/min, bandwidth 1 nm, response 0.5 sec, data pitch 0.5 nm, sensitivity 100 mdeg, with a 1 cm pathlenght quartz cell (Hellma, Ltd) and is an average of 16 scans. Each spectrum was subtracted of the solvent and corrected for the dilution.

Thermal stability studies

AS and ligand solutions were prepared at concentrations of 5 µM and 17.5 µM in distilled water and ethanol/water (1:4 v/v), respectively. SRCD spectra from 190 to 260 nm were collected at the beamline B23 module end station B, at Diamond Light Source Ltd (UK) with bandwidth of 1.2 nm, integration time of 1s, 1 nm digital resolution, 39 nm/min scan speed, and one repeated scan per spectrum, using Suprasil cells (Hellma Ltd.) with 0.1 cm pathlengths. Thermal stability has been monitored in the 10° - 90°C temperature range (increment steps of 5°C) using a Peltier temperature controller. Temperature was left to equilibrate for 10 min before spectra collecting. The data set of 17 spectra has been analyzed using Global fitting with singular value decomposition (SVD) method to obtain information about the number of possible AS conformations present in solution.

Preliminary aggregation studies

A solution of AS 100 µM in 20 mM phosphate buffer pH 6.8 was prepared and added with 0.03% NaN3 to avoid any bacterial growth. Solution was filtered through a 0.1 µm filters to remove any aggregated material. Compounds to be tested were dissolved in ethanol and added to the protein solution to achieve a final concentration of 200 µM in a total volume of 1 ml. Ethanol did not exceed 8% of the volume. Each sample was then incubated in an Eppendorf Thermomixer Compact (Hamburg, Germany) at 37 °C and 500 rpm for 13 days. From each sample small aliquots were taken at different times and analyzed through UV-Vis studies with CR as a probe.

For each sample at different times, 18 µl aliquots were taken and added to a solution of 20 µM CR in 20 mM phosphate buffer pH 6.8 to achieve a final CR/protein ratio equal to 5:1 and absorption spectrum was immediately collected from 650 to 400 nm at 25 °C, bandwidth 1 nm, with a 1 cm pathlenght quartz cell (Hellma, Ltd). The spectra were measured at Diamond Light Source Ltd (UK) using a LAMBDA 950 UV/Vis/NIR Perkin-

Elmer spectrophotometer. For each analysis the spectrum of CR only was measured before adding the aliquots. Aggregation kinetics were followed by measuring the red-shift of CR absorption. For the sample containing AS and curcumin, the spectrum of the sample without CR was also measured and then subtracted to the overall spectrum.

CD spectra of the aliquots studied by UV-vis spectroscopy were acquired with a Chirascan^{TM}-plus spectrometer at 25 °C from 650 to 450 nm, with bandwidth 1 nm, step 2 nm, time per point 1 sec and 4 scans.

SRCD spectra from 180 to 260 nm were collected at the beamline B23 module end station B, with bandwidth of 1.2 nm, integration time of 1s, 1 nm digital resolution, 39 nm/min scan speed, and two repeated scan per spectrum, using Suprasil cells (Hellma Ltd.) with 0.1 cm pathlengths. Samples were dilutes with buffer to obtain a theoretical protein concentration of 5 μM.

Chelating ability studies

UV-Vis measures were performed with a Shimadzu UV-2501 spectrophotometer at room temperature with 1 cm pathlength quartz cell (Hellma Ltd). The spectra were recorded from 200 to 710 nm and processed with UV-probe program.

The six compounds tested were dissolved in ethanol to obtain a stock solution with a concentration of 0.2 mg/ml for monomers and 0.4 mg/ml for the biphenyls.
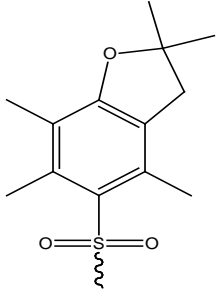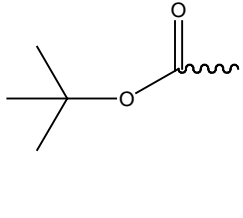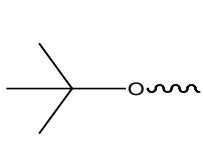
Solution 15 μM of DHZ and OMeDHZ, and their dimers, and 75 μM of zingerone and bizingerone in TRIS-HCl 10 mM buffer pH 6.8 were titrated with increasing aliquots of Cu^{2+}, Fe^{2+} and Fe^{3+} in 10 mM stock solution, in TRIS-HCl 10 mM buffer pH 6.8. The spectra were substracted of the solvent contribute and corrected for the dilution.

Peptide synthesis and purification

Peptide synthesis was performed by SPPS based on Fmoc-chemistry. A Rink-amide resin with a 0.06 mmol scale was used. Activation of the carboxylic group of the residue to be condensed was carried out utilizing TBTU as coupling reagent with HOBt and a three-fold molar excess of the Fmoc-aminoacid dissolved in DMF. Fmoc-Val-OH coupling for peptides containing the conformationally constrained aminoacid N-MePhe or Tic, both D- and L-, was achieved using DCC as activating reagent in presence of HOAT (DCC:HOAT:Fmoc-Val-OH 1,1,1). To avoid side reactions during peptide bond formation, active side chains of the aminoacid must be protected. Pbf (2,3-dihydro-2,2,4,6,7-

pentamethyl-5-benzofuranyl)sulfonyl) was used for the protection of the guanido group of arginine, for lysine and tryptophan Boc group (tert-butyloxycarbonyl) was used, while for tyrosine and threonine we used OtBu (tert-butyl ester). The protecting groups can be easily removed at the end of the synthesis in acidic conditions [115].

Table 3: List of the protecting group used.

Structure	Protecting group	abbreviation	function	cleavage	Stability
	2,3-dihydro-2,2,4,6,7-pentamethyl-5-benzofuranyl)sulfonyl	**Pbf**	**Protection of guanido group**	90-95% TFA	Basic conditions
	tert-butyloxycarbonyl	**Boc**	**Amine protecting group**	90-95% TFA	Basic conditions
	tert-butyl ester	**OtBu**	**Carboxylic protecting group**	90-95% TFA	Basic conditions

A 20% piperidine solution was used for the removal of Fmoc group, while peptide cleavage from resin and deprotection of side chains was performed by treatment with TFA-anisole-TIS-H2O solution (95:2.5:2.0:0.5 v/v). Peptides were purified by preparatice RP-HPLC utilizing a Jupiter C18 column, 10μm, 250 x 4.6 mm, 12 ml/min flow, λ = 216 nm, isocratic eluition at low B concentration for 5 minutes, then linear gradient 20%-35% B solvent for 30 minutes for BB1-mePhe, BB1-D-mePhe, BB2, BB2-D, BB1-Tic e BB1-D-Tic peptides; 10%-30% linear gradient of B for 30 minutes for BB1-Ala peptide and 20%-40% B linear gradient for 25 minutes for BB1 e BB1-D peptides. Solvent used for purification are: A, 0.05% TFA in acqua and B, 0.05% TFA in 9:1 v/v acetonitrile/water. Molecular weight and purity were checked by ESI-MS and analytic RP-HPLC.

Tryptophan fluorescence studies

A solution of the peptide 1.5μM in 20 mM phosphate buffer pH 6.8 was titrated with increasing aliquots of AS wt (stock solution 66 μM in the same buffer). To avoid tyrosines contributes of AS we set the excitation wavelength at 295 nm and the spectra were collected from 305-500 nm with a Perkin Elmer LS50B at 25 °C, excitation and emission slit 5 nm and are the average of 4 scans.

Förster resonance energy transfer studies

AS was expressed with a cisteine residue at C-terminal domain (Ct) and was then labeled with the fluorophore Oregon Green 488 (OG) through an addition reaction between the maleimido group and the SH moiety of the cysteine side chain.

Peptides were conjugated to a cysteine residue at N-terminal position (Nt) using the same method described for the peptides synthesis. Each peptide was then labeled with the fluorophore IAEDANS trough a S_N reaction between the iodide as leaving group and the SH group of the cysteine side chain.

Fluorescence spectra were collected with a Perkin Elmer LS50B at 25 °C from 350 to 650 nm, with a scan speed 150 nm/min, $\lambda_{excitation} = 336$ nm, excitation ad emission slit 3.5 nm, 4 scans with a 1 cm pathlenght quartz cell (Hellma, Ltd). A solution of 0.17 μM AS-Ct-OG in 10 mM Tris-HCl pH 6.8 was titrated with increasing amounts of each peptide (21 μM in the same buffer) up to a final ratio protein peptide 1:5.

Far-UV CD studies

AS (4 μM) in 20 mM phosphate buffer, pH 6.8, at 25 °C was titrated with small aliquots of each peptide (200 μM, same buffer) with minimal dilution. CD spectra were recorded on a Jasco J715 spectropolarimeter from 190 to 260 nm, scan speed 10 nm/min, bandwidth 2 nm, response 4 sec, data pitch 0.2 nm, sensitivity 100 mdeg, with a 1 mm pathlenght quartz cell (Hellma, Ltd) and are an average of four scans. Each CD spectrum was subtracted of the solvent and peptide contributes, and corrected for the dilution.

Correction of fluorescence emission spectra

The presence of different substances in the same solution can influence the observed fluorescence intensity in several ways because of the absorption by the incident light or the reabsorption of the the emitted light. For these reasons, correction of the observed fluorescence intensity values might be necessary.

We can distinguish two cases: coabsorption and reabsorption of the exciting light and reabsorption of the emitting light. In the first case light is absorbed eithr by the fluorophore of interest, but also by other chromophore, that act like filters at the excitation wavelength. If the species do not interact in the ground state, the absorption spectrum of the solution is equal to the sum of the spectrum of each component. At the excitation wavelength the fraction of light absorbed by fluoreophore is:

$$Fl(\lambda_{ex}) = \frac{A_l(\lambda_{ex})}{A(\lambda_{ex})}$$

Where $A_l(\lambda_{ex})$ is the absorbance of the fluorophore and $A(\lambda_{ex})$ is the total absorption of the solution at the excitation wavelength.

In the second case, a fraction of the lighted emitted by the fluorophore can be reabsorbed by the fluorophore itself or by another species and this can be a problem in the determination of the fluorescence intensity. The reabsorption effect depends on the geometry of the cell where the solution is contained. The excitation beam, whose thickness is considered negligible with respect to

the width of the cell, inceases perpendicularly the cell windows, excites the solution, and it is emitted again parallel with respect to the cell windows. For this reason, the emission of the fluorophore can be considered limited to a restricted area of the solution, According to the Lambert-Beer law, the fraction of the emitted light through the pathlength b and at emission wavelength λ_{em} can be written:

$$T_l(\lambda_{em}) = 10^{-A(\lambda_{em}).b}$$

Where $A(\lambda_{em})$ is the absorbance of the solution at emission wavelength. The fluorescence obtained is then:

$$I_l(\lambda_{ex}, \lambda_{em}) = I_l^0(\lambda_{ex}, \lambda_{em}).Tl(\lambda_{em})$$

Where I_l^0 id the fluorescence intensity without reabsorbing effect, whereas $Tl(\lambda_{em})$ is the correction factor fro the riabsorption of the emitted light, also called *emission inner filter* (EIF).

The b value must be known in order to calculate the EIF correction: b can be obtained by experimental measurements. What is needed is a solution containing the fluoropfhore and a non-interacting species absorbing in the spectral region where the fluorophore emits. When the fluorophore is excited, the fluorescenc intensity is measured at the absorption wavelength of the other species: this measure is repeated for solution with increasing concentration of the absorbing species. From the plot of the logarithm of fluorescence values versus the absorbance of the solution at the emission wavelength, one should obtain

a linear correlation. The slope gives the pathlength b, that is the width of the solution that the emitted light must pass through to leave the cell [127].

Results and discussion

α-synuclein

Expression and purification

AS was expressed and purified as described in the "Materials and Methods" section. The purity of AS after FPLC anion exchange chromatography step was checked by SDS-PAGE and characterized by MALDI-TOF mass spectroscopy. Figure 35 shows different steps of the purification protocol in which the band relative to AS is evidenced.
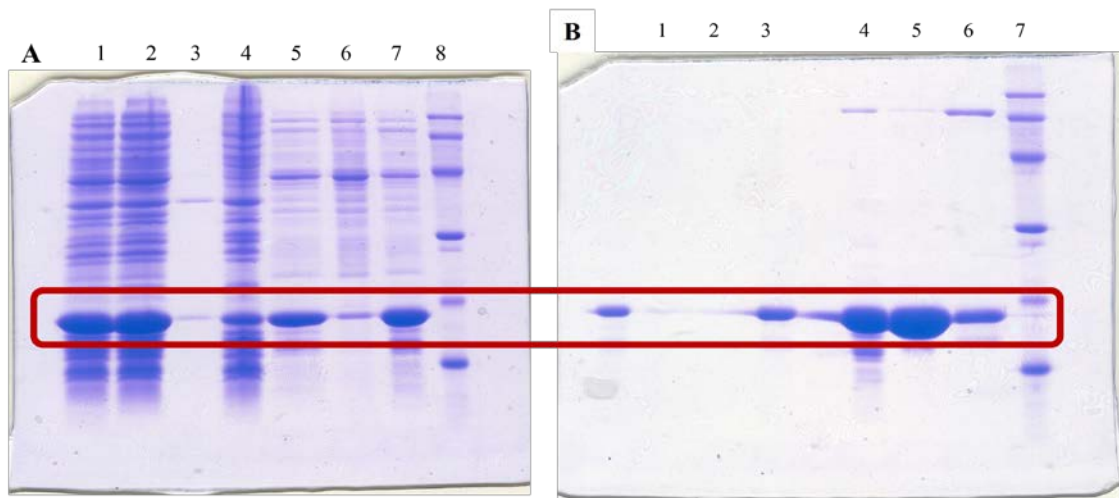
Figure 35: SDS-PAGE of different AS purification steps; Loading order: (A) (1) induced wt AS, pellet (2) and supernatant (3) of AS after osmotic shock buffer addition, pellet (4) and supernatant (5) after resuspension in cold water, pellet (6) and supernatant (7) after boiling, LMW markers(8); (B) pellet (1) and supernatant (2) after first ammonium sulfate treatment, pellet (3) after second ammonium sulfate treatment, crude wt AS (4), fraction 1 (5) and fraction 2 (6) of wt AS after FPLC purification, LMW markers (7).
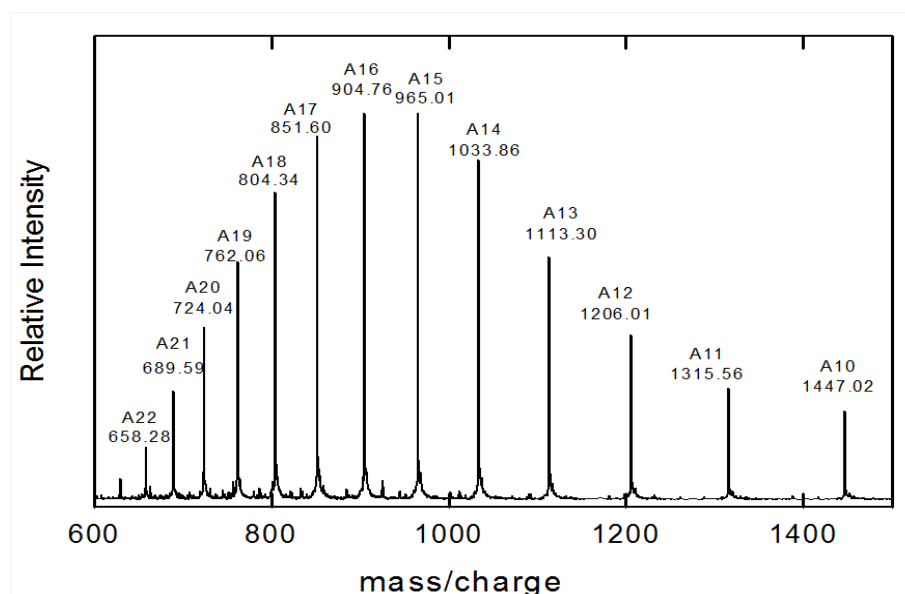
Figure 36: MALDI-TOF mass spectrum of α-synuclein wild-type.

59

Curcumin and its derivatives

Stability studies

The stability of curcumin in aqueous solution at different pH values was evaluated using UV-Vis spectroscopy. Curcumin has a strong absorption band in phosphate buffer, with maximum absorbance at 425 nm, and its degradation may be detected by the decrease of this band and the appearance of a shoulder at about 350 nm. As shown in figure 38, curcumin rapidly undergoes degradation in aqueous solution with a biphasic behaviour. A linear regression of first part of the curve of curcumin degradation was used to determinate the yield of degradation in all the experimental conditions tested (Table 4).
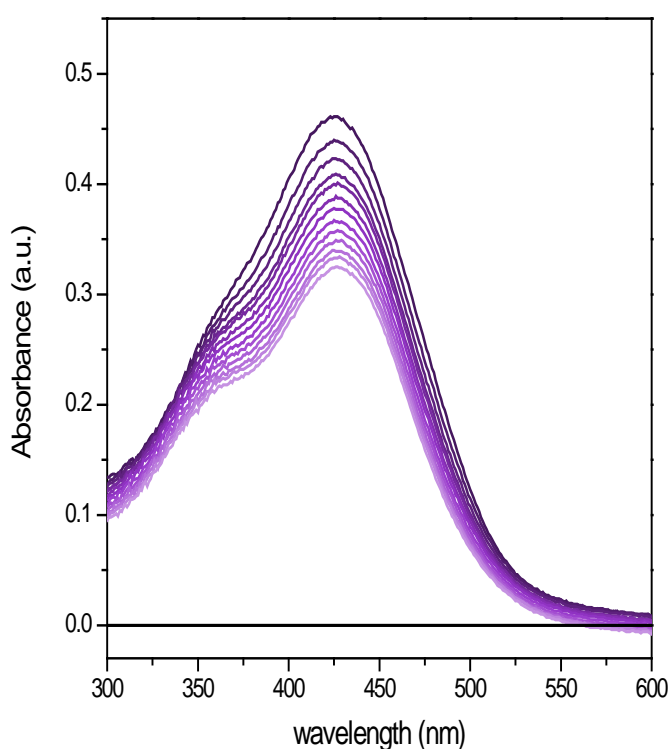
Figure 37: UV-Vis spectra of curcumin (20 µM in 20 mM phosphate buffer, pH 6.8) over the course of 36 minutes.
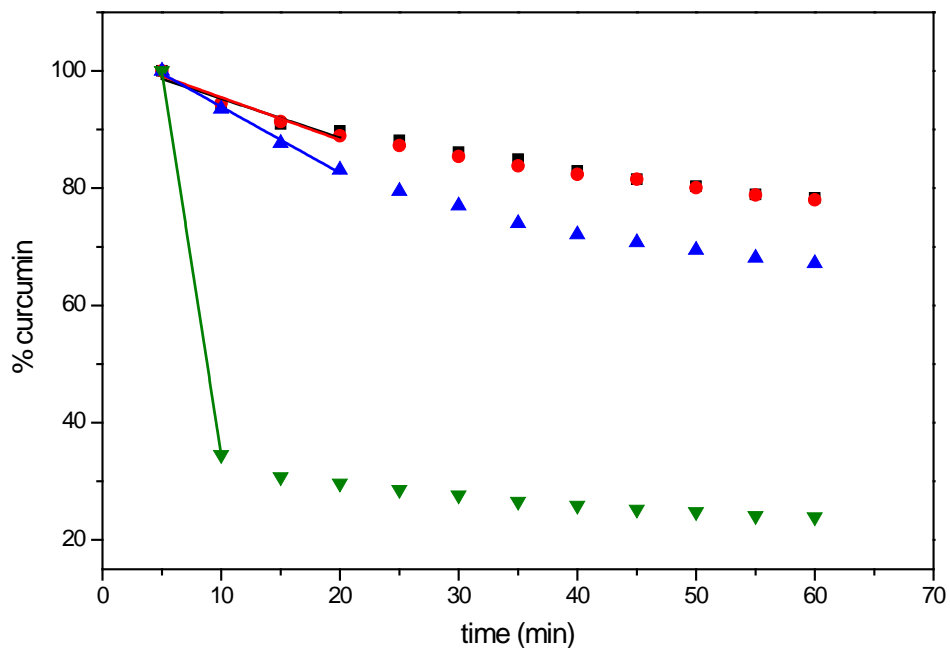
Figure 38: Stability of curcumin in phosphate buffer at different pH values: 1.9 (black), 2.6 (red), 6.2 (blue) and 8.4 (olive).

Table 4: Yield of curcumin's degradation at different pH values. *=calculation based on only two points.

pH	yield of degradation ($\% \text{ min}^{-1}$)	% of curcumin detected after 36 min
1.9	0.90±0.17	85
2.6	0.86±0.14	84
6.2	1.08±0.06	75
6.8	1.04±0.11	76
8.2	13.10*	27

Leung et al. [95] demonstrated that the binding of curcumin to either human serum albumin (HSA) or fibrinogen protects it from degradation. Consequently, the capability of α-synuclein to prevent the degradation of curcumin at pH 6.8 was checked. The results, compared to that obtained in the presence of BSA, showed that AS interacts with curcumin protecting it from degradation.
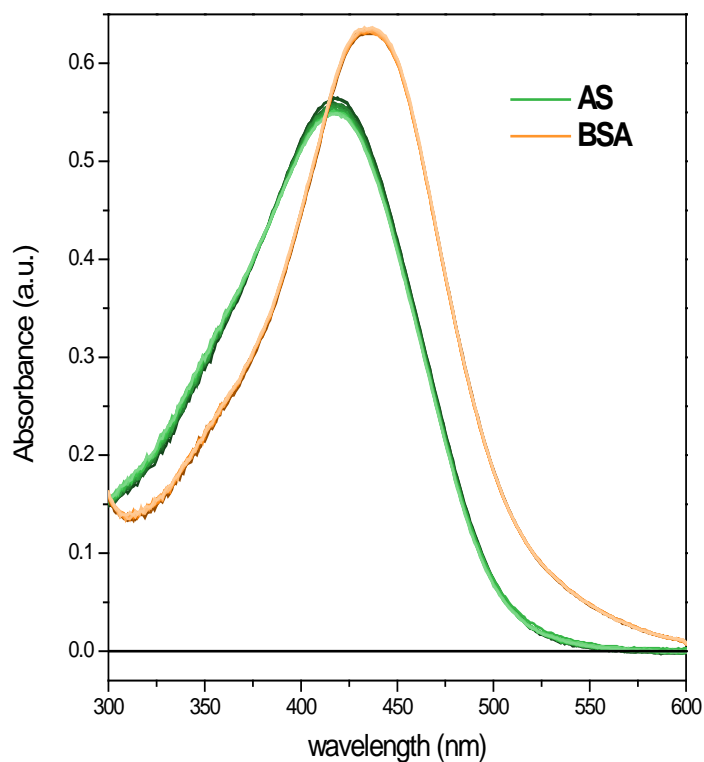
Figure 39: UV-Vis spectra of curcumin in presence of BSA (orange) and synuclein (green) over the course of 36 minutes. The concentration ratio of protein to curcumin is 1:2, where [BSA] and [AS] are 10.2 and 9.8 μM, respectively.
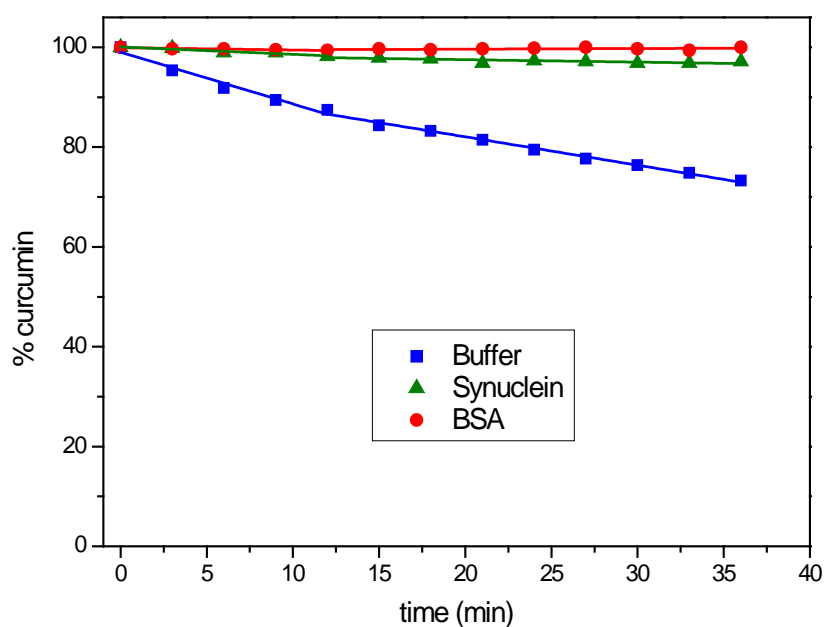

Figure 40: Stability of curcumin in phosphate buffer (blue) and with AS (green) or BSA (red) over the course of 36 min.

A linear regression of the first part of the curve of curcumin degradation was used to determine the yield of degradation in all the experimental condition. (fig. 40). Curcumin

degrades rapidly at pH 6.8 in the first 10 minutes ($1.04\pm0.11\%$ min^{-1}), then the degradation slows down, showing a biphasic behavior. The capability of both BSA and AS to protect curcumin from degradation was calculated using the following equation:

$$\text{Yield of suppression} = [(q_{buffer} - q_{protein})/q_{buffer}] \times 100\%$$

where q is the degradation yield in buffer or in the presence of protein. The result are summarized in table 5.

Table 5: Kinetic data of curcumin degradation in phosphate buffer (20 mM pH 6.8) and in the presence of BSA or AS.

	yield of degradation (% min^{-1})	% suppression degradation	% of curcumin detected after 36 min
Phosphate b. (pH 6.8)	1.04±0.11		76
BSA	0.05±0.01	95±15	100
α-sinuclein	0.15±0.02	85±14	97

Using the same conditions described for curcumin, the stability of dehydrozingerone and its analogues in aqueous environment was checked. First, the molar absorptivity of each compound was determined (table 6).

Table 6: Molar absorbivity and absorption maximum of the examined compound.

Compound	ε (M^{-1} cm^{-1})	λ$_{max}$ (nm)
DHZ	21000	339
OMe-DHZ	20000	333
Zing	3000	281
Bi-DHZ	11500	342
Bi-OMeDHZ	34400	315
Bi-Zing	5560	291

Stability studies showed that dehydrozingerone and its analogues do not degrade either in phosphate buffer (20 mM pH 6.8) or in the presence of proteins (α-synuclein or BSA).

Table 7: Yield of compound present in aqueous solution after 36 minutes.

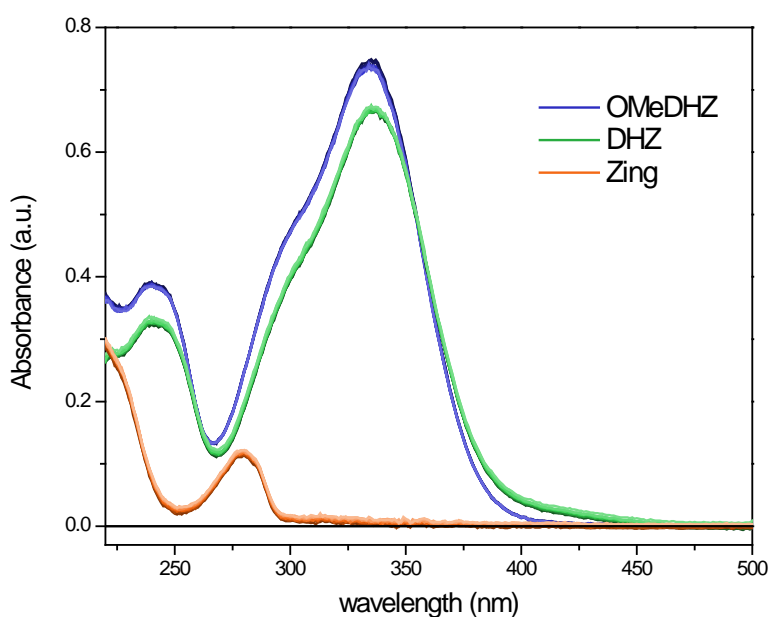| Compound	% compound after 36 min
DHZ	100
OMe-DHZ	98
Zing	100
Bi-DHZ	100
Bi-OMeDHZ	99
Bi-Zing	100

Figure 41: UV-Vis spectra of DHZ, OMe-DHZ and zingerone in 20 mM phosphate buffer pH 6.8 over the course of 36 min.

Fluorescence quenching studies

Fluorescence is widely used to study the interaction between small molecules and biological macromolecules. Fluorescence quenching is defined as the reduction of the fluorescence yield of a fluorophore. This can be due either to different processes that may occur during the lifetime of the excited state (e.g., collisional quenching, energy transfer, charge transfer or photochemical reactions) or to the formation of a stable non-fluorescent complex in the ground electronic state (static quenching). Dynamic or collisional quenching depends on the diffusion rate of the molecules and occurs when the fluorophore and the quencher collide during the lifetime of the excited state: the fluorophore returns to the ground state without photon emission [116].

Dynamic and static quenching can be distinguished using either lifetime measurements or fluorescence titration at different temperatures. Molecule diffusion increases with temperature, determining an increase in collisional quenching. On the contrary, static quenching decreases as a consequence of the changes in the of dissociation of the complex at higher temperatures.
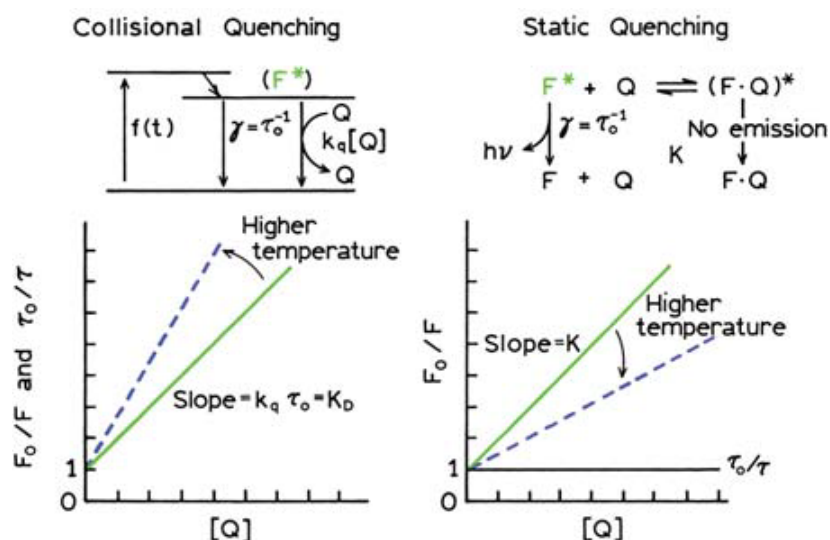

Figure 42: Comparison between collisional and static quenching [119].

AS contains four tyrosine residues: one in the N-terminal domain (position 39) and three in the C-terminal domain (positions 125, 133 and 136). Quenching of AS tyrosine fluorescence was used to evaluate the curcumin binding to the protein. Titrations and lifetime measurements of curcumin and curcumin-bound to AS at two different temperatures were performed to determine the type of quenching involved in the interaction between AS and curcumin.
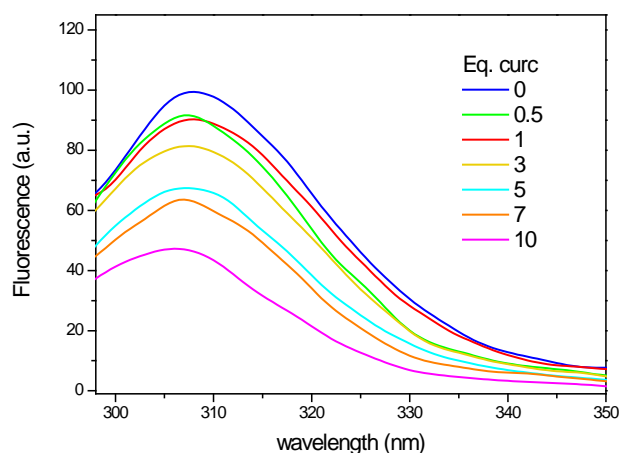

Figure 43: Fluorescence spectra for the titration of synuclein (3 µM in 20 mM phosphate buffer, pH 6.8) with curcumin (3 mM in ethanol), at 25 °C.

65

For the AS-curcumin complex, the slope in the Stern-Volmer plot decreases increasing the temperature, suggesting a static quenching mechanism that permits us to hypothesize the presence of a AS-curcumin complex.
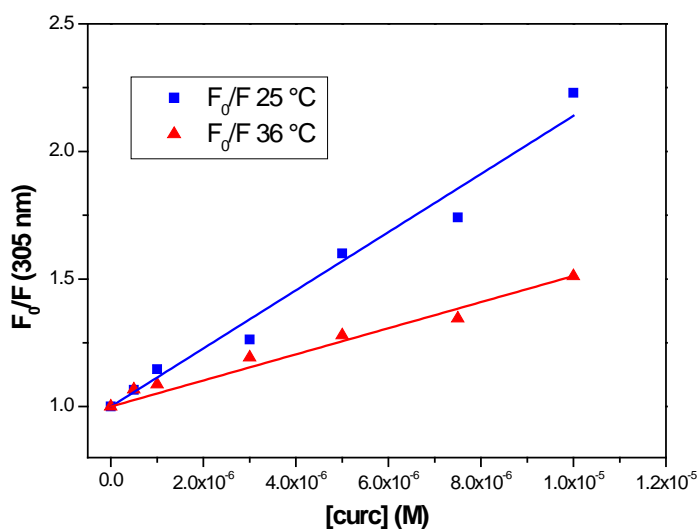

Figure 44: Stern-Volmer graph for the titration of synuclein (1 µm in 20 mM phosphate buffer, pH 6.8) with curcumin (0.8 mM in ethanol), at 25 °C (blue) and 36 °C (red).

This conclusion was confirmed by lifetime studies carried out at the "Istituto per la Sintesi Organica e la Fotoreattività" of CNR by Dr. Sandra Monti. AS has biexponential decay with lifetimes of t1 = 0.85 ns and t2 = 2.2 ns. In the presence of curcumin, the lifetime did not shown any appreciable variations. At protein ligand ratio of 1:2, t1 and t2 values of 0.85 ns and 2.1 ns, respectively, were determined; t1 and t2 values of 0.78 ns and 2.05 ns, respectively, were obtained at a protein:ligand ratio of 1:5.
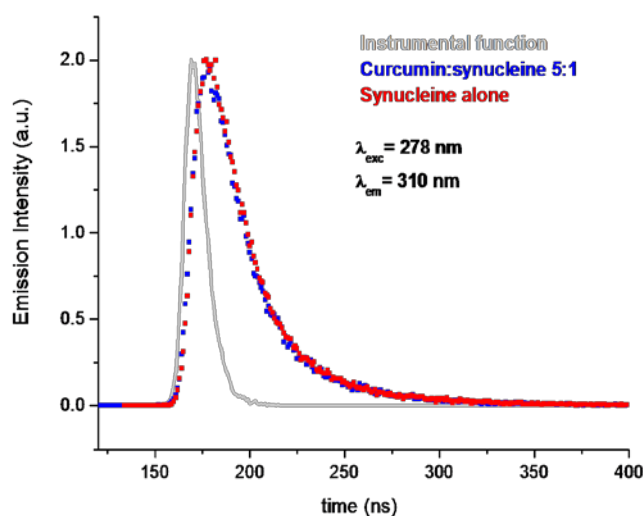

Figure 45: Lifetime measurements of AS alone and in the presence of 5 equivalents of curcumin.

66

These data confirm the presence of a static quenching, where the quencher (here curcumin) removes a fraction of the fluorophore, in this case the AS tyrosines, from the observable fraction. The complex is not fluorescent, so the only fluorescence observed is due to the free protein. The observable fraction remains unaffected and the lifetime as well [116]. The quenching reaction can be written as [117]:

$$nQ + AS \Leftrightarrow Q_n AS$$
(1)

where n is the number of binding sites of the protein, Q is the quencher, and AS is synuclein.

The binding constant can be obtained from the following equation:

$$K_a = \frac{[Q_n AS]}{[Q]^n [AS]}$$
(2)

where [Q] and [AS] are the concentrations of quencher and protein, respectively, and [QnAS] is the concentration of the non-fluorescent complex. If [AS]0 is the total AS concentration, equation (2) can be written as:

$$K_a = \frac{[AS_0] - [AS]}{[Q]^n [AS]}$$
(3)

Since fluorescence intensity is proportional to the concentration of the protein:

$$\frac{[AS]}{[AS_0]} = \frac{F}{F_0}$$
(4)

Combining equations (3) and (4), we obtain:

(5)
$$\log \frac{(F_0 - F)}{F} = \log K_a + n \log[Q]$$

where F_0 and F represent the fluorescence of AS without and with quencher, respectively. This equation permits us to estimate the binding stoichimetry, n, and the binding constant, K_a. For the AS/curcumin complex, we found: n = 0.95 and K_d = 7.77 μM.
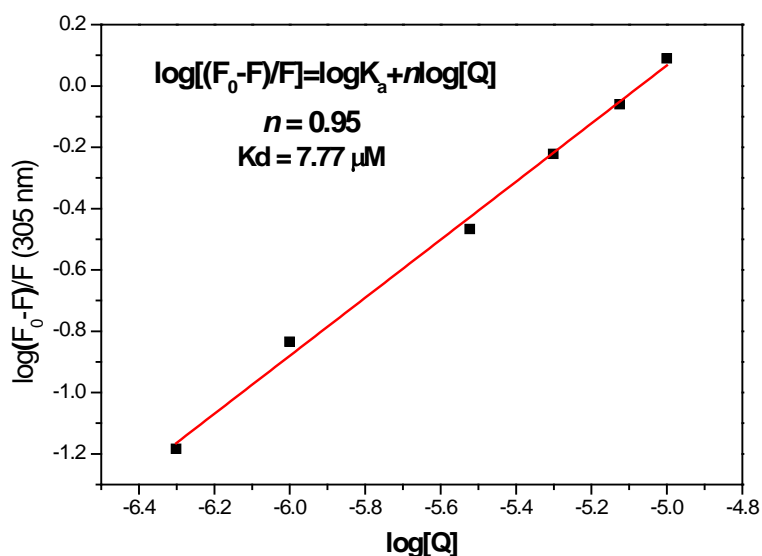
Figure 46: Graph of log[(F_0-F)/F] versus log [Q] for the determination of the binding constant of the AS/curcumin complex.

Additionally, quenching fluorescence measurements were performed to evaluate the interaction of DHZ and its analogues to AS. Since the absorbance and fluorescence of DHZ analogues fall in the same regions as tyrosines, each fluorescence spectrum was corrected for the inner filter effect as reported in the Materials and Methods section.

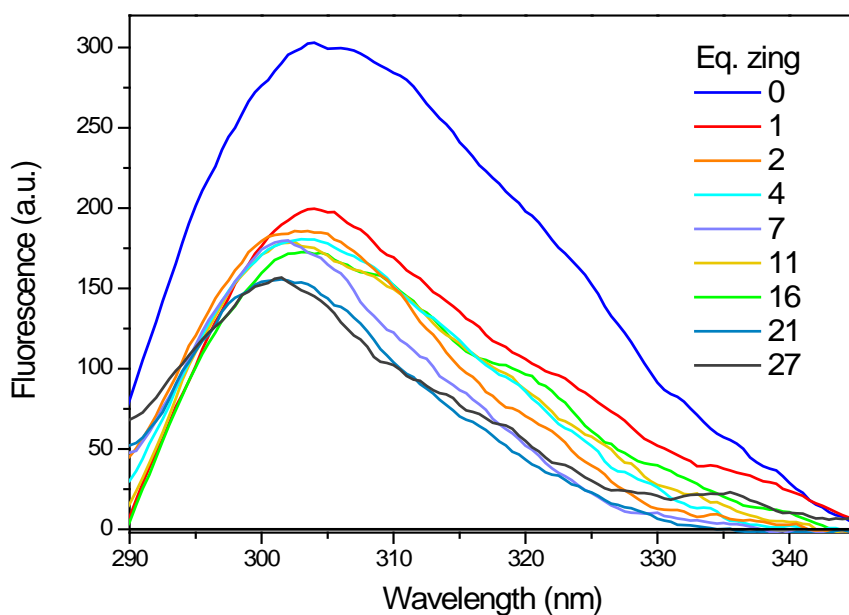As example the titration of AS with zingerone is reported.

Figure 47: Fluorescence spectra for the titration of synuclein (3 μm in 20 mM Tris-HCl buffer, pH 6.8) with zingerone (3 mM in ethanol), at 25 °C.

Tyrosine fluorescence emission of AS changes in every titration suggesting that each compound binds to AS, although with different affinity. Binding constant values for each compound are reported in table 8.

Table 8: K_d and n values for each protein-ligand complex.

Molecule	K_d (μM)	n
DHZ	13.1	0.97
OMe-DHZ	25.6	1.07
Zing	5.2	1.09
Bi-DHZ	2.6	1.41
Bi-OMeDHZ	0.7	1.33
Bi-Zing	0.1	1.03

Zingerone shows a tighter interaction than DHZ and OMe-DHZ and dimerization generally increases the affinity; and among the biphenyl compounds, bizingerone binds with higher affinity than Bi-DHZ and Bi-OMeDHZ. Each compound binds with a 1:1 stoichiometry with the exception of Bi-DHZ and Bi-OMeDHZ, for which n values of 1.41 and 1.33, respectively, have been determined.

Circular dichroism

Binding studies

Circular dichroism is one of the most sensitive spectroscopic techniques to examine the structure of proteins/polypeptides and interactions between macromolecules and their ligands. Analysis of the far-UV region permits one to investigate the secondary structure of proteins.

CD spectroscopy, both in the far-UV and in the visible region, was used to identify the interaction between curcumin and the AS monomer.

In the far-UV CD region, the main chromophore is the peptide bond that shows different dichroic signals when different secondary structure contributions are present. For AS, a negative band at about 195 nm is present: this signature is typical of an unfolded structure. Upon binding with curcumin the CD signal of the protein changes and this is indicative of an interaction between AS and curcumin, although the secondary structure of AS is not markedly influenced and remains essentially unstructured.
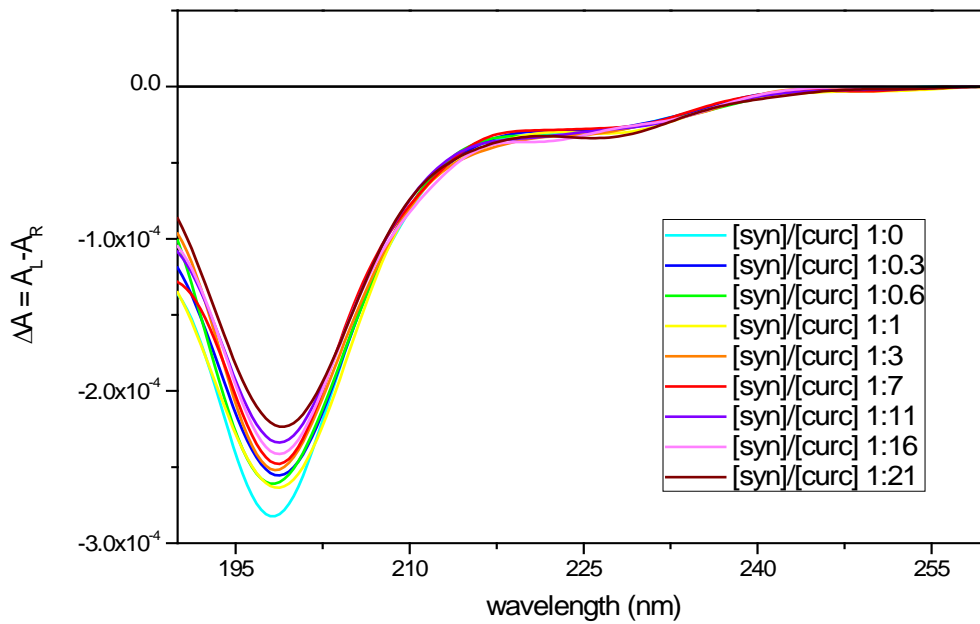
Figure 48: Far UV-CD spectra for the titration of synuclein (4 µM in 20 mMphosphate buffer pH 6.8) with curcumin (2 mM in ethanol) at 25 °C, 1 mm pathlength.

Variations of the CD signal in the far-UV region were used to evaluate the binding constant for the AS/curcumin complex. In general, the equilibrium between a receptor R and a ligand L can be described as:

(7) $$R + L \Leftrightarrow RL$$

and the binding constant is:

(8) $$K_d = \frac{[R][L]}{[RL]}$$

At equilibrium, the CD signal is due to the contribution of each species, for each λ:

(9) $$\Delta A_{obs} = \Delta A_R + \Delta A_L + \Delta A_{RL}$$

In an ideal system, one of the elements involved in the formation of the complex (here curcumin) is transparent in the region where signal variations are detected. Thus the equation (9) will contain only the contributions due of the bound and free receptor. Using the Lambert-Beer law, the equation can be written as:

(10) $$\Delta A_{obs} = \Delta \varepsilon_R [R]_{eq} + \Delta \varepsilon_{RL} [RL]_{eq}$$

where $\Delta \varepsilon_R$ and $\Delta \varepsilon_{RL}$ are the differences between the absorption extinction coefficients of the left and right circularly polarized light of R and RL, respectively. We can obtain these

70

values by measuring the CD spectra of a solution of the receptor only ($\Delta\varepsilon_R$) and of the receptor bound to the ligand ($\Delta\varepsilon_{RL}$).

If we have the initial concentration and introducing some substitutions, we can obtain the following non linear regression equation, formulated by Siligardi et al. [118], based on a 1:1 binding stoichiometry:

(11)

$$A = \left\{ \left(\Delta\varepsilon_{RL} - \Delta\varepsilon_R \right) \left[\frac{1 + K_a[R]_0 + K_a[L]_0 - \sqrt{\left(1 + K_a[R]_0 + K_a[L]_0\right)^2 - 4K_a^2[R]_0[L]_0}}{2K_a} \right] + \Delta\varepsilon_R[R]_0 \right\}$$

where $[R]_0$ and $[L]_0$ are the initial concentration of R and L and K_a is the binding constant. The binding constant for the complex AS/curcumin was determined using equation (11), giving a $K_d = 10$ μM, a value close to that obtained from fluorescence quenching measurements.
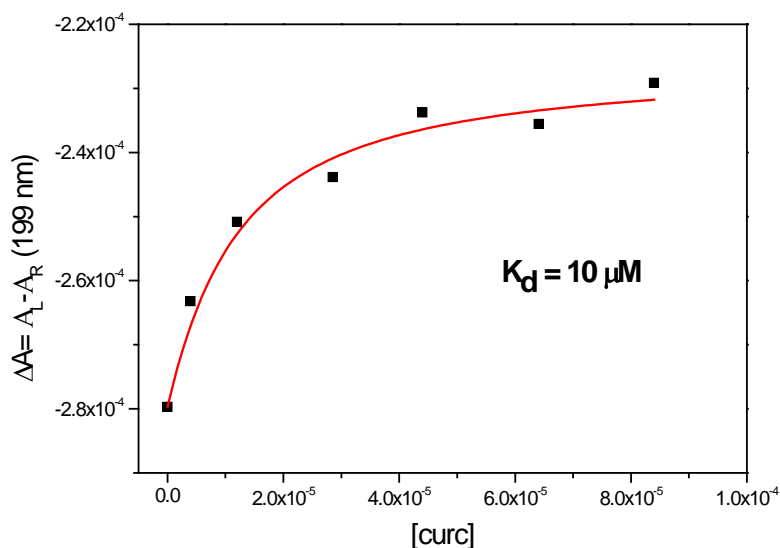

Figure 49: Binding curve for the titration of AS (4 μm in 20 mM phosphate buffer, pH 6.8) with curcumin (2 mM in ethanol), 25 °C.

The visible region of the spectrum was also evaluated, where the only chromophore is curcumin. Curcumin is achiral but can become optically active upon binding to AS. The phenomenon is known as "protein-induced chirality" and occurs when the ligand is constrained in the asymmetric binding site of the protein. As a consequence, when bound to AS, curcumin may experience a chiral environment and acquire optical activity in a region where AS does not absorb. In this particular case, no CD signal was detected at low

curcumin concentrations (≤ 1 equivalent of curcumin), whereas a negative band at 425 nm and a positive band at 374 nm appear at higher concentrations of curcumin typical of an exciton splitting. Exciton splitting occurs when two or more identical chromophores are fixed in close proximity in space and arises from electronic interactions between excited and nonexcited chromophores within the sets.

The binding of curcumin to HSA was extensively studied [119,120]. Specifically, visible CD spectra of curcumin bound to HSA showed a strong positive Cotton band at 496 nm and a negative Cotton band at 427 nm. The bisignate nature of the CD spectra was explained by assuming a non-planar conformation for curcumin, with its two halves being twisted relative to each other at the protein binding site and molecular modeling calculations determined a right-handed conformation for curcumin inserted in the hydrophobic domain of HSA [119]. An opposite trend is observed in the visible CD signal for the AS/curcumin complex and this suggests that probably AS induces an opposite conformation on curcumin during the interaction, resulting in the exciton splitting shown in figure 50.

The CD spectrum of curcumin alone cannot be collected because it rapidly degrades in the conditions used (20 mM phosphate buffer, pH 6.8).
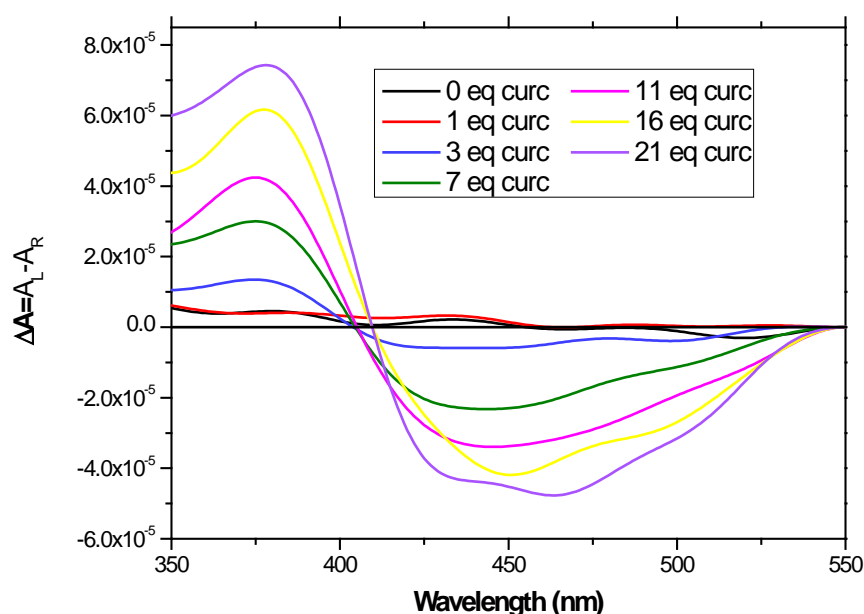

Figure 50: Visible CD spectra for the titration of synuclein (4 μM in 20 mM phosphate buffer pH 6.8) with curcumin (2 mM in ethanol) at 25 °C, 1 cm pathlength.

Circular dichroism measurements were performed also to evaluate the interaction between DHZ and its analogs and AS. As an example, titration of AS with DHZ is reported below.
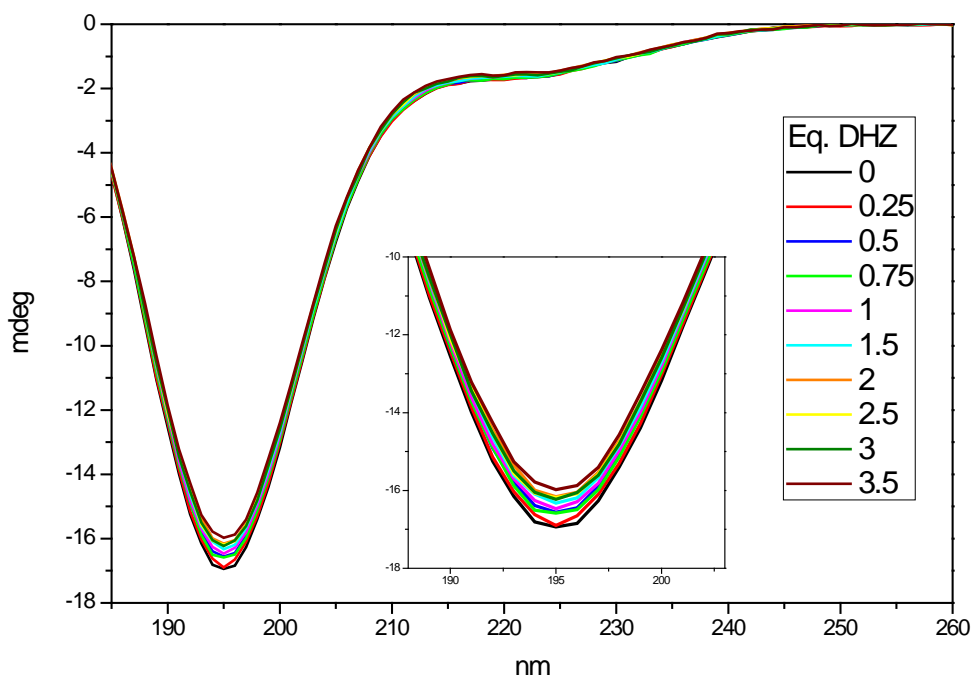
Figure 51: Far-UV CD spectra for the titration of synuclein (5 µM in 20 mM phosphate buffer, pH 6.8) with DHZ (100 and 200 µM 20 mM phosphate buffer pH 6.8/20%EtOH) at 25 °C, 1 mm pathlength.
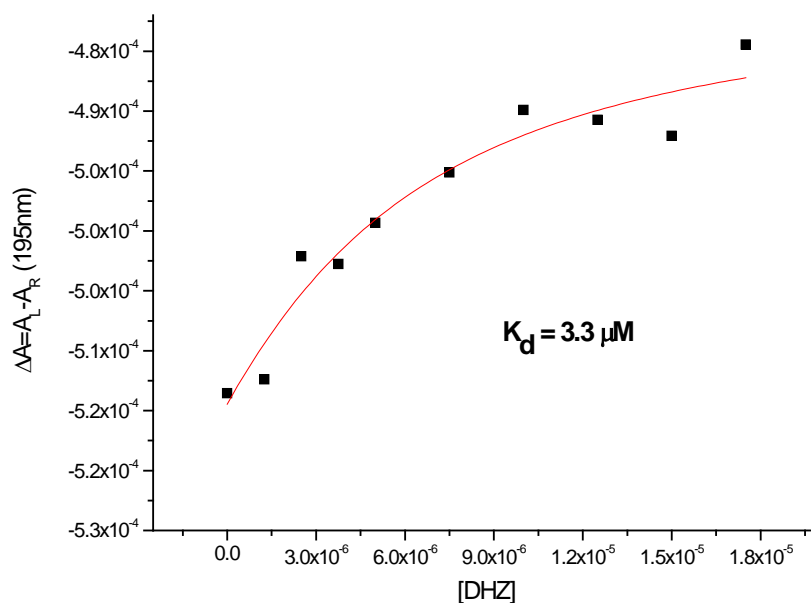

Figure 52: Binding curve for the titration of synuclein (5 µM in 20 mM phosphate buffer pH 6.8) with DHZ (100 and 200 µM 20 mM phosphate buffer pH 6.8/20%EtOH) at 25 °C, 1 mm pathlength.

Table 9 summarizes the K_d values for the complexes of AS with curcumin, DHZ and analogues bound to AS.

The use of a very sensitive instrument such as Chirascan[TM]-plus allowed us to detect very small signal changes such as those seen in this study. Every spectrum shows a small but reasonable change of the dichroic signal at about 197 nm attesting the binding between AS and DHZ-like compounds. Equation (11) was used to estimate the value of the binding

73

constant. The equation did not fit the data of Bi-DHZ and Bi-OMeDHZ titrations: this suggests that these compounds do not bind AS in a 1:1 binding stoichiometry, thus confirming the results obtained by fluorescence quenching. The K_d values are similar to those determined from fluorescence (K_d in μM range) except for zingerone that, from CD studies, reveals a very strong binding ($K_d < 0.1$ μM). It must be taken into account that the many corrections used in fluorescence studies for the inner filter effect cause a noticeable deviation of the results.

Table 9: K_d values for each complex protein/ligand.

Composto	Kd (μM)
Curc	10
DHZ	3.2
OMeDHZ	1.9
Zing	< 0.1
Bi-DHZ	*
Bi-OMeDHZ	*
Bi-Zing	2.9

Stability studies

The thermal stability of free and complexed AS with curcumin and DHZ-like molecules was assessed following the CD changes in the far-UV region as a function of temperature.

In all the systems analyzed (free AS and the seven AS complexes), the thermal stability can be described by using only two spectra: the starting spectrum (at 10 °C) characterized by a strong negative band at about 197-199 nm, and the final spectrum (at 90 °C) in which this band is reduced. The change in the intensity of the negative band at 198 nm as a function of temperature was used to estimate the relative stability of AS (free and complexed). The decrease of the intensity of the negative band with temperature has been fitted with a logistic sigmoid curve for a simple two-state unfolding process. The resulting melting temperatures (MT) are reported in Table 10. The thermal unfolding of free AS is reversible (figure 53) and addition of EtOH (3%) decreases the melting temperaures of free AS of about 3 °C. Results show that for each complex, except for zingerone and bidehydrozingerone, the melting temperature increases, especially for DHZ and OMeDHZ where a ΔMT of about 10 and 20 °C, respectively, was determined. This suggests a higher

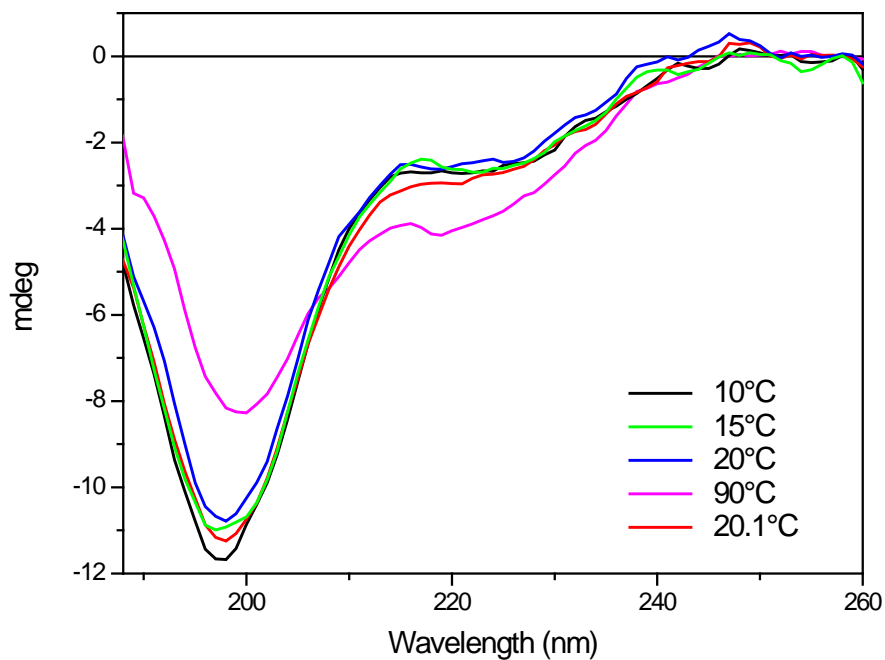stability of bound AS compared to free AS, with the exception of AS/zing and AS/BiDHZ complexes.

Figure 53: Far-UV CD spectra of AS (5 µM) in aqueous solution in the presence of 2.5 equiv. of OMe-DHZ.
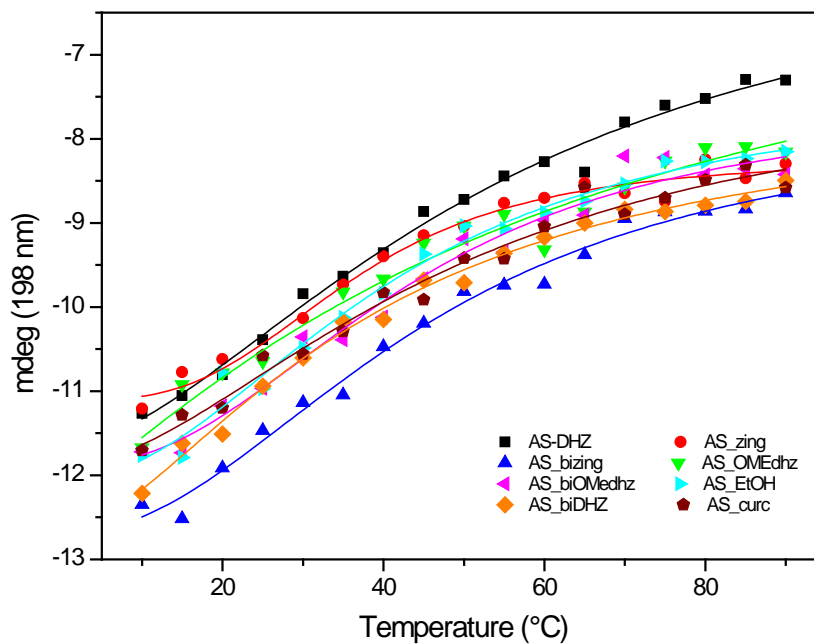

Figure 54: CD melting curves generated by monitoring the absorbance at 198 nm.

Table 10: Melting temperatures of free AS and AS bound to the ligands.

System	MT (°C)
AS	43.5
AS with 3% EtOH	40.6
AS/DHZ	53.1
AS/OMeDHZ	63.8
AS/Zing	36.2
AS/BiDHZ	37.9
AS/BiOMeDHZ	43.3
AS/BiZing	45.4
AS/Curc	47.5

Preliminary aggregation study

Thioflavine T (ThT) fluorescence emission is widely used to detect and quantify amyloid fibrils: today, this technique represents the principal method for real-time fibrillation kinetics assays. When ThT is added to compounds that contains rich β-sheet structure deposits, such as amyloid fibrils, it strongly fluoresces with an emission maximum at 490 nm and an absorption maximum at 440 nm, whereas it shows a very weak fluorescence spectrum and a blue shift to an emission maximum at 440 nm and absorption maximum at 350 nm when free in solution. Unfortunately, chromophores like curcumin with an absorption spectrum that matches the ThT fluorescence or absorption can bias ThT fluorescence emission because of quenching effects: as a consequence, the results obtained will not represent the real kinetics of aggregation [121]. In this study, to compare the ability of curcumin, DHZ and analogs to inhibit AS aggregation we decided to use Congo Red (CR) as a probe for aggregation. CR is able to partially inhibit fibril formation; thus, its use is not feasible for *in-situ* measurements, but it is used for real-time assays where CR is added to fibrils being formed and its absorbance is measured immediately. CR binding to fibrils induces an increased intensity in the absorption spectrum and a red-shift from 490 nm in aqueous solution and neutral pH to about 540 nm (depending on the aggregates formed). Curcumin absorption is comparable to CR absorption, but it has been demonstrated that if the spectrum of curcumin in the presence of the amyloidogenic peptide model RCMκ-CN is subtracted to that obtained in the presence of CR, the resulting spectrum is due to CR absorption only [121]. Moreover, Hoyer et al. [122] demonstrated that wild-type AS can give aggregates with different morphologies, depending on pH and

ionic strength, and this might influence ThT fluorescence. Indeed, ThT strongly fluoresces with fibrils grown in 10mM $MgCl_2$ or 0.2 M NaCl, whereas its emission is markedly reduced without salts. This second aspect strenghthened our proposal to use CR as a probe for fibrils.
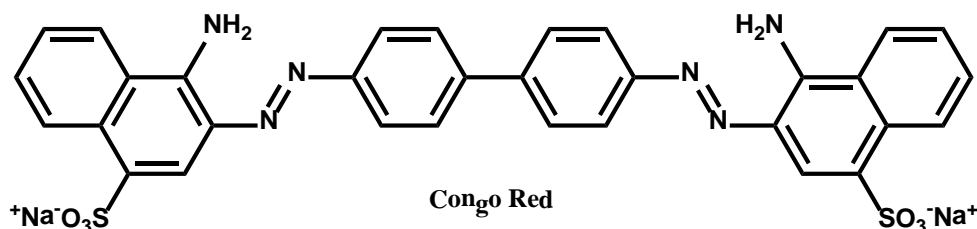

Figure 55: Structure of Congo Red

Aggregation studies were performed to evaluate the inhibitory activity of curcumin and DHZ-like molecules against aggregation of AS and the kinetics was monitored through changes in the absorption spectrum of CR as described in Materials and Methods section. Samples examined are listed in table 11:

Table 11: List of the samples tested.

Sample nr.	Description
1	AS 100 μM
2	AS 100 μM + DHZ 200 μM
3	AS 100 μM + OMeDHZ 200 μM
4	AS 100 μM + Zing 200 μM
5	AS 100 μM + Bi-DHZ 200 μM
6	AS 100 μM + Bi-OMeDHZ 200 μM
7	AS 100 μM + Bi-Zing 200 μM
8	AS 100 μM + Curc 200 μM

As an example, the absorption spectra of aliquots of sample 1 taken at different days are reported. The intensity of CR absorbance increases with time accompanied by a red shift from 489 nm to about 510 nm: this is indicative that aggregation is proceeding. We measured the wavelength values for each sample at different times and the variation was plotted as a function of time (fig.57). Each sample shows a sigmoidal trend and data were fitted using a sigmoidal computer fit: for samples 2 and 3 the fitting was not achievable, perhaps because there are only few points in the slope segment. In general the lag phase is quite short and aggregation starts after few hours, with the exception of sample 8 in which we do not observe any lag phase and aggregation starts immediately.
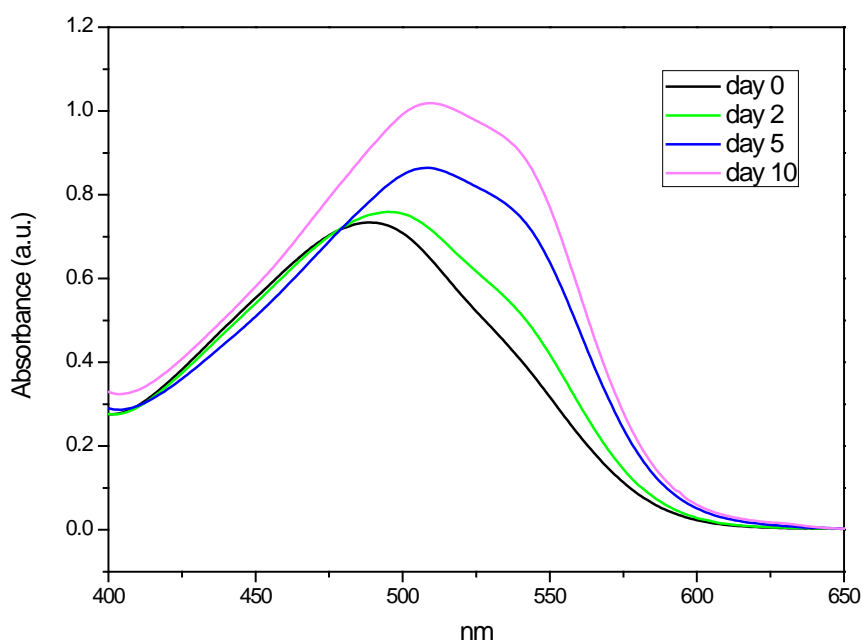
Figure 56: Absorption spectrum of aliquots containing 20 µM CR in phosphate buffer pH 6.8 with 4 µM AS taken at different times.
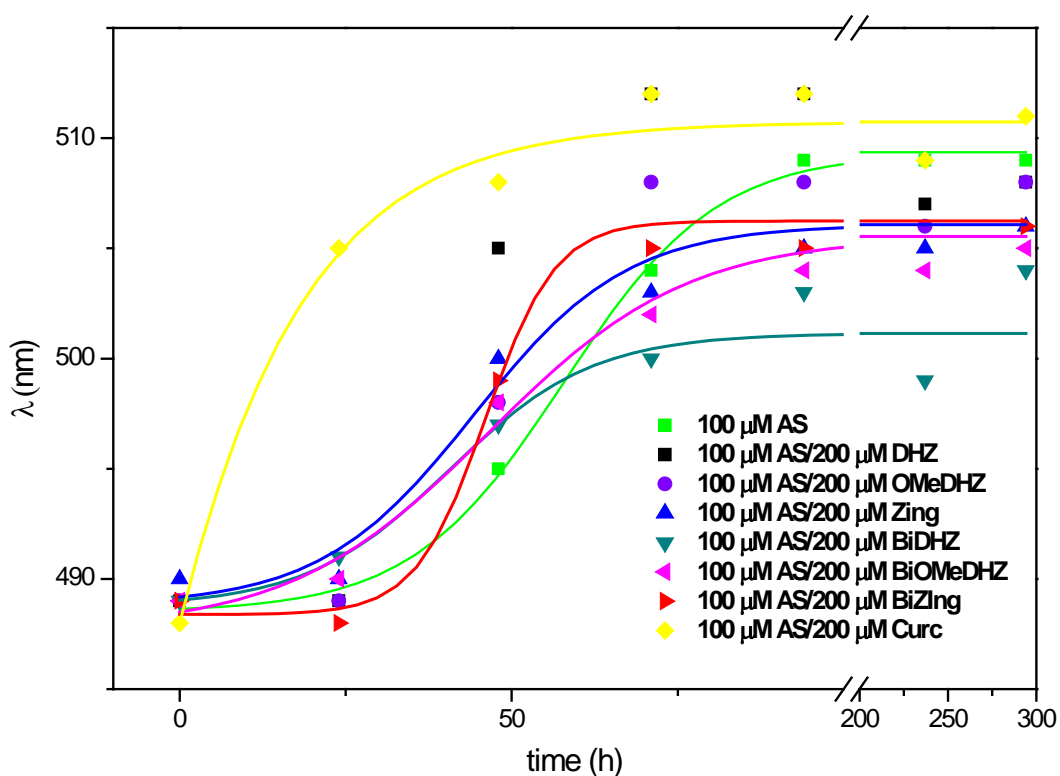

Figure 57: Aggregation kinetics of AS in absence (sample 1) and presence of the tested compounds (samples 2-8).

Hence, for curcumin (sample 8) we did not observe the inhibitory activity reported in the literature. On the other hand, the red shift of sample 5 does not go beyond 500 nm,

78

suggesting that aggregation stops at an intermediate step while, for all the other samples, the aggregation kinetics are quite similar to that of the reference sample 1.

The experiment should be repeated collecting the aliquots more frequently to obtain a better analysis of the lag time and slope.

Aggregation was also studied by analyzing changes in the CD spectra of CR when it binds to AS aggregates. Like curcumin, CR is achiral, but it might assume a chiral character upon binding to AS thanks to the "protein-induced chirality" phenomenon.
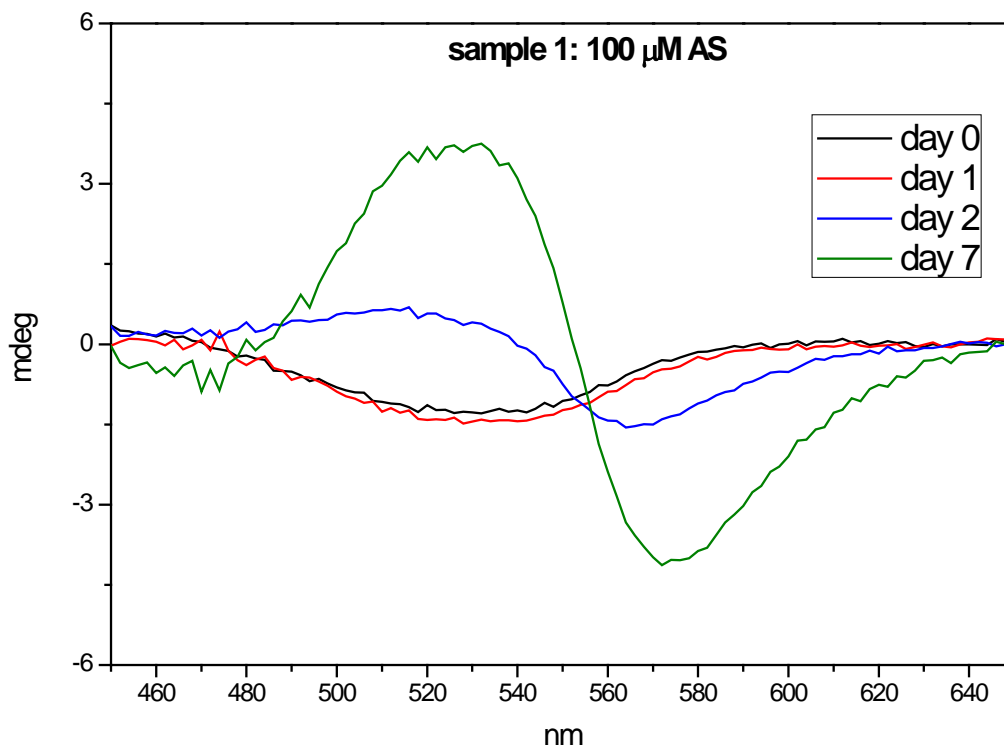

Figure 58: Induced CD spectra of 20 µM CR in phosphate buffer, pH 6.8 with 4 µM AS taken at different times.

Interestigly, when bound to the AS monomer (sample 1, figure 58), the dichroic signal of CR displays only a negative band at 520 nm. As the aggregation proceeds, the CD signal changes and shows a negative band at 570 nm and a positive one at 520 nm and this trend is similar to the exciton chiral interaction of curcumin bound to AS (figure 50), suggesting that Congo Red experiences a similar situation when it binds to AS.

The same analysis was performed for all the other samples: a similar behavior was found, with the exception of sample 5 (AS/BiDHZ) where we never observed an exciton splitting, but only a negative band at about 520 nm (figure 59).
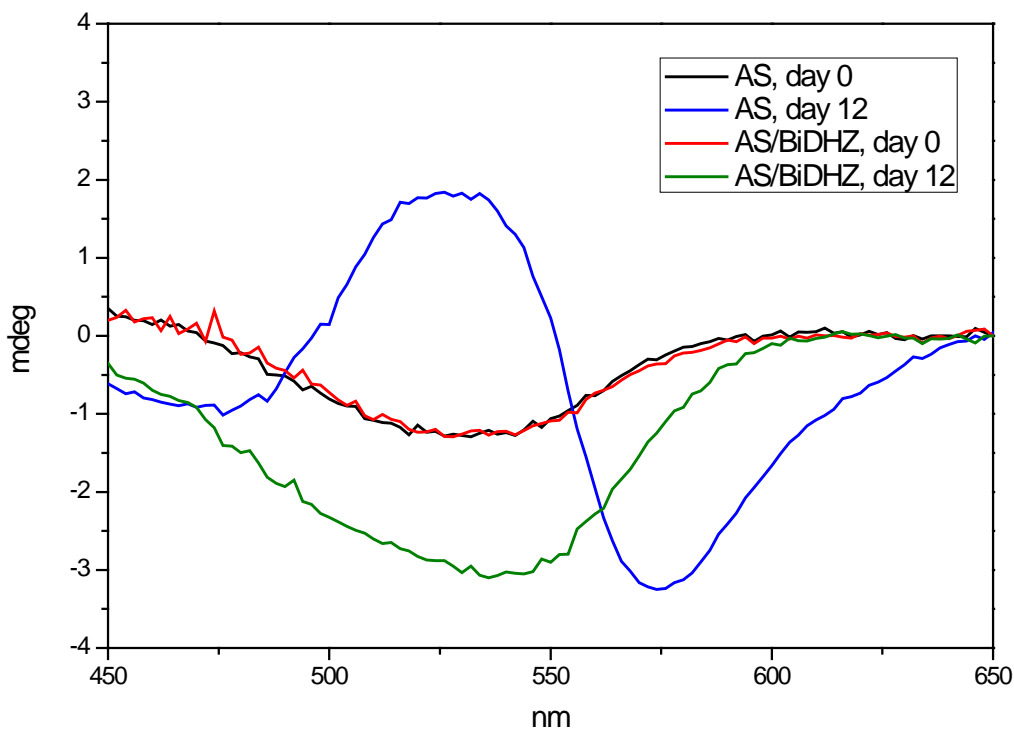
Figure 59: Comparison between induced CD spectra of Congo Red

The secondary structure at the end of aggregation was also analysed for each sample. CD spectra were collected at Diamond Light Source Ltd (UK) using a synchrotron light source. SRCD has a high photon flux and micro beam dimensions that permits collection of spectra in very short times and using very small samples. It also allows samples in turbid solutions or in absorbing buffer (e.g. Tris-HCl) to be examined and permits the spectral region to be expanded at wavelengths usually inaccessible with bench-top instruments.

The far-UV CD spectra were collected for all the samples, then CR was added to each sample and the spectrum recorded again. Spectra with and without CR for each sample are superimposable, indicating that CR did not change the secondary structure of the protein (data not shown). All spectra, except that of sample 5 (AS/BiDHZ), showed a negative band at about 220 nm and a positive one at about 197 nm, characteristic of a β-sheet structure; SRCD spectrum of sample 1 is reported as an example. The SRCD spectrum of fresh synuclein (sample 1, day 1) is also reported for comparison.
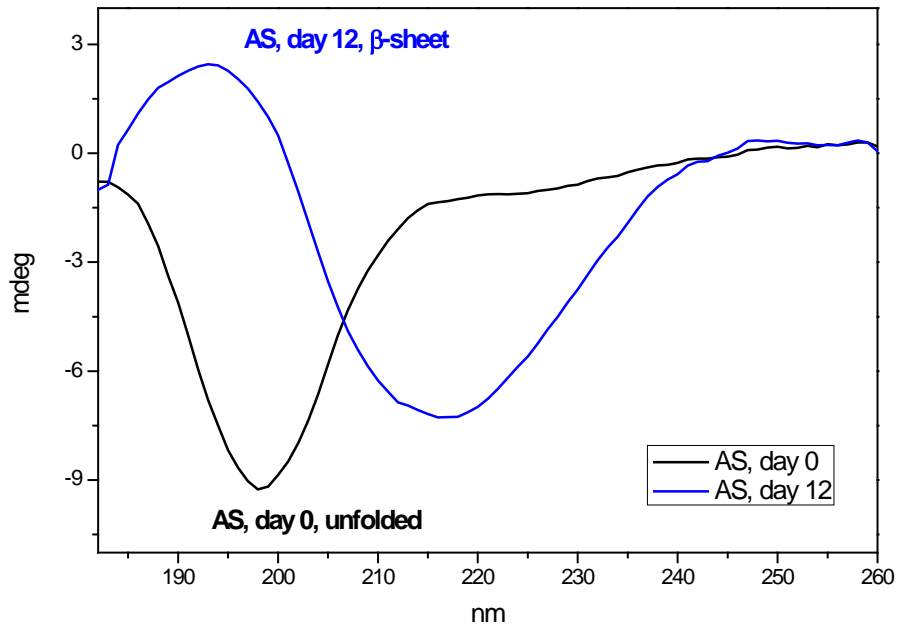
Figura 60: SRCD spectra of sample 1 collected at the beginning (day 0) and at the end (day 12) of the aggregation experiment.

The SRCD spectra of sample 5 (AS/Bi-DHZ) shows a different behavior: a small negative band at 220 nm appears that may be representative of β-sheet contribution, but a negative band at about 195 nm is also present and it is characteristic of an unfolded structure. Considering the SRCD spectrum of sample 1 at day 0 as 100% unfolded and supposing that the SRCD spectrum of sample 1 at day 12 is due to a 100% β-sheet contribution, the two spectra can be combined at different ratios to estimate the theoretical unfolded and/or β-sheet contribution: in this approximation, no other contribution of further structures, such as α-helix and β-turn was considered and the only two species admitted are unfolded and β-sheet structures. Results are reported in figure 61 together with experimental SRCD spectrum of sample 5 at day 12 for comparison.

Analysing figure 61, the theoretical spectrum that mostly resembles the SRCD spectrum of sample 5 is the red one, which corresponds to a theoretical 50% of unfolded and β-sheet content. This suggests that sample 5 contains an ensemble of species that equally contribute to the final spectrum, whereas in all the other samples the main contribution is from species rich in β-sheet structure.

These findings, accompanied by the previous differences revealed in CD signal of CR suggest that the analysis of the CD spectra of Congo Red during protein aggregation might be a useful technique to detect appreciable differences in the content of the species tested and can be a complementary method to study the aggregation.
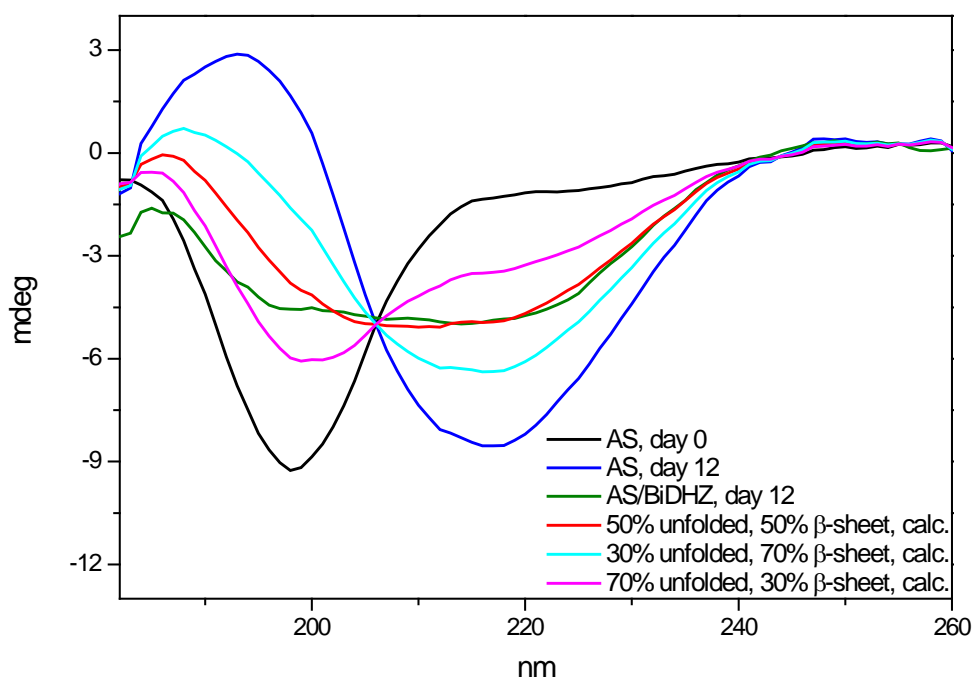
Figure 61: Experimental SRCD spectra of sample 5 at day 12 (green), sample 1 at day 1 (black) and day 12 (blue) and theoretical SRCD spectra obtained from the combination of black and blue spectra with different ratio (red, cyan and magenta).

Antioxidant activity

Among the several activities confirmed by scientific studies, curcumin shows antioxidant properties. Antioxidant acitivity was reported for many other polyphenols and, since one of the factors that worsen PD is oxidative stress, antioxidant compounds may be beneficial for PD treatment.

The free-radical scavenging capacity of DHZ-like compounds were initially evaluated by EPR spectroscopy using the DPPH radical. The measurements were performed at "Istituto di Chimica Biomolecolare" of CNR, Sassari Unit. The EPR spectrum (a quintet with hyperfine splitting of 8.7 G) in Figure 62 (black) is characteristic of the DPPH radical.

As seen in Figure 62, the addition of increasing amounts of a selected compound (as an example, BiDHZ) to the control, reduces the intensity of the DPPH signal. To quantify the relative amounts of the DPPH present in a given sample, the central peak of each spectrum was used for calculations. The results demonstrated that each compounds reduced the DPPH signal in a concentration-dependent manner.
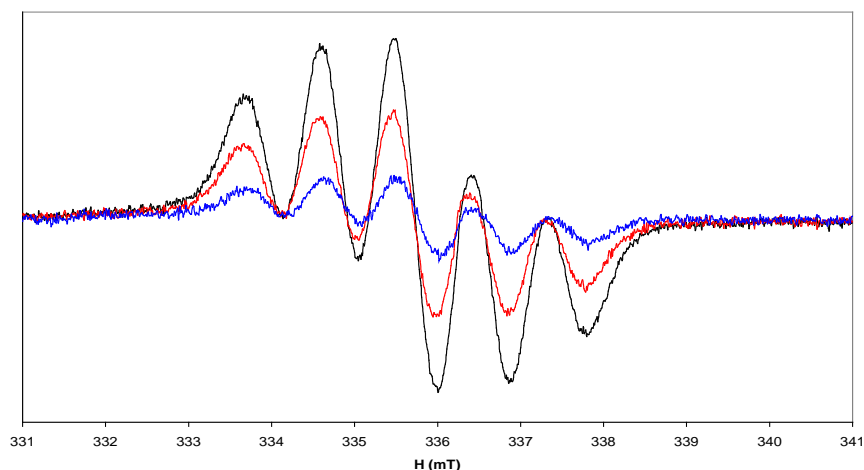
Figure 62: Typical EPR spectra of 50 µM ethanol solutions of DPPH radical in the absence (black) or in the presence of different amounts of 4: 16 µM (red) and 32 µM (blue).

The free radical scavenging activity of DHZ and analogs is expressesed as EC50 (Table 12). The radical-scavenging properties of the molecules were also determined by UV-Vis measurements and the calculated EC_{50} values are reported in Table 12. Variations in EC_{50} values may be due to the technique used but in general results show a similar behavior, where for both techniques OMeDHZ and its biphenyl derivative have the highest EC_{50}, Zingerone the lowest and Bi-DHZ show a lower EC_{50} value than its monomer DHZ.

Table 12: Inhibitory properties of compounds tested on DPPH radical.

Compound	EPR EC50 (µM)	UV-Vis EC50 (µM)
DHZ	54.8	117.0
OMe-DHZ	5620.0	7130.0
Zing	25.1	31.5
Bi-DHZ[a]	35.2	57.4
Bi-OMeDHZ[a]	2000.0	2000.0
Bi-Zing[a]	22.8	nd[b]
[a] concentration expressed as phenolic group; [b] not detectable		

Since OMe-DHZ and Bi-OMeDHZ have no hydroxyl groups that may contribute to scavenge the DPPH radical, they exhibit a much lower activity than the other compounds. These results are consistent with published data since flavonoids and other phenolic compounds act as radical scavengers due to the presence of phenolic moiety, which is able to neutralize radicals by hydrogen donation to form a poorly reactive phenoxy radical. The dimerization process of DHZ and zingerone affects the DPPH radical scavenging activity in a different way. As shown in Table 12, the EC_{50} value of Bi-DHZ is significantly lower than that of the parent compound DHZ while zingerone and bizingerone show comparable

EC50 values (data obtained from only EPR studies). Zingerone and its biphenyl dimer showed the lowest EC50 values in free radical scavenging tests.

Metal ion chelating activity

High metal ions levels are present in tissue of PD patients, especially iron and copper and are associated with oxidative stress because they can produce highly toxic free radicals. Thus, another strategy for PD therapy may be the development of small molecules that display both antioxidant and chelating activity.

The chelating properties of DHZ-like molecules towards Cu^{2+}, Fe^{2+}, and Fe^{3+} was evaluated by UV-Vis spectroscopy. As an example, spectra of the titration of Bi-OMeDHZ with Cu^{2+} are reported.

The interaction studies of DHZ-like molecules with Cu(II), Fe(II) and Fe(III) by UV-Vis spectroscopy, underline the capacity of biphenylic derivatives to interact with the metal ions considered. The chelating properties of byphenilic compounds is probably due to the presence of two hydroxyl groups (Bi-DHZ and bizingerone) or of the two methoxy groups (Bi-OMeDHZ) in 4,4' position, that permits the interaction with different metal ions. The analysis of the binding curves (not shown) underlines that the different complexes experience a different stoichimetry from 1:1.
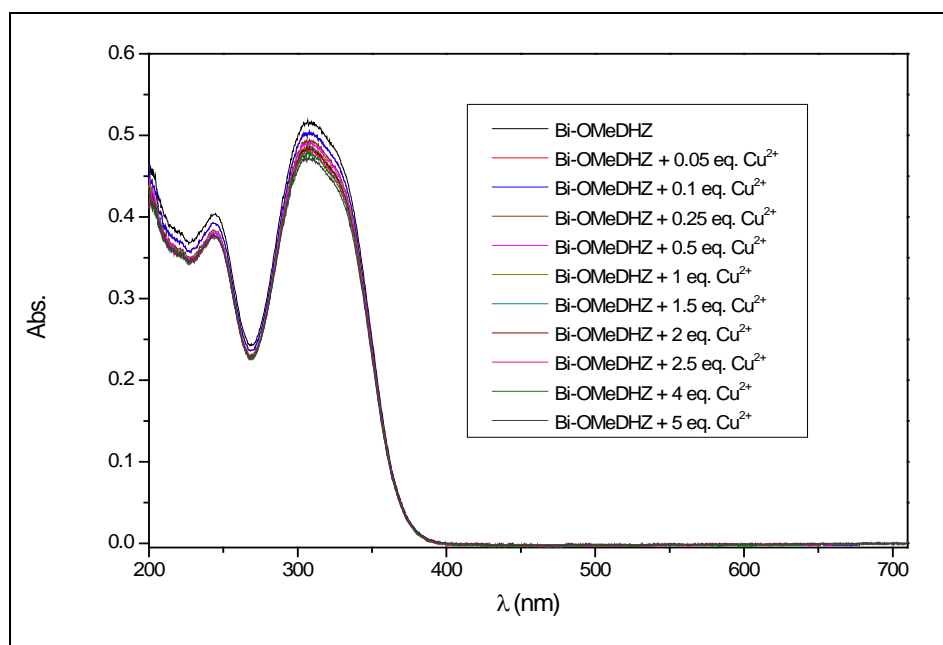

Figure 63: UV-Vis spectra of the titration of 15 µM Bi-OMeDHZ in 10 mM Tris-HCl buffer, pH 6.8 with Cu2+ (10 mM stock solution in 10 mM Tris-HCl buffer pH 6.8) at room temperature.
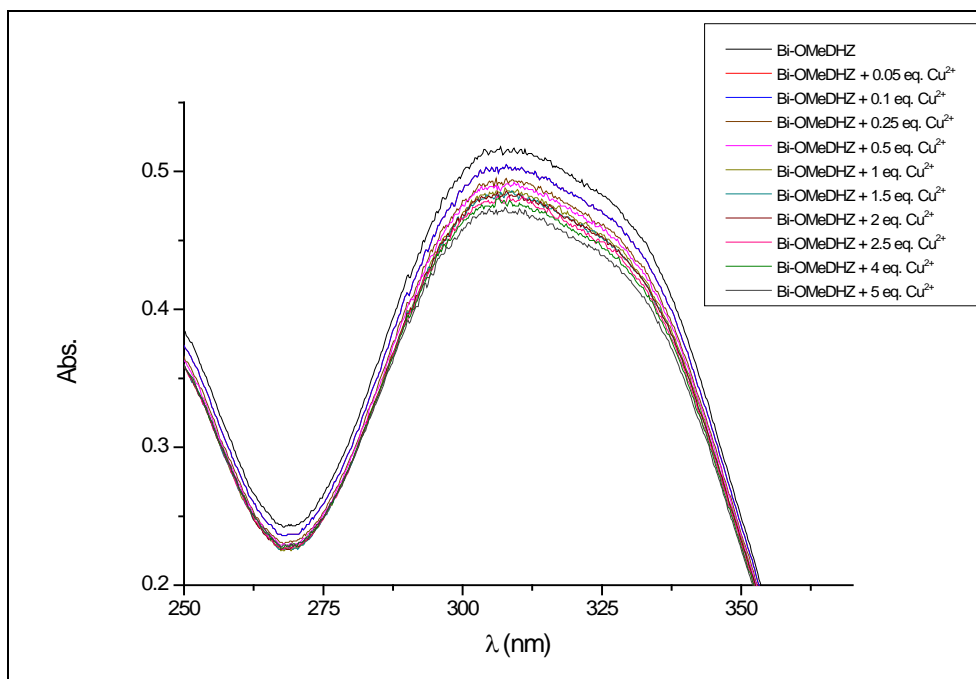
Figure 64: Enlargement of figure 65.

The stoichiometric values were calculated by the extrapolation of the two straight segments, at the origin and at saturation and are summarized in table 13.

Table 13: Stoichiometric values of the complexes of the biphenyl derivatives with Fe^{3+}, Fe^{2+} e Cu^{2+}.

Compounds	Cu^{2+}	Fe^{3+}	Fe^{2+}
Bi-DHZ	0.5	0.2-0.3	0.5
Bi-OMeDHZ	0.25-0.33	0.6-0.7	0.5
Bi-Zing	nd	0.5-0.6	nd

If we compare the binding curves of the same compound with the different metal ions, we observe a different affinity of biphenyl derivatives to metal ions examined. Thus, Bi-DHZ and Bi-OMeDHZ show to be good chelator for metal ions, whereas for Bi-Zing the chlating activity seems to be restricted to Fe^{3+} only.

Cell viability test

This analysis was conducted at the "Istituto di Chimica Biomolecolare" of CNR, Sassari Unit. The *in vitro* neuroprotective activity of DHZ-like molecules was evaluated analyzing cell death induced by H_2O_2, MPP^+ and $MnCl_2$ in PC12 cells. This cell line is a good model to study oxidative stress associated with PD [126]. Cell viability at 24 h after exposure to H_2O_2 (75 μM), MPP^+ (0.5 mM) or $MnCl_2$ (0.75 mM) was reduced respectively to 55%, 64% and 54% of the control values. As shown in Figure 63, the viability of PC12 cells was

significantly reduced by exposure to compounds OMe-DHZ (81%), Bi-DHZ (80%) and BiOMeDHZ (12%) compared with controls.
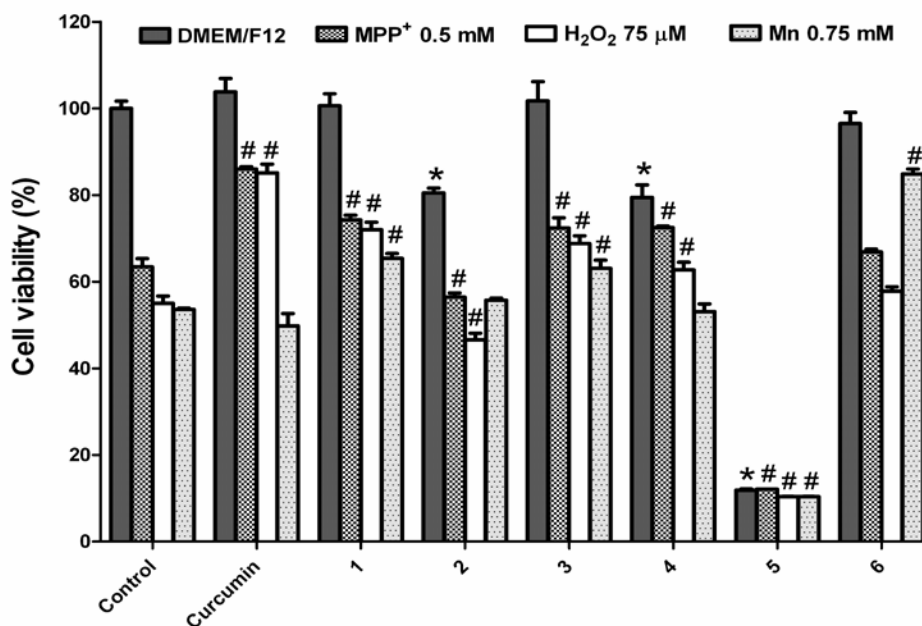

Figure 65: Effects of curcumin or dehydrozingerone-like compounds (40 µM) on viability of PC12 cells in their culture medium alone (DMEM/F12) or supplemented with H_2O_2 (75 µM), MPP^+ (0.5 mM) or $MnCl_2$ (0.75 mM).*,# = P<0.05 versus the corresponding control. 1 = DHZ; 2 = OMeDHZ; 3 = Zing; 4 = BiDHZ; 5 = BiOMeDHZ; 6 = BiZing.

Dose-response studies (Figure 64) confirmed the cytotoxicity of these compounds. Specifically, Bi-OMeDHZ significantly reduced cell viability already at the concentration of 10 µM (65%), while OMe-DHZ shows slight toxicity at 20 µM concentration. In the whole range of tested concentrations (from 10 to 80 µM), none of these compounds protects cells from toxic compounds to a significant level. DHZ and zingerone protect injured cells in all studied models. Surprisingly, bizingerone, the dimer of zingerone, protected cells only against $MnCl_2$ damage. Curcumin significantly protected cells from H_2O_2 and MPP^+ toxic effects while failed to protect cells exposed to $MnCl_2$.

In conclusion, the protective effect on PC12 cells of bizingerone against the toxic effect of $MnCl_2$ is noteworthy. Surprisingly, both the dimerization process (except for bizingerone) and the introduction of methoxy group in 4-position of 3-buten-2-one derivatives (OMeDHZ and BiOMeDHZ) increased the cytotoxic properties of these compounds, hampering their possible therapeutic use.
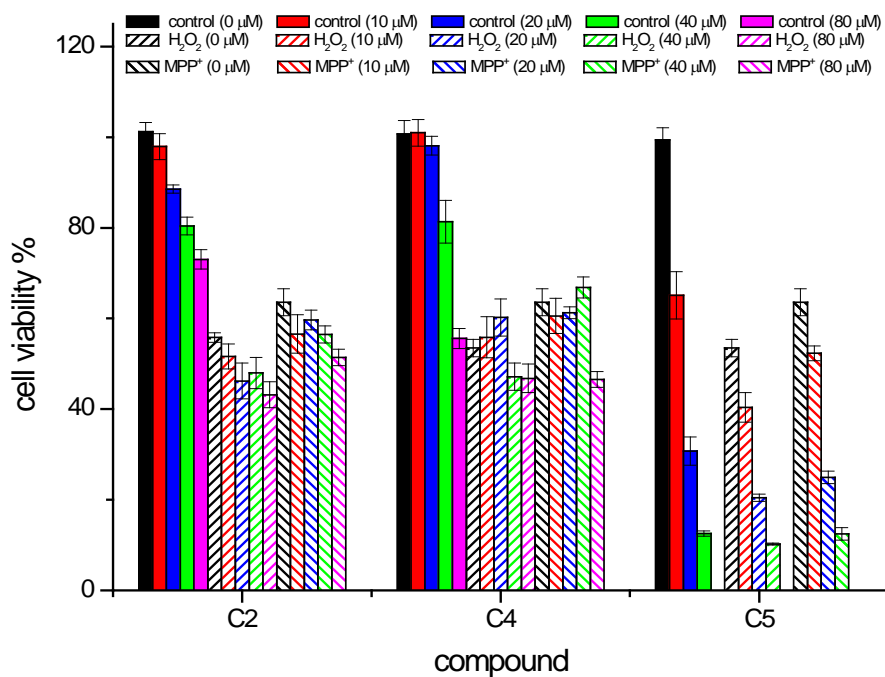
Figure 66: . Effects of OMeDHZ (C2), BiDHZ (C4) and BiOMeDHZ (C5) concentration (reported in parentheses) on viability of PC12 cells in their culture medium alone (control) or supplemented with either H_2O_2 (75 μM) or MPP^+ (0.5 mM).

β-sheet breaker peptides

Synthesis

We synthesized nine peptide whose basic sequence was taken from two β-sheet breaker peptide already known in literature. To overcome intrinsic disadvantages in the therapeutic use of peptide (proteolytic degradation and poor BBB permeation) and to improve the ability to act as β-sheet breakers, two main modifications were introduced: the phenylalanine residue was substituted with its constrained analogs N-MePhe and Tic, using both D- and L-series aminoacid. This substitution permits us also to understand the role of the Phe residue in the binding with AS.

The introduction of conformational restrictions in peptides represent an efficient method to study substrate selectivity toward a specific ligand. These conformational constraints involve different torsional angles of the peptide chain and can be divided in three main groups: "local constraints" reduce conformational mobility of a single residue, "regional constraints" influence a group of residues to form secondary structures like β-turns, and "global constraints" involve the entire peptide structure. The use of local constraints allows one to explore the topology of amino acid side chains that is defined by the torsional angles χ^i. In general, local constraints are due to substituents that cause an increase in steric hindrance, thus reducing mobility of adjacent angles. When aromatic residues are involved, local constraints often entail the formation of cyclic structures between the aromatic ring and the backbone. Side chain conformation can be limited through the introduction of an alkyl group in β-position or on the aromatic ring of the amino acid residue. These substitutions do not perturb the backbone excessively permitting a certain degree of mobility to both backbone and side chains, but the orientation of the aromatic ring can be reduced.
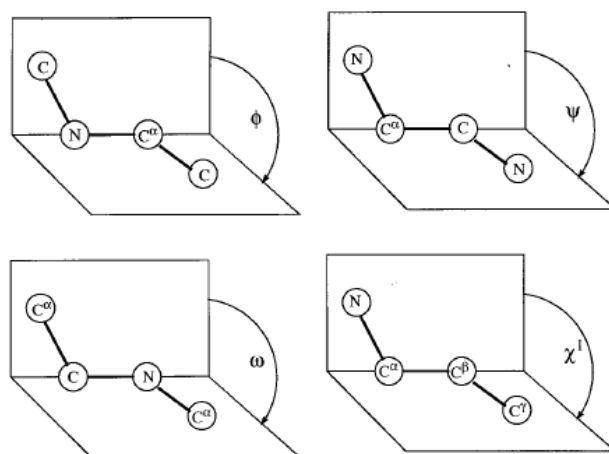

Figure 67: Definition of torsional angles φ, ψ, ω, χ[1] [123].

Moreover, alkyl groups enhance the lipophilic character of the peptide, favoring its blood-brain barrier permeation. The addition of a covalent bond between the aromatic ring and the backbone N^α of the backbone allows one to introduce conformational limitations to the amino acid residue. For example, the Tic residue (1,2,3,4-tetrahydroisoquinoline-3-carboxylic acid) is a cyclic, constrained phenylalanine analogue, with a methylene bridge between the backbone N^α and the $C^{2'}$ of the aromatic side chain [123]. The Tic residue is characterized by only two allowed side-chain orientations, the g(-) or g(+) conformations (fig. 68).
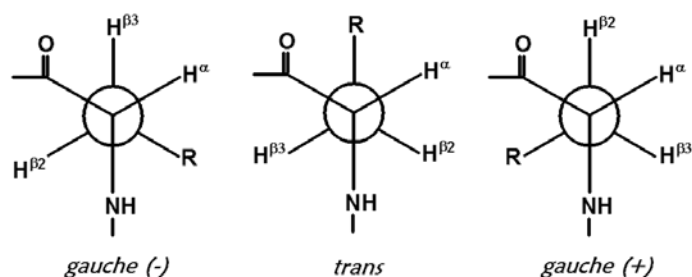
Figure 68: Newman projections of three staggered x1 rotamers in L-amino acids [123].

The preferred conformation of the D-Tic residue in a peptide chain is g(-), which corresponds to g(+) for an L-residue in the same position [124]. For the L-NMePhe residue, all three side-chain conformations are possible in principle, but mostly the t and g(-) conformations are observed in peptides (fig. 68) [125]. The presence of a methyl group on the nitrogen constrains the ψ angle of the preceding residue to a large value typical of those found in extended or β-structures. In addition to providing topographic restrictions, constraint residues can impart other properties to peptides, such as increased resistance to proteolysis.

The substitution of the phenylalanine residue with N-MePhe, D-N-MePhe, Tic e D-Tic residues in the BB1 peptide was carried out to evaluate the orientation of the side chain and the effect of the conformational constraints introduced upon binding to AS. Phenilalanine was also substituted with alanine to estimate the importance of the aromatic residue for the interaction with AS.

Figure 69: Tic and N-MePhe structure.

Peptides were synthesized and subsequently purified following the procedures explained in the Materials and Methods section. Each peptide was obtained in good purity and high yield.

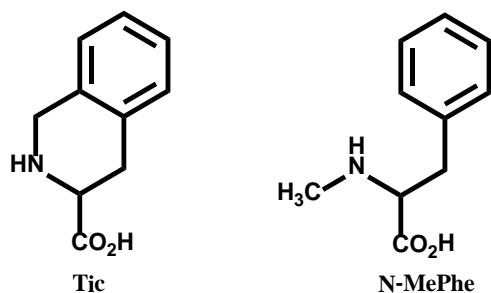Table 14: List of the peptides synthesized and their molecular weight determined by ESI-MS.

Peptide		MW		
			Calculated	*Determined*
BB1	RKVFYTW-NH$_2$	C$_{50}$H$_{71}$N$_{13}$O$_9$	997.55	997.55
BB1-D	rkvfytw-NH$_2$	C$_{50}$H$_{71}$N$_{13}$O$_9$	997.55	997.55
BB1-MePhe	RKV-**N-MePhe**-YTW-NH$_2$	C$_{51}$H$_{73}$N$_{13}$O$_9$	1011.57	1011.56
BB1-D-MePhe	RKV-**me-phe**-YTW-NH$_2$	C$_{51}$H$_{73}$N$_{13}$O$_9$	1011.57	1011.59
BB1-Tic	RKV-**Tic**-YTW-NH$_2$	C$_{51}$H$_{71}$N$_{13}$O$_9$	1009.55	1009.59
BB1-D-Tic	RKV-**tic**-YTW-NH$_2$	C$_{51}$H$_{71}$N$_{13}$O$_9$	1009.55	1009.56
BB1-Ala	RKVAYTW-NH$_2$	C$_{44}$H$_{67}$N$_{13}$O$_9$	921,52	921.54
BB2	RGAVVTGR-NH$_2$	C$_{33}$H$_{63}$N$_{15}$O$_9$	813.49	813.49
BB2-D	rgavvtgr-NH$_2$	C$_{33}$H$_{63}$N$_{15}$O$_9$	813.49	813.49

Lower case = D-series aminoacids

Fluorescence studies

Tryptophan fluorescence

The tryptophan contained in the sequence of the BB1 group of peptides was used as a fluorescence probe to monitor the binding of each peptide with to AS. Fluorescence spectra were collected as described in the Materials and Methods section using an excitation wavelength of 295 nm to abolish the tyrosine contribution from α-synuclein.

For each peptide, we observed an increased intensity of the emission fluorescence upon binding to AS, but the emission maxima value do not change noticeably, with only a small blue-shift. Thus, we can conclude that the environment surrounding the tryptophan residue does not change and that binding to AS causes only a minimal increase of hydrophobicity. This is not surprising because the AS monomer is unfolded in aqueous solution, so it cannot bury the peptide inside a hydrophobic core like globular proteins such as BSA. As a consequence, the peptide fluorescence is essentially influenced by the external aqueous environment. The increased intensity corresponds to a higher rigidity of the peptide because the binding to AS reduces its degrees of freedom.
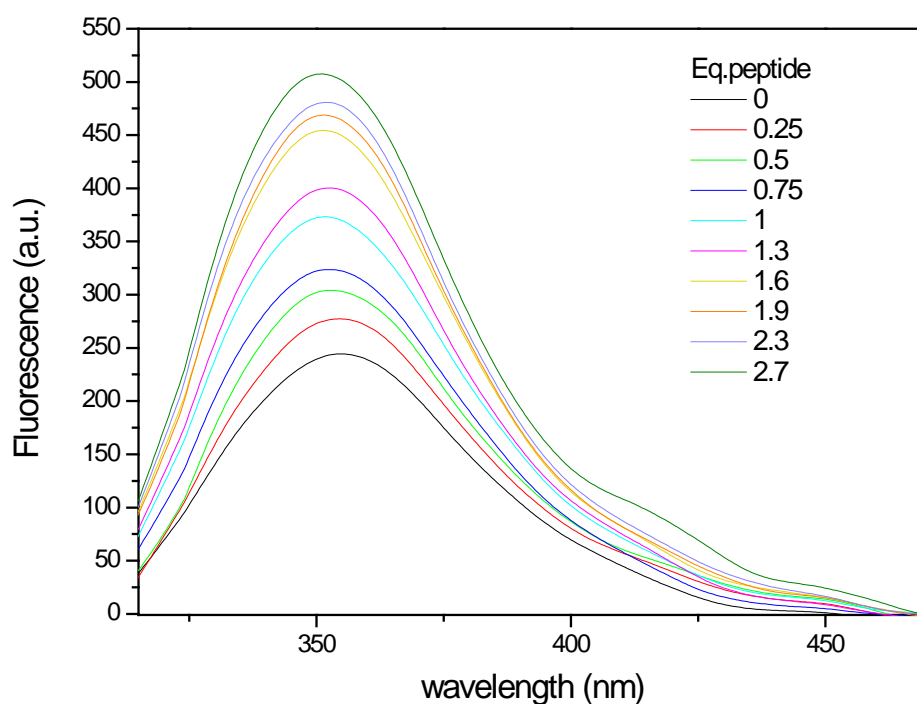
Figure 70: Tryptophan fluorescence emission spectra for the titration of BB1 (1.5 µM in 20 mM phosphate buffer, pH 6.8) with AS (66 µM of the same buffer) at 25 °C, 1 cm pathlength.

Table 15 reports the emission maximum of tryptophan alone and complexed with AS.

Table 15: Tryptophan emission maximum for each peptide in the absence ($\lambda_{em\ max}$) and in excess($\lambda_{em\ saturation}$) of AS.

Peptide	$\lambda_{em\ max}$ (nm)	$\lambda_{em\ saturazione}$ (nm)
BB1	358	352
BB1-D	354	353
BB1-MePhe	360	358
BB1-D-MePhe	357	353
BB1-Tic	359	355
BB1-D-Tic	360	356
BB1-Ala	356	353

The binding of the peptide (L) to AS (R) can be described as follows :

(12)
$$L + R \Leftrightarrow RL$$

where the binding constant is:

(13)
$$K_d = \frac{[L][R]}{[RL]}$$

K_d can be obtained from single titration data using the non-linear least square computer fit based on the equation valid for a 1:1 binding stoichiometry [126]:

(14) $$\Delta F = F_{obs} - F_0 = \Delta F_{max} \cdot \frac{[L]+[R]+K_d - \sqrt{([L]+[R]+K_d)^2 - 4[L][R]}}{2[L]}$$

Where F_{obs} and F_0 are the values of the observed and initial fluorescence intensity, respectively, [L] and [R] the total concentrations of the peptide and AS, $\Delta F_{max} = F_{max} - F_0$ where F_{max} is the peptide fluorescence saturated with AS. When the saturation is not achieved, we estrapolated the value from the graph of 1/F versus 1/[AS]. As an example, we report the binding curve for the AS/BB1 complex.
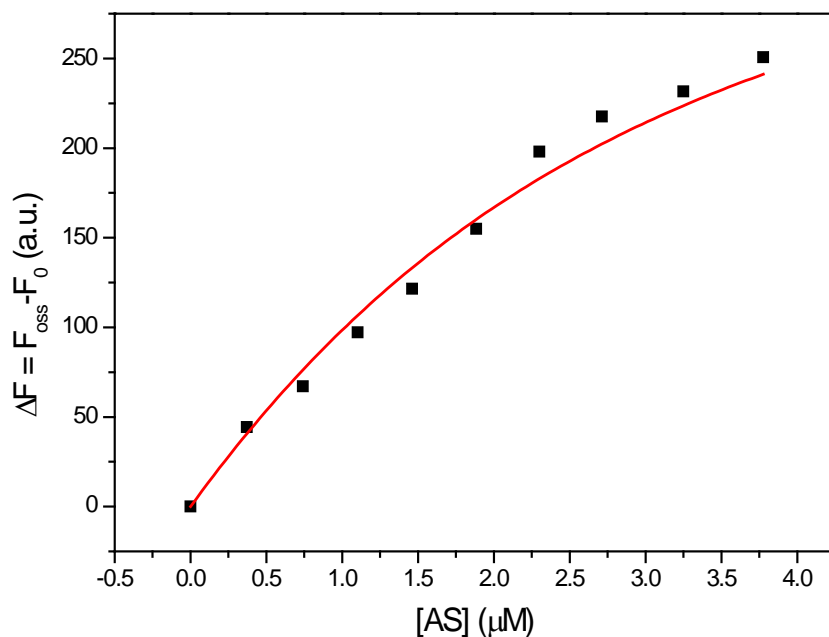
Figure 71: Binding curve for the titration of BB1 peptide (1.5 μM in 20 mM phosphate buffer, pH 6.8) with increasing amounts of AS (66 μM, same buffer).

The peptides BB1 and BB1-D peptides show similar binding affinity. The affinity of the peptide toward the protein is decreased by the introduction of constraints at the Phe position, whereas it is increased by the introduction of an alanine residue in the same position. From these findings we conclude that the aromatic residue is not important for binding to AS or rather that it has a negative effect on the interaction. Table 16 shows the binding dissociation constant for each peptide/protein complex.

Table 16: K_d values for each peptide tested.

Peptide	K_d (μM)
BB1	2.43±0.21
BB1-D	2.12±0.33
BB1-MePhe	2.94±0.36
BB1-D-MePhe	3.38±0.52
BB1-Tic	4.68±0.59
BB1-D-Tic	5.59±1.20
BB1-Ala	1.04±0.13

Förster resonance energy transfer (FRET)

FRET studies were performed to better analyze the binding between the peptides and AS and to determine the preferred protein domain for the interaction with each peptide. Wild type AS was labeled with the fluorophore Oregon Green 488 that displays an absorption maximum at 491 nm with a molar absorbity ε_{491} = 81000 M-1 cm-1 and a strong emission with a maximum at 524 nm. Peptides were labeled with the fluorophore IAEDANS that absorbs at 336 nm with a molar absorbity ε_{336} = 5700 M-1 cm-1 and emits at 490 nm. The emission spectrum of IAEDANS partially overlaps the absorption spectrum of Oregon Green, thus the two fluorophore can be used as FRET probes, with an R_0 value of 46 Å (R_0 is the Förster distance, that is the distance equivalent to a 50% energy transfer efficiency). FRET is a useful technique for the aim of this study, that is the identification of the region in the protein where the peptides bind. If the peptide labeled with IAEDANS binds the protein in a region far from where the protein is labeled with OG (> 1.5R_0), we will not detect energy transfer. Fluorescence measurements were performed as described in Materials and Methods section.

As an example, the titration of C-terminally labeled AS with BB1-D-Tic-IAEDANS is reported in figure 72.

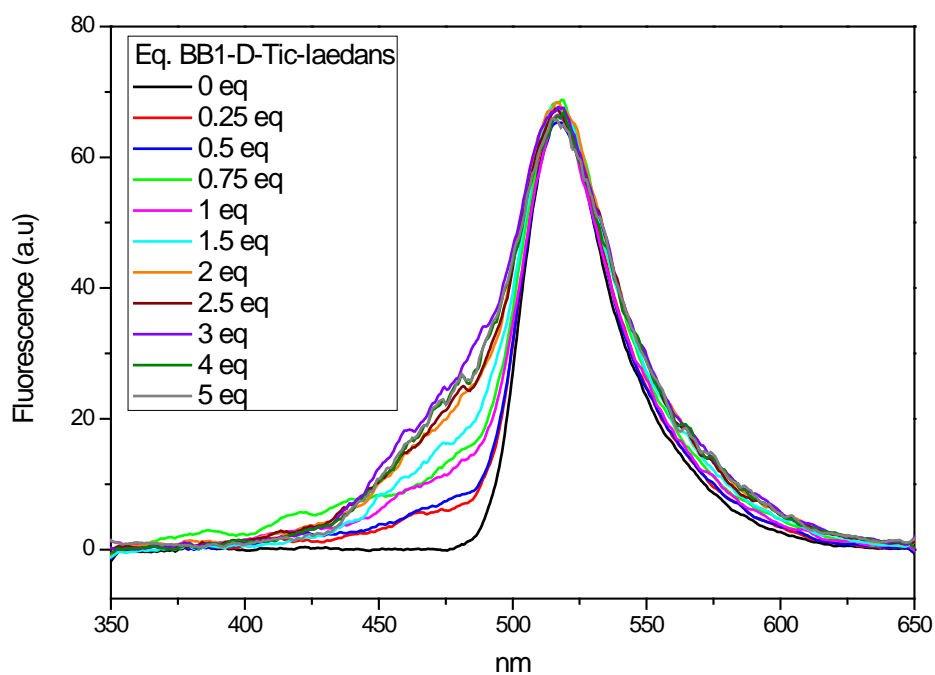**Figure 72: Difference fluorescence emission spectr for the titration of AS-Ct-OG 0.2 μM in 20 mM phosphate buffer pH 6.8 with increasing amounts of BB1-D-Tic-Nt-IAEDANS (21 μM in 20 mM phosphate buffer, pH 6.8). Fluorescence spectra were excited at 336 nm and recorded from 350 to 650 nm.**

No change in the emission fluorescence of the acceptor (OG) was detected, as the fluorescence spectra of OG in the presence and in the absence of the peptide (fig. 72) are super imposable. Similar results were obtained for all the other peptides and suggest that no energy transfer occurs, i.e., that the peptides do not interact with the C-terminal domain of AS. A small shoulder at about 480 nm, corresponding to the emission region of IAEDANS (fig. 72), is present at increasing amounts of the peptide,. The increase of the fluorescence emission at 480 nm suggest that IAEDANS experiences a different and more rigid environment, leading us to conclude that the peptide interacts with AS but in a region far from the C-terminal domain. It would be interesting to label AS in other positions and repeat the same measurements to identify the binding site of the peptides.

Circular dichroism studies

The peptides BB2 and BB2-D do not have any aromatic residue that can be used as fluorescent probe. Therefore, circular dichroism in the far-UV region was analyzed to evaluate if the peptides interact with AS.
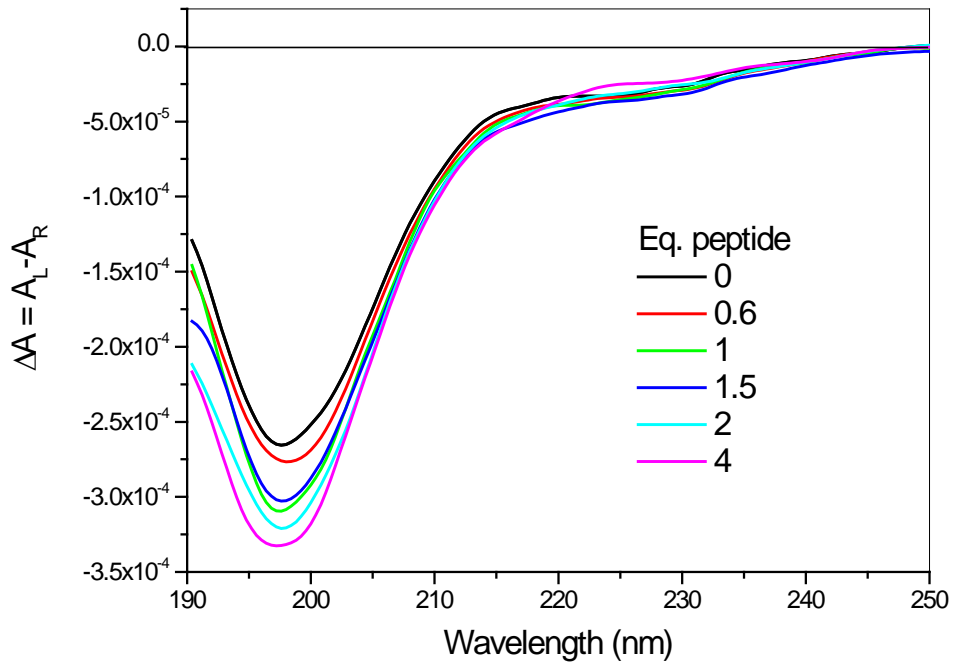
Figure 73: Far-UV CD spectra for the titration of synuclein (4 μM in 20 mM phosphate buffer, pH 6.8) with BB2 (200 μM in the same buffer) at 25 °C, 1 mm pathlength.
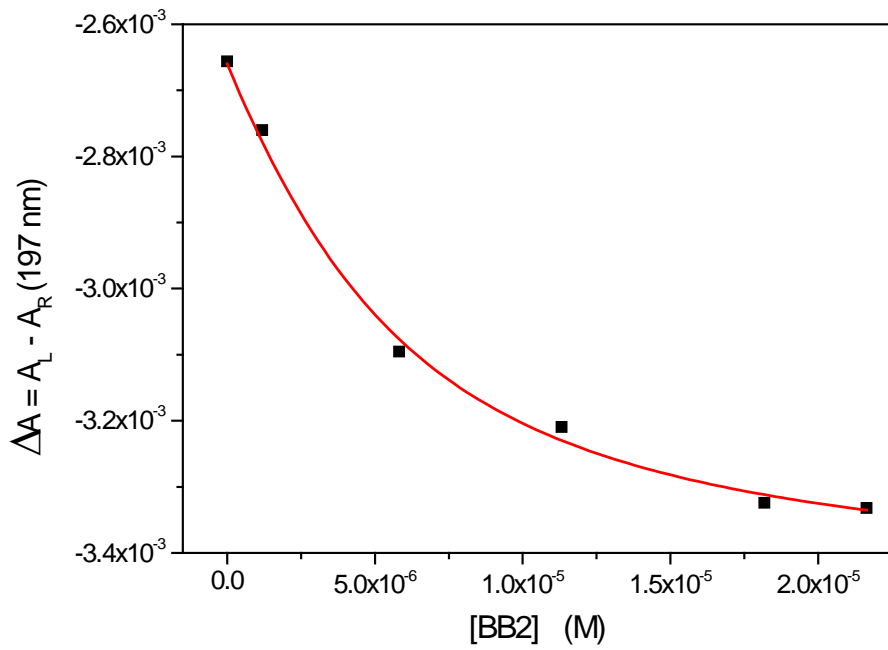
Figure 74: Binding curve for the titration of synuclein (4 μM in 20 mM phosphate buffer pH 6.8) with BB2 (200 μM in the same buffer) at 25 °C, 1 mm pathlength.

CD spectra show a change in the signal intensity at about 197 nm that reveal the binding between AS and the peptides tested, although the secondary structure is not greatly influenced and AS remains essentially unstructured.

Analyzing the data obtained, the BB2 series shows higher affinity in the binding to AS, but the measurements were performed with a different technique, which might make direct comparison not feasible.

Equation (11) was used to estimate the binding constant (table 17) where we consider the $\Delta\varepsilon_{RL}$ value due only to the protein contribution to the signal and the contribute of changes in the conformation of the protein and peptide upon binding. As an example, the titration of AS with BB2 and its binding curve are reported.

Table 17: K_d values for the complexes AS/BB2 and AS/BB2-D

Peptide	K_d (μM)
BB2	0.50±0.10
BB2-D	0.35±0.08

Conclusions

Peptides synthesized by SPPS were obtained in high yields and elevated purity. Circular dichroism and fluorescence studies demonstrated that all the peptides can interact with α-synuclein. Specifically, we introduced some substitutions in the BB1 group (at Phe position) to evaluate the importance of this aromatic residue in the binding to AS. The results obtained by spectroscopic studies show that N-MePhe and Tic (both D- and L-) did not improve the binding. Moreover, the stronger affinity of BB1-Ala peptide towards AS leads us to affirm that the aromatic residue is not important for the binding with AS and on the contrary it hampers it. FRET studies performed to identify the preferential region of peptides on AS were carried out using C-terminal Oregon Green labeled synuclein and N-terminal labeled IAEDANS peptides. Fluorescence spectra revealed the absence of energy transfer between the two fluorophores, suggesting that peptides do no bind near the C-terminal residues of AS.

Interaction of curcumin and DHZ-like with AS monomer was studied by both circular dichroism and fluorescence spectroscopy. All the compounds can bind AS although with different affinity. Synuclein thermal stability studies in the presence of these ligands were performed by SRCD spectroscopy at Diamond Light Source (UK). Results show that synuclein melting temperature is increased in all the samples with the exception of Zingerone and Bidehydrozingerone, suggesting suggesting a positive effect on stabilization of AS structure. Preliminary aggregation studies were performed to test the activity of these compounds to inhibit AS aggregation and the kinetics was followed by either UV-Vis or CD spectroscopy. No particular differences were detected for the complexed tested compared to the aggregation of AS alone, with the only exception of the sample containing Bi-DHZ, in which the aggregation seems to stop at an intermediate stage. Moreover, analysis of the secondary structure by far-UV CD spectroscopy revealed the presence of an intermediate situation, a mixture of both unfolded and β-sheet contribution compared to the distinct β-sheet signal of the other samples. Antioxidant properties were evaluated by DPPH test and the results suggest that OMeDHZ and its biphenyl derivative are not very good free radicals scavenger, probably due to the absence of hydroxyl groups, usually involved in the mechanism of free radical scavenging. Metal ion chelating activity was also evaluated. Among the tested compounds, only the biphenyl derivatives showed a good chelation of the ions tested (Cu^{2+}, Fe^{2+} and Fe^{3+}). Finally, the toxicity of these compounds and their protective effect toward oxidative stress insults agents were evaluated, and

BiOMeDHZ was shown to be the most toxic compound. Taking into account all these results we may conclude that the molecules examined could be beneficial for Parkinson's disease in two way: by interfering the oxidative stress process involved in PD or by hampering the aggregation of AS by direct binding to the protein. In addition, they are more soluble in aqueous solutions than curcumin and do not degrade at neutral/basic pH and this represents a significant advantage in their administration for a hypothetical use in therapy. Before this use can be proposed, modifications need to be introduced to eliminate their citotoxicity

Bibliography

1. Y. Chen *et al.*, Protein folding: Then and now. *Archives of Biochemistry and Biophysics* **469**, 4 (Jan 1, 2008).
2. C. Soto, Protein misfolding and disease; protein refolding and therapy. *Febs Letters* **498**, 204 (Jun 8, 2001).
3. C. M. Dobson, The structural basis of protein folding and its links with human disease. *Philosophical Transactions of the Royal Society of London Series B-Biological Sciences* **356**, 133 (Feb 28, 2001).
4. C. M. Dobson, Protein folding and misfolding. *Nature* **426**, 884 (Dec 18, 2003).
5. T. R. Jahn, S. E. Radford, The Yin and Yang of protein folding. *Febs Journal* **272**, 5962 (Dec, 2005).
6. N. Gregersen, Protein misfolding disorders: Pathogenesis and intervention. *Journal of Inherited Metabolic Disease* **29**, 456 (Apr, 2006).
7. C. B. Lucking, A. Brice, Alpha-synuclein and Parkinson's disease. *Cellular and Molecular Life Sciences* **57**, 1894 (Dec, 2000).
8. C. W. Olanow, K. McNaught, Parkinson's Disease, Proteins, and Prions: Milestones. *Movement Disorders* **26**, 1056 (May, 2011).
9. C. M. Dobson, Protein misfolding, evolution and disease. *Trends in Biochemical Sciences* **24**, 329 (Sep, 1999).
10. M. Stefani, C. M. Dobson, Protein aggregation and aggregate toxicity: new insights into protein folding, misfolding diseases and biological evolution. *Journal of Molecular Medicine-Jmm* **81**, 678 (Nov, 2003).
11. C. Soto, Unfolding the role of protein misfolding in neurodegenerative diseases. *Nature Reviews Neuroscience* **4**, 49 (Jan, 2003).
12. R. Morales, K. M. Green, C. Soto, Cross Currents in Protein Misfolding Disorders: Interactions and Therapy. *Cns & Neurological Disorders-Drug Targets* **8**, 363 (Nov, 2009).
13. O. S. Makin, L. C. Serpell, Examining the structure of the mature amyloid fibril. *Biochemical Society Transactions* **30**, 521 (Aug, 2002).
14. H.-Y. Kim *et al.*, Structural Properties of Pore-Forming Oligomers of alpha-Synuclein. *Journal of the American Chemical Society* **131**, 17482 (Dec 2, 2009).
15. R. Kayed *et al.*, Permeabilization of lipid bilayers is a common conformation-dependent activity of soluble amyloid oligomers in protein misfolding diseases. *Journal of Biological Chemistry* **279**, 46363 (Nov 5, 2004).
16. R. G. Booth, in *Foye's principles of medicinal chemistry,* T. L. Lemke, D. A. Williams, Eds. (Lippincott Williams & Wilkins, Philadelphia, PA, 2008), pp. 679-697.
17. B. Thomas, M. F. Beal, Parkinson's disease. *Human Molecular Genetics* **16**, R183 (Oct 15, 2007).
18. J. Lotharius, P. Brundin, Pathogenesis of Parkinson's disease: Dopamine, vesicles and alpha-synuclein. *Nature Reviews Neuroscience* **3**, 932 (Dec, 2002).
19. O. Rascol, A. Lozano, M. Stern, W. Poewe, Milestones in Parkinson's Disease Therapeutics. *Movement Disorders* **26**, 1072 (May, 2011).
20. J. E. Galvin, Interaction of alpha-synuclein and dopamine metabolites in the pathogenesis of Parkinson's disease: a case for the selective vulnerability of the substantia nigra. *Acta Neuropathologica* **112**, 115 (Aug, 2006).
21. A. H. V. Schapira, Mitochondrial dysfunction in Parkinson's disease. *Cell Death and Differentiation* **14**, 1261 (Jul, 2007).

22. K. J. Barnham, C. L. Masters, A. I. Bush, Neurodegenerative diseases and oxidative stress. *Nature Reviews Drug Discovery* **3**, 205 (Mar, 2004).

23. M. Gu *et al.*, Mitochondrial function, GSH and iron in neurodegeneration and Lewy body diseases. *Journal of the Neurological Sciences* **158**, 24 (Jun 11, 1998).

24. T. M. Dawson, V. L. Dawson, Molecular pathways of neurodegeneration in Parkinson's disease. *Science* **302**, 819 (Oct 31, 2003).

25. M. R. Cookson, The biochemistry of Parkinson's disease. *Annual Review of Biochemistry* **74**, 29 (2005).

26. M. Windisch, H. Wolf, B. Hutter-Paier, R. Wronski, The role of alpha-synuclein in neurodegenerative diseases: A potential target for new treatment strategies? *Neurodegenerative Diseases* **5**, 218 (2008, 2008).

27. D. F. Clayton, J. M. George, The synucleins: a family of proteins involved in synaptic function, plasticity, neurodegeneration and disease. *Trends in Neurosciences* **21**, 249 (Jun, 1998).

28. L. Maroteaux, J. T. Campanelli, R. H. Scheller, Synuclein: a Neuron-Specific Protein Localized to the Nucleus and Presynaptic Nerve-Terminal. *Journal of Neuroscience* **8**, 2804 (Aug, 1988).

29. M. G. Spillantini, M. Goedert, in *Molecular Basis of Dementia,* J. H. W. R. J. C. S. N. R. M. Growdon, Ed. (2000), vol. 920, pp. 16-27.

30. O. M. A. El-Agnaf, G. B. Irvine, Review: Formation and properties of amyloid-like fibrils derived from alpha-synuclein and related proteins. *Journal of Structural Biology* **130**, 300 (Jun, 2000).

31. M. Goedert, Alpha-synuclein and neurodegenerative diseases. *Nature Reviews Neuroscience* **2**, 492 (Jul, 2001).

32. V. N. Uversky, Amyloidogenesis of natively unfolded proteins. *Current Alzheimer Research* **5**, 260 (Jun, 2008).

33. B. I. Giasson, I. V. J. Murray, J. Q. Trojanowski, V. M. Y. Lee, A hydrophobic stretch of 12 amino acid residues in the middle of alpha-synuclein is essential for filament assembly. *Journal of Biological Chemistry* **276**, 2380 (Jan 26, 2001).

34. E. Palecek, V. Ostatna, M. Masarik, C. W. Bertoncini, T. M. Jovin, Changes in interfacial properties of alpha-synuclein preceding its aggregation. *Analyst* **133**, 76 (2008, 2008).

35. M. Bisaglia, S. Mammi, L. Bubacco, Structural insights on physiological functions and pathological effects of alpha-synuclein. *Faseb Journal* **23**, 329 (Feb, 2009).

36. P. K. Auluck, G. Caraveo, S. Lindquist, alpha-Synuclein: Membrane Interactions and Toxicity in Parkinson's Disease. *Annual Review of Cell and Developmental Biology* **26**, 211 (2010).

37. P. T. Lansbury, Evolution of amyloid: What normal protein folding may tell us about fibrillogenesis and disease. *Proceedings of the National Academy of Sciences of the United States of America* **96**, 3342 (Mar 30, 1999).

38. V. N. Uversky *et al.*, Biophysical properties of the synucleins and their propensities to fibrillate - Inhibition of alpha-synuclein assembly by beta- and gamma-synucleins. *Journal of Biological Chemistry* **277**, 11970 (Apr 5, 2002).

39. J. Y. Park, P. T. Lansbury, beta-synuclein inhibits formation of alpha-synuclein protofibrils: A possible therapeutic strategy against Parkinson's disease. *Biochemistry* **42**, 3696 (Apr 8, 2003).

40. M. Hashimoto, E. Rockenstein, M. Mante, M. Mallory, E. Masliah, beta-synuclein inhibits alpha-synuclein aggregation: A possible role as an anti-parkinsonian factor. *Neuron* **32**, 213 (Oct 25, 2001).

41. W. Hoyer, D. Cherny, V. Subramaniam, T. M. Jovin, Impact of the acidic C-terminal region comprising amino acids 109-140 on alpha-synuclein aggregation in

vitro. *Biochemistry* **43**, 16233 (Dec 28, 2004).

42.   J. R. Mazzulli, M. Armakola, M. Dumoulin, I. Parastatidis, H. Ischiropoulos, Cellular oligomerization of alpha-synuclein is determined by the interaction of oxidized catechols with a c-terminal sequence. *Journal of Biological Chemistry* **282**, 31621 (Oct 26, 2007).

43.   M. M. Dedmon, K. Lindorff-Larsen, J. Christodoulou, M. Vendruscolo, C. M. Dobson, Mapping long-range interactions in alpha-synuclein using spin-label NMR and ensemble molecular dynamics simulations. *Journal of the American Chemical Society* **127**, 476 (Jan 19, 2005).

44.   C. W. Bertoncini *et al.*, Release of long-range tertiary interactions potentiates aggregation of natively unstructured alpha-synuclein. *Proceedings of the National Academy of Sciences of the United States of America* **102**, 1430 (Feb 1, 2005).

45.   T. Bartels, J. G. Choi, D. J. Selkoe, alpha-Synuclein occurs physiologically as a helically folded tetramer that resists aggregation. *Nature* **477**, 107 (Sep 1, 2011).

46.   R. Cappai *et al.*, Dopamine promotes alpha-synuclein aggregation into SDS-resistant soluble oligomers via a distinct folding pathway. *Faseb Journal* **19**, 1377 (Jun, 2005).

47.   M. G. Spillantini *et al.*, alpha-synuclein in Lewy bodies. *Nature* **388**, 839 (Aug 28, 1997).

48.   H. Braak *et al.*, Staging of brain pathology related to sporadic Parkinson's disease. *Neurobiology of Aging* **24**, 197 (Mar-Apr, 2003).

49.   S. J. Wood *et al.*, alpha-synuclein fibrillogenesis is nucleation-dependent - Implications for the pathogenesis of Parkinson's disease. *Journal of Biological Chemistry* **274**, 19509 (Jul 9, 1999).

50.   O. M. A. El-Agnaf, R. Jakes, M. D. Curran, A. Wallace, Effects of the mutations Ala(30) to Pro and Ala(53) to Thr on the physical and morphological properties of alpha-synuclein protein implicated in Parkinson's disease. *Febs Letters* **440**, 67 (Nov 27, 1998).

51.   M. Vilar *et al.*, The fold of alpha-synuclein fibrils. *Proceedings of the National Academy of Sciences of the United States of America* **105**, 8637 (Jun 24, 2008).

52.   M. S. Celej, W. Caarls, A. P. Demchenko, T. M. Jovin, A Triple-Emission Fluorescent Probe Reveals Distinctive Amyloid Fibrillar Polymorphism of Wild-Type alpha-Synuclein and Its Familial Parkinson's Disease Mutants. *Biochemistry* **48**, 7465 (Aug 11, 2009).

53.   M. R. H. Krebs, E. H. C. Bromley, A. M. Donald, The binding of thioflavin-T to amyloid fibrils: localisation and implications. *Journal of Structural Biology* **149**, 30 (Jan, 2005).

54.   K. A. Conway *et al.*, Acceleration of oligomerization, not fibrillization, is a shared property of both alpha-synuclein mutations linked to early-onset Parkinson's disease: Implications for pathogenesis and therapy. *Proceedings of the National Academy of Sciences of the United States of America* **97**, 571 (Jan 18, 2000).

55.   L. C. Serpell, J. Berriman, R. Jakes, M. Goedert, R. A. Crowther, Fiber diffraction of synthetic alpha-synuclein filaments shows amyloid-like cross-beta conformation. *Proceedings of the National Academy of Sciences of the United States of America* **97**, 4897 (Apr 25, 2000).

56.   H. A. Lashuel *et al.*, alpha-synuclein, especially the Parkinson's disease-associated mutants, forms pore-like annular and tubular protofibrils. *Journal of Molecular Biology* **322**, 1089 (Oct 4, 2002).

57.   H. A. Lashuel, D. Hartley, B. M. Petre, T. Walz, P. T. Lansbury, Neurodegenerative disease - Amyloid pores from pathogenic mutations. *Nature* **418**, 291 (Jul 18, 2002).

58. K. A. Conway, J. D. Harper, P. T. Lansbury, Accelerated in vitro fibril formation by a mutant alpha-synuclein linked to early-onset Parkinson disease. *Nature Medicine* **4**, 1318 (Nov, 1998).

59. J. Yu, Y. L. Lyubchenko, Early Stages for Parkinson's Development: alpha-Synuclein Misfolding and Aggregation. *Journal of Neuroimmune Pharmacology* **4**, 10 (Mar, 2009).

60. J. M. Souza, B. I. Giasson, Q. P. Chen, V. M. Y. Lee, H. Ischiropoulos, Dityrosine cross-linking promotes formation of stable alpha-synuclein polymers - Implication of nitrative and oxidative stress in the pathogenesis of neurodegenerative synucleinopathies. *Journal of Biological Chemistry* **275**, 18344 (Jun 16, 2000).

61. E. H. Norris, B. I. Giasson, H. Ischiropoulos, V. M. Y. Lee, Effects of oxidative and nitrative challenges on alpha-synuclein fibrillogenesis involve distinct mechanisms of protein modifications. *Journal of Biological Chemistry* **278**, 27230 (Jul 18, 2003).

62. H. Fujiwara *et al.*, alpha-Synuclein is phosphorylated in synucleinopathy lesions. *Nature Cell Biology* **4**, 160 (Feb, 2002).

63 V. N. Uversy et al., Accelerated alpha-synuclein fibrillation in crowded milieu. *FEBS Lett* **515**, 99 (Mar 27, 2002)

64. S. R. Paik, H. J. Shin, J. H. Lee, Metal-catalyzed oxidation of alpha-synuclein in the presence of copper(II) and hydrogen peroxide. *Archives of Biochemistry and Biophysics* **378**, 269 (Jun 15, 2000).

65. A. Binolfi *et al.*, Interaction of alpha-synuclein with divalent metal ions reveals key differences: A link between structure, binding specificity and fibrillation enhancement. *Journal of the American Chemical Society* **128**, 9893 (Aug 2, 2006).

66. S. L. Leong, R. Cappai, K. J. Barnham, C. L. L. Pham, Modulation of alpha-Synuclein Aggregation by Dopamine: A Review. *Neurochemical Research* **34**, 1838 (Oct, 2009).

67. M. Hashimoto *et al.*, Oxidative stress induces amyloid-like aggregate formation of NACP/alpha-synuclein in vitro. *Neuroreport* **10**, 717 (Mar 17, 1999).

68 G. Heisenhofer et al., Catecholamine Metabolism: A Contemporary View with Implications for Physiology and Medicine. *Pharmacol Rev*, 56, 331 (Sep, 2004)

69. T. F. Outeiro *et al.*, Dopamine-Induced Conformational Changes in Alpha-Synuclein. *Plos One* **4**, (Sep 4, 2009).

70. A. H. Schapira, P. Jenner, Etiology and Pathogenesis of Parkinson's Disease. *Movement Disorders* **26**, 1049 (May, 2011).

71. D. A. M. Amer, G. B. Irvine, O. M. A. El-Agnaf, Inhibitors of alpha-synuclein oligomerization and toxicity: a future therapeutic strategy for Parkinson's disease and related disorders. *Experimental Brain Research* **173**, 223 (Aug, 2006).

72. V. M. Y. Lee, J. Q. Trojanowski, Mechanisms of Parkinson's disease linked to pathological alpha-synuclein: New targets for drug discovery. *Neuron* **52**, 33 (Oct 5, 2006).

73. A. Goel, A. B. Kunnumakkara, B. B. Aggarwal, Curcumin as "Curecumin": From kitchen to clinic. *Biochemical Pharmacology* **75**, 787 (Feb 15, 2008).

74. L. Pari, D. Tewas, J. Eckel, Role of curcumin in health and disease. *Archives of physiology and biochemistry* **114**, 127 (2008-Apr, 2008).

75. B. B. Aggarwal, C. Sundaram, N. Malani, H. Ichikawa, Curcumin: The Indian solid gold. *Molecular Targets and Therapeutic Uses of Curcumin in Health and Disease* **595**, 1 (2007, 2007).

76. B. B. Aggarwal, B. Sung. Pharmacological basis for the role of curcumin in chronic diseases: an age-old spice with modern target. *Archives of physiology and biochemistry* **114**, 127 (2008-Apr, 2008).

77. K. I. Priyadarsini, Photophysics, photochemistry and photobiology of curcumin: Studies from organic solutions, bio-mimetics and living cells. *Journal of Photochemistry and Photobiology C-Photochemistry Reviews* **10**, 81 (Jun, 2009).

78. H. Hatcher, R. Planalp, J. Cho, F. M. Tortia, S. V. Torti, Curcumin: From ancient medicine to current clinical trials. *Cellular and Molecular Life Sciences* **65**, 1631 (Jun, 2008).

79. F. Jasim, F. Ali, Measurements of Some Spectrophotometric Parameters of Curcumin in 12 Polar and Nonpolar Organic-Solvents. *Microchemical Journal* **39**, 156 (Apr, 1989).

80. P. H. Bong, Spectral and photophysical behaviors of curcumin and curcuminoids. *Bulletin of the Korean Chemical Society* **21**, 81 (Jan 20, 2000).

81. C. F. Chignell *et al.*, Spectral and Photochemical Properties of Curcumin. *Photochemistry and Photobiology* **59**, 295 (Mar, 1994).

82. N. Pandey, J. Strider, W. C. Nolan, S. X. Yan, J. E. Galvin, Curcumin inhibits aggregation of alpha-synuclein. *Acta Neuropathologica* **115**, 479 (Apr, 2008).

83. A. Y. Sun, Q. Wang, A. Simonyi, G. Y. Sun, Botanical Phenolics and Brain Health. *Neuromolecular Medicine* **10**, 259 (2008, 2008).

84. F. S. Yang *et al.*, Curcumin inhibits formation of amyloid beta oligomers and fibrils, binds plaques, and reduces amyloid in vivo. *Journal of Biological Chemistry* **280**, 5892 (Feb 18, 2005).

85. H. Shoval *et al.*, Polyphenol-induced dissociation of various amyloid fibrils results in a methionine-independent formation of ROS. *Biochimica Et Biophysica Acta-Proteins and Proteomics* **1784**, 1570 (Nov, 2008).

86. M. Masuda *et al.*, Small molecule inhibitors of alpha-synuclein filament assembly. *Biochemistry* **45**, 6085 (May 16, 2006).

87. K. Ono, M. Yamada, Antioxidant compounds have potent anti-fibrillogenic and fibril-destabilizing effects for alpha-synuclein fibrils in vitro. *Journal of Neurochemistry* **97**, 105 (Apr, 2006).

88. A. A. Reinke, J. E. Gestwicki, Structure-activity relationships of amyloid beta-aggregation inhibitors based on curcumin: Influence of linker length and flexibility. *Chemical Biology & Drug Design* **70**, 206 (Sep, 2007).

89. A. Dairam, R. Fogel, S. Daya, J. L. Limson, Antioxidant and iron-binding properties of curcumin, capsaicin, and S-Allylcysteine reduce oxidative stress in rat brain homogenate. *Journal of Agricultural and Food Chemistry* **56**, 3350 (May 14, 2008).

90. G. K. Jayaprakasha, L. J. Rao, K. K. Sakariah, Antioxidant activities of curcumin, demethoxycurcumin and bisdemethoxycurcumin. *Food Chemistry* **98**, 720 (2006, 2006).

91. B. Jagatha, R. B. Mythri, S. Vali, M. M. S. Bharath, Curcumin treatment alleviates the effects of glutathione depletion in vitro and in vivo: Therapeutic implications for Parkinson's disease explained via in silico studies. *Free Radical Biology and Medicine* **44**, 907 (Mar 1, 2008).

92. G. Harish *et al.*, Bioconjugates of curcumin display improved protection against glutathione depletion mediated oxidative stress in a dopaminergic neuronal cell line: Implications for Parkinson's disease. *Bioorganic & Medicinal Chemistry* **18**, 2631 (Apr, 2010).

93. Y. J. Wang *et al.*, Stability of curcumin in buffer solutions and characterization of its degradation products. *Journal of Pharmaceutical and Biomedical Analysis* **15**, 1867 (Aug, 1997).

94. C. R. A. Souza, S. F. Osme, M. B. A. Gloria, Stability of curcuminoid pigments in model systems. *Journal of Food Processing and Preservation* **21**, 353 (Nov, 1997).

95. M. H. M. Leung, T. W. Kee, Effective Stabilization of Curcumin by Association to Plasma Proteins: Human Serum Albumin and Fibrinogen. *Langmuir* **25**, 5773 (May 19, 2009).

96. K. Ono, M. Hirohata, M. Yamada, Ferulic acid destabilizes preformed beta-amyloid fibrils in vitro. *Biochemical and Biophysical Research Communications* **336**, 444 (Oct 21, 2005).

97. P. C. Kuo *et al.*, Isolation of a natural antioxidant, dehydrozingerone from Zingiber officinale and synthesis of its analogues for recognition of effective antioxidant and antityrosinase agents. *Archives of Pharmacal Research* **28**, 518 (May, 2005).

98. E. K. Ryu, Y. S. Choe, K.-H. Lee, Y. Choi, B.-T. Kim, Curcumin and dehydrozingerone derivatives: Synthesis, radiolabeling, and evaluation for beta-amyloid plaque imaging. *Journal of Medicinal Chemistry* **49**, 6111 (Oct 5, 2006).

99. H. Kabuto *et al.*, Zingerone 4-(4-hydroxy-3-methoxyphenyl)-2-butanone prevents 6-hydroxydopamine-induced dopamine depression in mouse striatum and increases superoxide scavenging activity in serum. *Neurochemical Research* **30**, 325 (Mar, 2005).

100. K. L. Sciarretta, D. J. Gordon, S. C. Meredith, Peptide-based inhibitors of amyloid assembly. *Amyloid, Prions, and Other Protein Aggregates, Pt C* **413**, 273 (2006).

101. L. D. Estrada, C. Soto, Inhibition of protein misfolding and aggregation by small rationally-designed peptides. *Current Pharmaceutical Design* **12**, 2557 (2006, 2006).

102. C. Soto *et al.*, beta-sheet breaker peptides inhibit fibrillogenesis in a rat brain model of amyloidosis: Implications for Alzheimer's therapy. *Nature Medicine* **4**, 822 (Jul, 1998).

103. Jacobson Holman PLLC. K. Stott. Peptides containing N-substituted L-amino acids for preventing β-strand association, US 7125838 B1 (2000).

104. C. I. Stains, K. Mondal, I. Ghosh, Molecules that target beta-amyloid. *ChemMedChem* **2**, 1674 (2007-Dec, 2007).

105. C. Adessi, C. Soto, Beta-sheet breaker strategy for the treatment of Alzheimer's disease. *Drug Development Research* **56**, 184 (Jun, 2002).

106. I. Laczko *et al.*, Aggregation of A beta(1-42) in the presence of short peptides: conformational studies. *Journal of Peptide Science* **14**, 731 (Jun, 2008).

107. T. Takahashi, H. Mihara, Peptide and Protein Mimetics Inhibiting Amyloid beta-Peptide Aggregation. *Accounts of Chemical Research* **41**, 1309 (Oct, 2008).

108. F. Formaggio *et al.*, Disruption of the beta-sheet structure of a protected pentapeptide, related to the beta-amyloid sequence 17-21, induced by a single, helicogenic C-alpha-tetrasubstituted alpha-amino acid. *Journal of Peptide Science* **9**, 461 (Jul, 2003).

109. P. Santhoshkumar, K. K. Sharma, Inhibition of amyloid fibrillogenesis and toxicity by a peptide chaperone. *Molecular and Cellular Biochemistry* **267**, 147 (Dec, 2004).

110. O. M. A. El-Agnaf *et al.*, A strategy for designing inhibitors of alpha-synuclein aggregation and toxicity as a novel treatment for Parkinson's disease and related disorders. *Faseb Journal* **18**, 1315 (Jun, 2004).

111. K. E. Paleologou, G. B. Irvine, O. M. A. El-Agnaf, alpha-Synuclein aggregation in neurodegenerative diseases and its inhibition as a potential therapeutic strategy. *Biochemical Society Transactions* **33**, 1106 (Nov, 2005).

112. J. Madine, A. J. Doig, D. A. Middleton, Design of an N-methylated peptide inhibitor of alpha-synuclein aggregation guided by solid-state NMR. *Journal of the American Chemical Society* **130**, 7873 (Jun 25, 2008).

113. M. Windisch, B. Hutter-Paier, E. Schreiner, R. Wronski, beta-synuclein-derived peptides with neuroprotective activity - An alternative treatment of

neurodegenerative disorders? *Journal of Molecular Neuroscience* **24**, 155 (2004, 2004).

114   huang et al

115.   J. Jones, in *Amino acid and peptide synthesis*. (Oxford University Press, 2002, Oxford, UK, 1991), pp. 25-41.

116.   J. R. Lackovitz, in *Principles of Fluorescence Spectroscopy*. (Springer, Singapore, 2006), pp. 277-327.

117.   M. Jiang *et al.*, Spectroscopic studies on the interaction of cinnamic acid and its hydroxyl derivatives with human serum albumin. *Journal of Molecular Structure* **692**, 71 (Apr 5, 2004).

118   G. Siligardi et al., Regulation of Hsp90 ATPase activity by the co-chaperone Cdc37p/p50cdc37.*J Biol Chem*, **277**, 20151 (Mar, 2002).

119.   F. Zsila, Z. Bikadi, M. Simonyi, Molecular basis of the Cotton effects induced by the binding of curcumin to human serum albumin. *Tetrahedron-Asymmetry* **14**, 2433 (Aug 15, 2003).

120.   F. Zsila, Z. Bikadi, M. Simonyi, Unique, pH-dependent biphasic band shape of the visible circular dichroism of curcumin-serum albumin complex. *Biochemical and Biophysical Research Communications* **301**, 776 (Feb 14, 2003).

121.   S. A. Hudson, H. Ecroyd, T. W. Kee, J. A. Carver, The thioflavin T fluorescence assay for amyloid fibril detection can be biased by the presence of exogenous compounds. *Febs Journal* **276**, 5960 (Oct, 2009).

122.   W. Hoyer *et al.*, Dependence of alpha-synuclein aggregate morphology on solution conditions. *Journal of Molecular Biology* **322**, 383 (Sep 13, 2002).

123.   V. J. Hruby, G. G. Li, C. HaskellLuevano, M. Shenderovich, Design of peptides, proteins, and peptidomimetics in chi space. *Biopolymers* **43**, 219 (1997, 1997).

124.   G. Valle *et al.*, Constrained Phenylalanine Analogs - Preferred Conformation of the 1,2,3,4-Tetrahydroisoquinoline-3-Carboxylic Acid (Tic) Residue. *International Journal of Peptide and Protein Research* **40**, 222 (Sep-Oct, 1992).

125.   P. W. Schiller *et al.*, Differential Stereochemical Requirements of Mu vs Delta-Opioid Receptors For Ligand-Binding And Signal Transduction - Development of a Class of Potent and Highly Delta-Selective Peptide Antagonists. *Proceedings of the National Academy of Sciences of the United States of America* **89**, 11871 (Dec 15, 1992).

126.   T.-C. Fan *et al.*, Characterization of molecular interactions between eosinophil cationic protein and heparin. *Journal of Biological Chemistry* **283**, 25468 (Sep 12, 2008).

127   M. Montalti et al. Handbook of photochemistry, 3rd edition, (CRC, 2006), pp 561-572.